Design Synthesis of NLMPC-based Tracking Controller for Autonomous Vehicles with Active Aerodynamic Control

by

Chunyu Mao

A thesis submitted to the
School of Graduate and Postdoctoral Studies in partial
fulfillment of the requirements for the degree of

Master of Applied Science in Automotive Engineering

Faculty of Engineering and Applied Science

University of Ontario Institute of Technology (Ontario Tech University)

Oshawa, Ontario, Canada

December 2022

© Chunyu Mao, 2022

THESIS EXAMINATION INFORMATION

Submitted by: **Chunyu Mao**

Master of Applied Science in **Automotive Engineering**

Thesis title: A Comprehensive Active Control System for Road Vehicles Path Following and Aerodynamic Devices

An oral defense of this thesis took place on November 14, 2022, in front of the following examining committee:

Examining Committee:

Chair of Examining Committee	Sayeed Ali Hosseini
Research Supervisor	Yuping He
Research Co-supervisor	Martin Agelin-Chaab
Examining Committee Member	Xianke Lin
Thesis Examiner	Mohamed Youssef

The above committee determined that the thesis is acceptable in form and content and that a satisfactory knowledge of the field covered by the thesis was demonstrated by the candidate during an oral examination. A signed copy of the Certificate of Approval is available from the School of Graduate and Postdoctoral Studies.

ABSTRACT

The past three decades have witnessed extensive studies on tracking-control for autonomous vehicles (AVs). However, there is a lack of studies on effective design methods in this field. To tackle this problem, this thesis proposes a design synthesis method which is featured a design framework with two layers: at the upper layer, a particle swarm optimization algorithm is used to find optimal solutions with desired trajectory-tracking performance; at the lower layer, a comprehensively coupled dynamic analysis is conducted among the three subsystems, including a nonlinear vehicle model with active aerodynamic control for mechanical vehicle representation, a motion-planning module with given perception data, and a tracking controller based on non-linear model predictive control (NLMPC) for direction and lateral stability control. The design optimization demonstrates that the proposed method can effectively determine the desired design variables to achieve optimal trajectory-tracking performance. The insightful findings from this study will provide valuable guidelines for designing autonomous vehicles.

Keywords: autonomous vehicles; autonomous steering control; trajectory-tracking; non-linear model predictive control; active aerodynamic control; particle swarm optimization; design optimizations

AUTHOR'S DECLARATION

I hereby declare that this thesis consists of original work of which I have authored. This is a true copy of the thesis, including any required final revisions, as accepted by my examiners.

I authorize the University of Ontario Institute of Technology (Ontario Tech University) to lend this thesis to other institutions or individuals for the purpose of scholarly research. I further authorize University of Ontario Institute of Technology (Ontario Tech University) to reproduce this thesis by photocopying or by other means, in total or in part, at the request of other institutions or individuals for the purpose of scholarly research. I understand that my thesis will be made electronically available to the public.

Chunyu Mao

STATEMENT OF CONTRIBUTIONS

I hereby certify that I am the sole author of this thesis and that no part of this thesis has been published. I have used standard referencing practices to acknowledge ideas, research techniques, or other materials that belong to others. Furthermore, I hereby certify that I am the sole source of the creative works described in this thesis.

ACKNOWLEDGEMENTS

First and foremost, I am incredibly grateful to my supervisors, Dr. Yuping He and Dr. Martin Agelin-Chaab, for giving me the opportunity to join their research group and providing me with valuable guidance throughout my research. Their motivation and endless help contributed tremendously to the successful completion of the whole journey of my graduate study and research. Dr. Yuping He has taught me the methodology to carry out the research and present the paperwork professionally, there will be no thesis without his constructive advice. Dr. Martin Agelin-Chaab has built the ladder for me to the fantastic and magical aerodynamics world, and it inspired me a lot during my thesis preparation and writing. Studying and working under their guidance was a great privilege and honour.

Besides my supervisors, I would like to express my heartfelt gratitude to my parents, Faming Mao and Meiqing Liu, for giving birth to me and supporting me unconditionally. Their love gave me the courage and confidence to get through all the hills and downs. To be their son made me feel that I am the luckiest person in the world, and I know they are always there for me no matter where I am and whom I became.

Last but not least, I would like to thank my friends in Canada and back in China. Regardless of where I am, you will always be my friend, and I will never forget our friendship. Your company is the biggest treasure in my life.

TABLE OF CONTENTS

LIST OF TABLES

LIST OF FIGURES

Appendix

LIST OF ABBREVIATIONS AND SYMBOLS

Abbreviations

AAC	Active aerodynamic control
AOA	Angle of attack
AVs	Autonomous vehicles
CFD	Computational fluid dynamics
DOF	Degrees of freedom
ECs	Evolutionary computations
FEM	Finite element method
GA	Genetic algorithm
GNSS	Global navigation satellite system
HSLC	Highway single lane-change
MIMO	Multi-input and multi-output
MPC	Model predictive control
NACA	National advisory committee for aeronautics
NLMPC	Non-linear model predictive control
ODE's	Ordinary differential equations
PSO	Particle swarm optimization
RMS	Root of mean square
SLC	Single lane-change
SST	Shear stress transport
UGV	Unmanned ground vehicle
USLC	Urban single lane-change

VS	VehicleSim

Symbols

C_D	Aerodynamic drag coefficient
C_L	Aerodynamic lift coefficient
ρ	Air density
A	Frontal area of the spoiler
V	Vehicle forward speed
F	Total tractive force
R_a	Aerodynamic resistance force
R_r	Total rolling resistance force
R_g	Grade resistance force
W	Vehicle weight
g	Gravity constant
μ	Coefficient of road adhesion
δ	Steering angle
L	Wheelbase
R	Curve radius
K_{us}	Understeer coefficient
$\boldsymbol{X}_D$	Design variable set
$\boldsymbol{X}_{Dt}$	Reference trajectories
$\boldsymbol{X}_{Dm}$	Tuning parameters of the controller
$\boldsymbol{X}_{Dv}$	Geometric and inertial parameters of the vehicle

$\boldsymbol{Z}_{D,i}$	i-th particle in the swarm
$\boldsymbol{V}_i$	Velocity of particle
$\boldsymbol{P}_i$	Position of local minimum fitness value in the search space
$\boldsymbol{P}_g$	Position of global minimum fitness value in the search space
w	Inertia weight
C_1	Positive constant
C_2	Positive constant
k	Sampling step
$\boldsymbol{u}(k)$	Control input
H_p	Prediction horizon
H_c	Control horizon
m	Vehicle mass
I	Moment of inertia about z axis
F_{cf}	Cornering force of the front tire
F_{cr}	Cornering force of the rear tire
l_f	Distance from the CG to the front axle
l_f	Distance from the CG to the rear axle
v_f	Velocity at the center of the contact area of the front wheel with the road
v_r	Velocity at the center of the contact area of the rear wheel with the road
α_i	Front or rear tire slip angle

F_{zi}	Vertical load on front or rear wheel
φ	Heading angle
φ_{ref}	Reference heading angle
Y_{ref}	Reference y coordinates in global coordinate system
v_x	Longitudinal velocity in vehicle inertial coordinate system
v_y	Lateral velocity in vehicle inertial coordinate system
e_1	Vehicle yaw angle error with respect to the target path
e_2	Vehicle lateral path deviation
X	x coordinates in global coordinate system
Y	y coordinates in global coordinate system
w_t	Track width of the vehicle
J_1	Path following off-tracking
J_2	Yaw angle deviation
J_3	Ride quality measure
a_y	Lateral acceleration
T_{slc}	Time duration for completing SLC maneuver
T_s	Sample time
$\boldsymbol{Q}$	Output weighting matrix
$\boldsymbol{R}$	Control input variation weighting matrix
q_1	Weight of yaw angle
q_2	Weight of y
R	Weight of steering input

ρ_i	Normalized weighting factors
J_i^{norm}	Performance measures
F_{z_aero}	Lift/down force generated by spoiler
Y_{err_Max}	Maximum peak lateral position deviation of the vehicle CG from the reference path
$Yaw\_ang_{err\_Max}$	Maximum peak vehicle yaw angle deviation from the reference value
$Steering\_angle_{Max}$	Maximum peak vehicle steering input
$F_{z\_diff\_front\_max}$	Maximum peak vehicle vertical load difference on front axle
$F_{z\_diff\_rear\_max}$	Maximum peak vehicle vertical load difference on rear axle
$Roll_{max}$	Maximum peak vehicle roll angle

Chapter 1

Introduction

1.1   Background and Motivation

The autonomous driving of an unmanned ground vehicle (UGV) can be described from three perspectives: perception, motion-planning, and tracking-control [1, 2]. The so-called navigation system takes an essential role in the stage of perception, and the processing of collected position information is called vehicle self-localization [3]. Then, in the decision stage, the motion-planning module generates an optimal path or trajectory toward the desired destination based on the information gathered from the perception stage. One approach, for example, using artificial intelligence aided online path planning to overcome the uncertainty in the operational environment [4]. With the consideration of static and dynamic obstacle avoidance, the generated path/trajectory is not only able to maintain transportation efficiency but also can ensure the vehicle operates in a safe condition [5]. The final stage is the implementation of automatic tracking control for the vehicle to follow the planned path/trajectory.

Among numerous tracking-control techniques, model predictive control (MPC), as one of the multi-input and multi-output (MIMO) control techniques, has gained massive popularity due to its capabilities of systematically handling model uncertainties, as well as state and control constraints, thus allowing tracking-control to operate at the limits of achievable performance. In conventional MPC-based tracking control designs, trial-and-error methods are usually used to tune these controllers. It was reported that the tuning of MPC-based tracking-controller parameters is difficult, and the tuning process is very time-

consuming [6]. Although the trial-and-error method may yield a good result if the designer is experienced, it is still identified as time-consuming and complicated. There is an auto- and optimal-tuning algorithms that implement a bi-level optimization process to solve this issue, in which the tuning parameters for MPC controllers were computed automatically at the upper-level using meta-heuristic search algorithms, e.g., particle swarm optimization (PSO) and genetic algorithm (GA), then the resulting parameters were sent to the lower-level MPC problem; the MPC used the tuned weights to calculate optimal control inputs for the plant [7].

Besides the tracking-control, vehicular aerodynamic control is aimed at improving vehicle ride quality and increasing safety without human intervention. Generally, the tire force in the longitudinal direction is called traction force or braking force, and the tire force in the lateral direction is called lateral/cornering force. Both forces are restricted by the maximum adhesion capability of the tire-road interface, while the maximum adhesion capability is directly proportional to the product of the tire friction coefficient and the vertical load on the tire. There are various road accidents that happen all over the world due to saturating longitudinal/lateral forces when the vehicle is travelling on slippery road surfaces or negotiating around a tight corner at high speed [8].

Vehicular aerodynamic devices, such as spoiler/flap, can provide extra downside or lift forces to the vehicle for increasing vehicle road holding capability and improving yaw and roll stability. It will be more effective with the increase of vehicle forward speed, although a higher drag force will degrade the fuel economy of the vehicle. Those extra downside forces will be counted to the vertical load on the tires and therefore enhance the maximum adhesion capability for the vehicle [9]. On the other hand, two rear spoilers installed in one

line but working independently can be used to generate a corrective yaw moment and reduce the vehicle's lateral load transfer by means of manipulating the angle of attack for each spoiler, thereby improving the roll and yaw stability of the vehicle [10].

Inspired by the aforementioned auto- and optimal-tuning methods for MPC controllers, as well as considering active vehicle aerodynamic control and their mechatronic nature, a novel design synthesis method that binds two distinct fields – vehicle dynamics control, and vehicle aerodynamic control – is proposed in this thesis. This design synthesis method is featured a design framework with two layers: at the upper layer, a particle swarm optimization algorithm is used to coordinate design criteria and various constraints for finding optimal solutions with desired trajectory-tracking performance; at the lower layer, a comprehensively coupled dynamic analysis is conducted among three subsystems, including a nonlinear vehicle model with active aerodynamic control for mechanical vehicle representation, a motion-planning module with given perception data, and a tracking-controller based on non-linear model predictive control (NLMPC) for direction control.

The active aerodynamic control system is composed of four independent NACA-0012 spoilers, and one spoiler is installed above each wheel located at four corners of the vehicle; thus precisely controlled extra lift/down force on each wheel will compensate for the lateral load transfer and improve the vehicle trajectory-tracking performance in the high-speed scenario. Figure 1.1 shows the NACA-0012 spoiler.
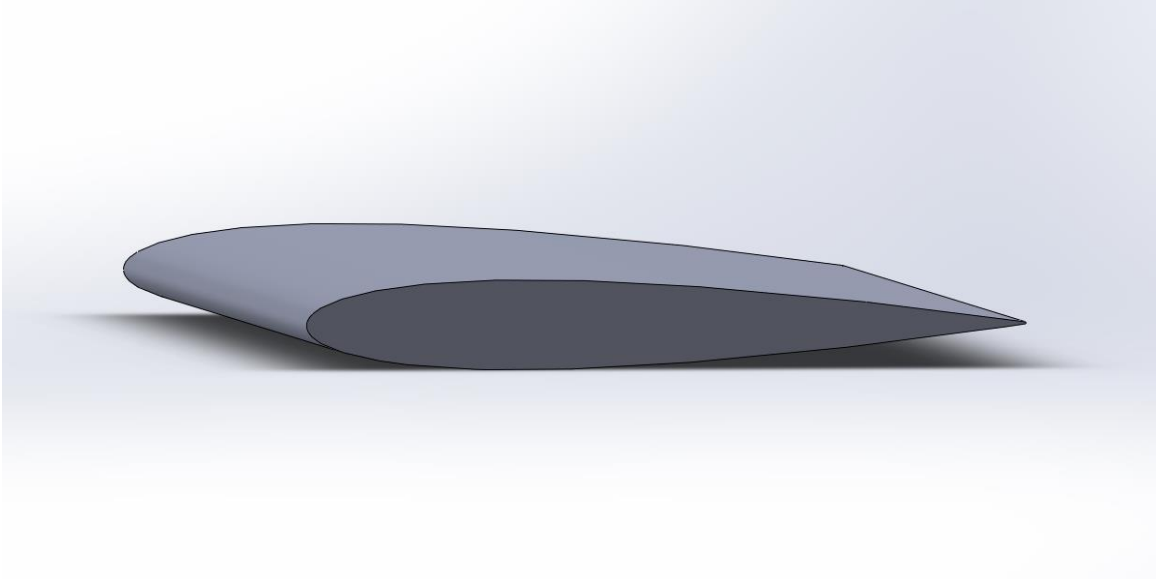
Figure 1.1: NACA-0012 Airfoil.

1.2   Thesis Objectives

The eventual target of the associated overall research program is to propose, develop, and validate a design methodology for autonomous vehicles. With the proposed methodology, the autonomous vehicle will be optimized to increase safety, improve driving performance, and ensure ride quality by means of finding optimal design variables characterizing mechanical vehicles, navigation system, actuation systems, etc. As a part of this research program, the objectives of this thesis are:

- To propose and develop a design synthesis framework with two layers: at the lower layer are the dynamically coupled motion-planning module, tracking-control module, and virtual vehicle plant with active aerodynamic control; and at the upper layer is an optimizer.

- To apply the proposed design synthesis method to the design optimization of a tracking-control oriented autonomous vehicle with active aerodynamic control. The design optimization is to simultaneously find the design variables of the mechanical vehicle and the tracking-controller to improve path-following performance, ensure yaw stability, and enhance ride quality under several operating conditions. The design variables for the mechanical vehicle may be inertial and geometric parameters, whereas the design variables for the tracking-controller can be weighting factors.

- To derive and validate a nonlinear 2 degrees of freedom (DOF) bicycle model and a 2-DOF four wheels model. In both vehicle models, the nonlinear magic formula tire model is used to mimic the tire/road interactions, and these vehicle models are applied as the prediction model for the design of the NLMPC-based tracking-controller.

- To modify MIRA (Motor Industry Research Association) car reference model with four NACA-0012 spoilers in SolidWorks and export to FLUENT software. To acquire aerodynamic data of the selected spoiler, i.e., NACA-0012, the CFD (Computational Fluid Dynamics) simulations are conducted in FLUENT software Then, the achieved aerodynamic data for the spoiler will be incorporated into the respective CarSim vehicle model, which is used as the vehicle plant in the NLMPC controller design considering the high-speed operating scenarios.

- To utilize the co-simulation by integrating the NLMPC controller designed in MATLAB/SimuLink with the virtual vehicle plant developed in CarSim to

evaluate the performance of the design of NLMPC-based tracking-controller for autonomous vehicles with active aerodynamic control.

1.3   Thesis organization

The remainder of the thesis is organized as follows. Chapter 2 reviews the state-of-the-art of studies on the topics concerned and identifies the associated knowledge gaps to be filled by this research. Besides, all the relevant background concepts/models and associated terminologies are introduced in this chapter. Chapter 3 presents the design synthesis method for autonomous vehicles. The proposed bi-layer design synthesis is introduced; a PSO search algorithm will be applied at the upper layer as the optimizer; the NLMPC tracking-controller is dynamically coupled with the CarSim vehicle model with active aerodynamic control. The active aerodynamic control functionality for the CarSim vehicle model is established. Chapter 4 presents the implementation of the design optimization of vehicles with autonomous steering control, and the simulation results are analyzed and discussed. Finally, Chapter 5 identifies the future research topics and concludes this thesis.

Chapter 2

Literature review

2.1 Autonomous driving systems

Advances in electronics, information, communications, computer, and control technologies have paved the road for developing autonomous vehicles (AVs). Three interrelated operating modules can characterize the autonomous driving of an AV: perception, motion-planning, and tracking-control [1, 2]. The perception module operates with two functions, including local traffic detection and global localization. An AV acquires information about its surrounding traffic environment using various sensors, e.g., ultrasonic, radar, Lidar, camera, etc., [11]; a global navigation satellite system (GNSS) may be utilized to identify the vehicle localization with its longitude, latitude, speed, and course [12]-[13], while an odometry technique or an inertial measurement unit, which combines accelerometers, gyroscopes and magnetometers, can be used in situations where the GNSS is unreliable [14]. To enhance the reliability, accuracy, and fault tolerance of environmental perception and localization, various sensor fusion techniques have been studied and developed for AVs, where large amounts of disparate sensor data are produced and analyzed [15, 16].

With the data of its surrounding environment and positioning acquired through perception, the AV operates in the motion-planning module, which is typically featured with hierarchically structured functions, including route-planning at the top level, behavioral-planning at the middle level, and local motion-planning at the bottom level [1]-[2]. The route planner determines a global route utilizing the user-defined destination and road network data; considering the perceived road users and signage, as well as preliminary

information about the traffic rules and vehicle dynamics, the behavioural decision maker decides on a local driving task with a motion specification (e.g., turn-left, lane-change, or cruise-in-lane), which progresses the vehicle along the selected route and abides by the traffic rules; with the estimated vehicle pose and collision-free space, the local motion planner then provides a feasible path/trajectory through the traffic environment to accomplish the motion specification.

Route-planning is a hot research topic, attracting significant attention in the transportation engineering community, and numerous practical algorithms for efficiently planning routes have been proposed and developed [17-19]. In behavioral-planning, appropriate driving behaviour is selected according to the observed behaviours of other traffic participants, road conditions, and signals from infrastructure. To predict the driving behaviours, intentions, and future trajectories of surrounding road users, various techniques have been proposed and studied [20-24]. The local motion planner is responsible for determining a safe, comfortable, and dynamically feasible trajectory from the vehicle's current state to the target state. A local motion-planning takes either the form of a path or a trajectory [1]. Path-planning handles static environments, and the resulting solution does not specify how the path should be tracked and one can select a velocity profile for the path, whereas trajectory-planning deals with a dynamic environment, and the determined solution stipulates how the vehicle dynamics evolve over time. The problem of path-planning has been studied extensively [25-28]. Trajectory-planning in dynamic environments is more challenging than path-planning in static environments [29-32]. However, less attention has been paid to trajectory-planning.

Given the reference path or trajectory determined by the motion-planning module, a tracking-control system chooses and generates appropriate actuator inputs (i.e., steering, throttle, and brake) to implement the planned motion and correct tracking errors for stable driving and desired path/trajectory following [33, 34]. The tracking errors that occurred over the execution of planned motions are attributed to various factors, e.g., modelling errors, external disturbances, operating condition uncertainties, etc. Many efforts have been made to explore the robustness and stability of tracking-control [35-37]. Various tracking-control techniques have been proposed and evaluated for executing the reference motions determined by motion-planning modules [38-40].

2.2 Vehicle aerodynamics

Aerodynamic analysis and design in automotive engineering performed either utilizing CFD simulations or wind tunnel tests [41, 42]. A road vehicle in a wind tunnel test is done by varying wind speed and operating conditions to simulate the different boundary conditions; the static-floor and rolling-road wind tunnel measurements; as a physical simulation of actual on-road driving. CFD is a more cost-effective way than the traditional wind tunnel; it is a mature, accurate and rapid digital progress in computational technology [43-44].

Vehicle aerodynamics plays a more important role in determining vehicle's driving performance when the vehicle runs at high speed, while aerodynamic drag and lift force dominate vehicle dynamics. The governing equations for these two forces as follows [45-47]:

$$Drag = \frac{C_D \rho A V^2}{2} \tag{2.1}$$

$$Lift = \frac{C_L \rho A V^2}{2} \tag{2.2}$$

where C_D and C_L are aerodynamic drag and lift coefficients, respectively, ρ is the air density, A is the frontal area of the spoiler, and V is the vehicle's forward speed. C_D and C_L are dependent on the angle of attack of the spoiler. Drag force has impact on vehicle fuel economy and longitudinal dynamics, while lift force on each tire of the front and rear axle is crucial for vehicle lateral load transfer and high-speed handling [44, 48].

Generic reference models have been applied widely in vehicle aerodynamics as test cases in the validation of computational techniques. The research aimed to investigate flow regimes and aerodynamic force and moment characteristics has been conducted primarily on small-scale versions of the models and then compared the results from the test in wind tunnels using the full-scale models [41]. Researchers are advocating that they choose existing reference geometries and their extended families for experimental and computational research purposes. Those shapes could be seen in three categories: simple bodies, basic car shapes, and production (series) cars [49].

The typical shapes of simple bodies are the Ahmed model and NRCC/SAE model. Ahmed et al. first identified the significance of the backlight angle on aerodynamic characteristics. They presented the simple model known as "the Ahmed Model" (see Figure 2.1) [50].
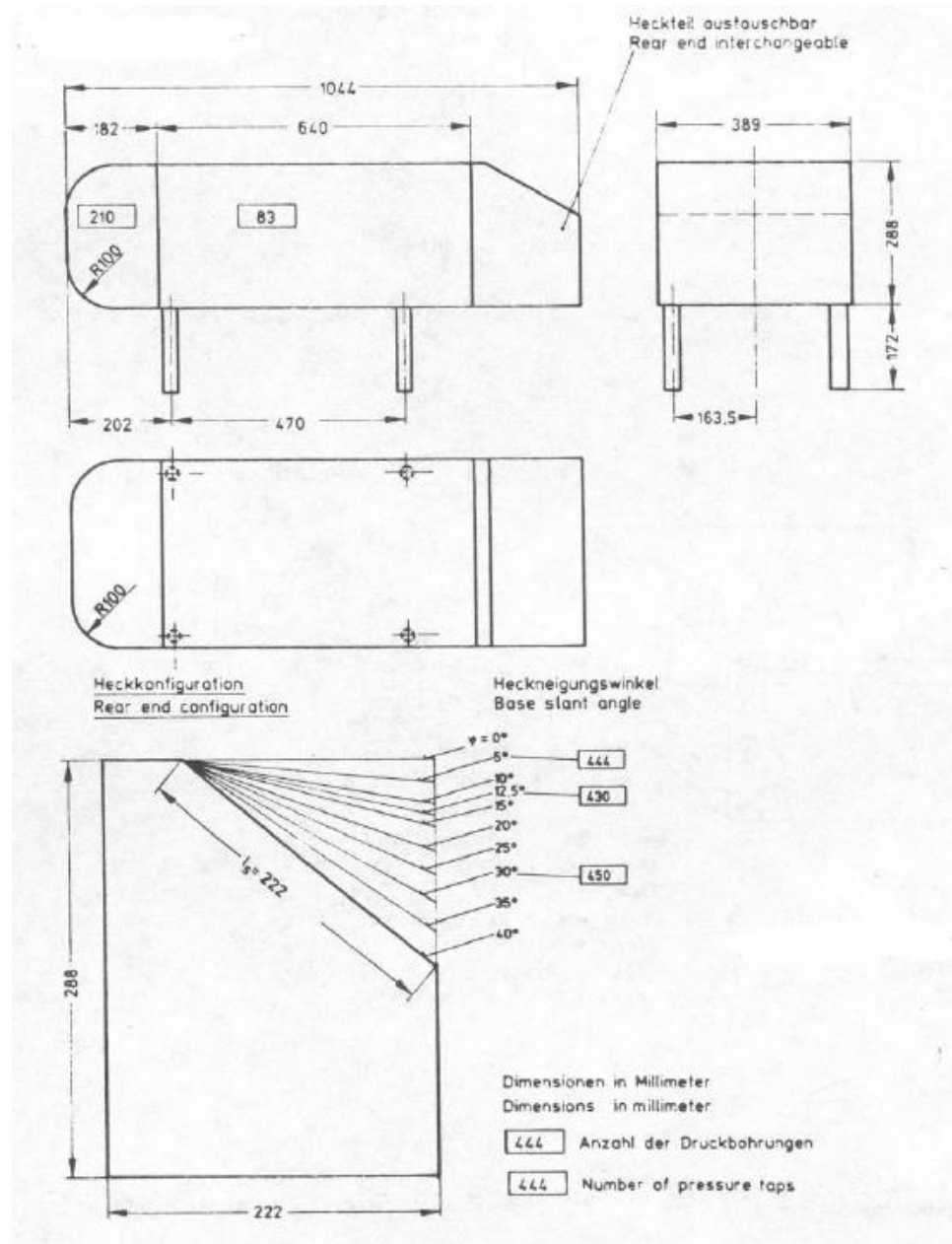
Figure 2.1: Ahmed model [50].

This model can be used to show the effect of backlight angle and the drag contribution of different regions of the model on aerodynamic characteristics and the associated flows. When the backlight angle of the model reaches 30°, i.e., the so-called critical backlight angle, a significant drag peak will appear. Another representative shape is the NRCC/SAE

model (shown in Figure 2.2) [46]. This geometry was developed to approximate the overall dimensions of average North American automobiles, and it has two designs of the forebody and one alternative back-ends. The different combinations will achieve attached or separated flows from the front end and either no significant trailing vortex structure or two strong longitudinal vortices attached to a slanted back of 27° in the back ends. Both models had no wheels and were tested with nominal ground clearance. The use of simple bodies leads much of the fundamental research in automotive aerodynamics and yields invaluable results on the flow characteristics.
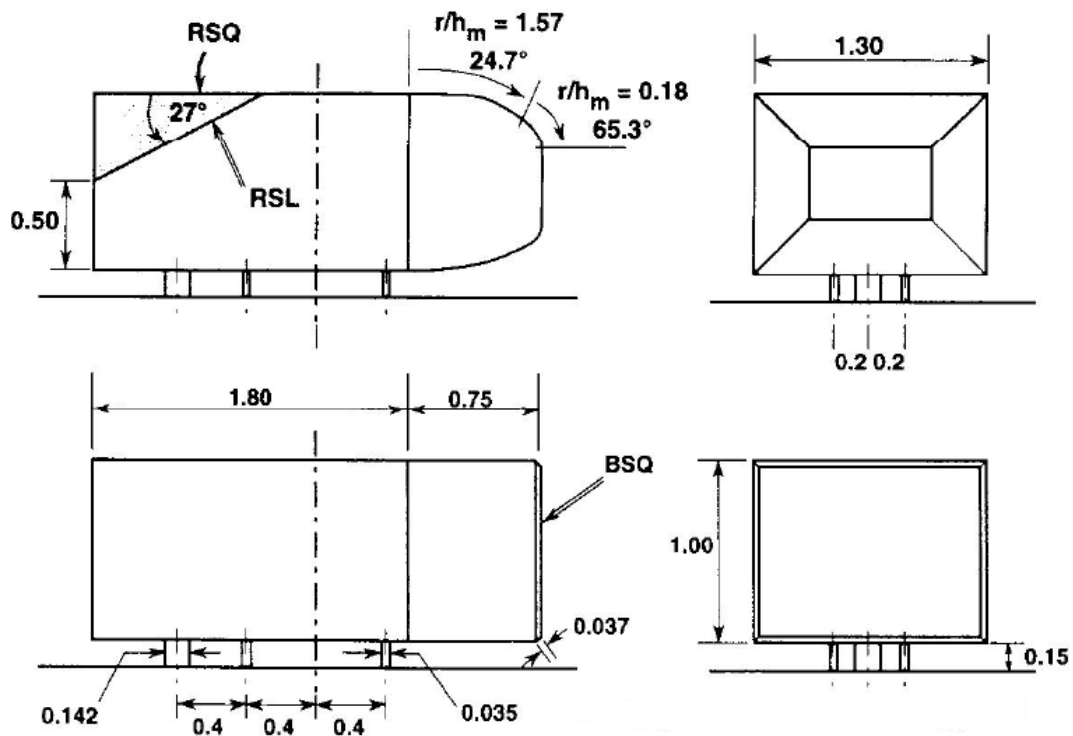
Figure 2.2: NRCC/SAE model [46].

The basic car shape reference model is more recognizable as automotive shapes than the simple bodies model. The MIRA reference car model (shown in Figure 2.3 and Table 2.1)

is the most well-known basic car shape, in which the geometries are from production cars but have simplified surfaces [41]. The back-ends of the MIRA reference car model are interchangeable to form four different automobile geometries, i.e., Notchback, Fastback, Estate-back, and Pick-Up shape. The first three shapes represent the most common passenger car, while the Pick-Up shape is obtained when none of the first three shapes is fitted. The MIRA Reference car model can be used in calibration and correlation tasks, refinement of wind tunnels, investigation of blockage correction techniques, and in evaluation of ground simulation for automotive development [49, 52]. The full-scale MIRA reference car model is being used and updated as part of MIRA's calibration process in their full-scale wind tunnel.
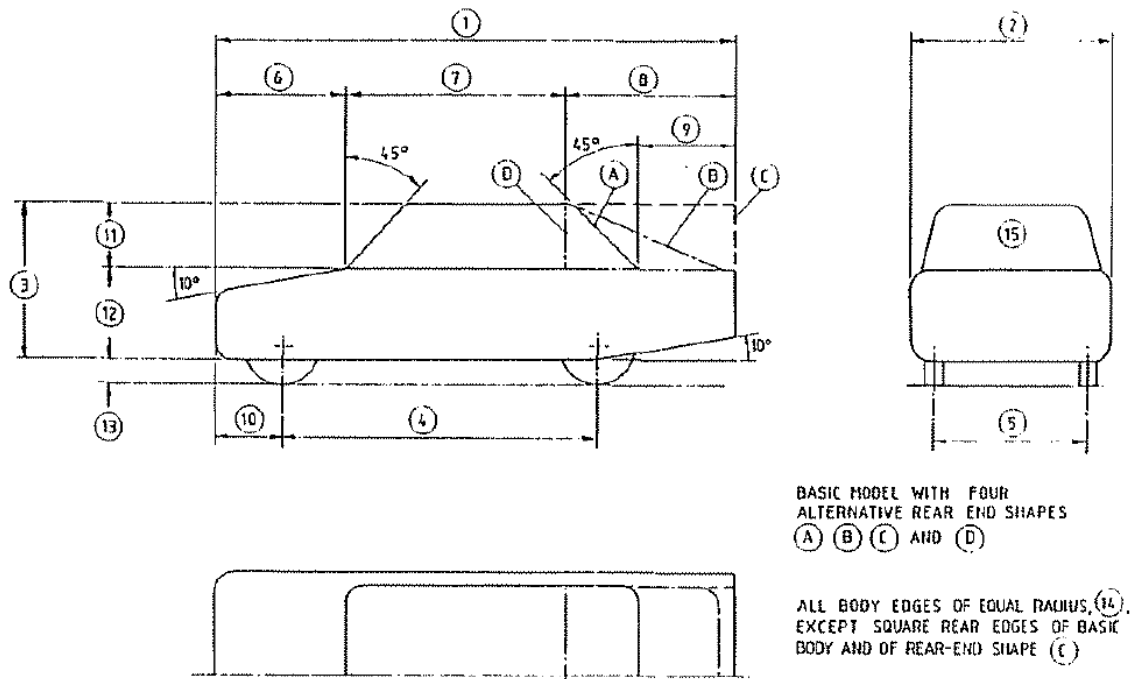
Figure 2.3: MIRA reference car model [52].

Table 2.1: Dimensions of MIRA reference car model [52].

Model Scale	1:5	1:4	1:3	1:1
1. Overall length	833	1041	1389	4165
2. Overall width	325	407	542	1625
3. Overall height	284	356	474	1420
4. Wheelbase	508	635	847	2540
5. Track, front and rear	254	318	423	1270
6. Bonnet length	211	264	351	1055
7. Front canopy length	358	447	597	1790
8. Rear-end length	264	330	440	1320
9. Boot length (notch-back)	150	187	250	750
10. Front overhang	107	134	178	535
11. Canopy height	102	127	169	508
12. Lower body height	142	177	237	708
13. Ground clearance	41	51	68	204
14. Radius of rounded edges	30	38	51	152
15. Frontal area, m^2	0.074	0.116	0.206	1.856

*All dimensions in mm, except stated otherwise

The last type of model is the production (series) cars, which have been used for the purpose of investigation and validation in both small-scale and full-size versions [49]. One example is the BMW validation model, which covers a range of BMW vehicle shapes that resemble actual production vehicles with different front end and rear end designs [44]. This model contained the engine bay and all the underbody details, and was tested in the AWT full-scale wind-tunnel at BMW with moving ground simulation and rotating wheels simulations. There are three different front fascia modules, fourteen different rear back-end modules and closing the front-end cooling openings on some of the configurations as the variations to the model.

Having established the vehicle body types above, the vehicle's aerodynamic characteristics can be investigated and analyzed. Consequently, the influence of wings and other aerodynamic adds-on have attracted much attention in automotive engineering as those

devices have the potential to affect a vehicle's aerodynamics characteristics and safety. Although extra drag force will be produced, the lift/down forces generated by the wings can be viewed as a cheap shortcut to improve the vehicle stability and aerodynamic characteristics without changing the entail vehicle body shapes. Flow around the front-end and rear-end of one vehicle are strongly correlated, and it should be noted that the position of the front wings influences the position of the stagnation point on the car body and the flow conditions around the whole vehicle [53-54]. Finding the optimal position to install the front wing is time-consuming and costly. The rear wing does the same job but without some of the issues listed above. One rear wing configuration – split rear wings – can be used to correct the vehicle yaw moment by manipulating different attacking angles for the left and right rear wings, thereby getting different downforces acting on the left and right rear tires [55]. The split wing is more adaptive and can be used to handle the lateral load transfer during cornering maneuvers.

There are many wing configurations that can be used to perform as a spoiler of a vehicle; one called the NACA-0012 was announced by the National Advisory Committee for Aeronautics (NACA) of the United States and further refined by the United States Air Force at Langley Research Center. NACA-0012 is a symmetrical airfoil with a 12% thickness to chord length ratio and no camber [51]. It is a mature and widely used airfoil, on which a lot of investigations have been conducted, including CFD analysis and numerical studies of its aerodynamic characteristics and applications in wind turbine designs [57-59]. Since it is a symmetric airfoil, the lift/drag forces should be the same if the absolute value of the angle of attack is the same. Figure 2.4 shows the shape of the

NACA-0012 [60]. Figures 2.5 and 2.6 visualize the relationship between the angle of attack and lift/drag coefficients.
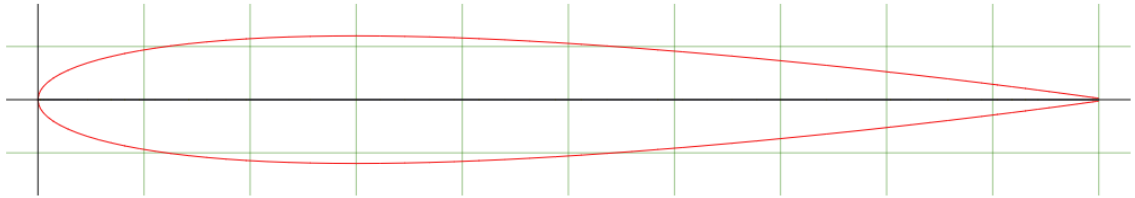
Figure 2.4: NACA-0012 Profile [55].
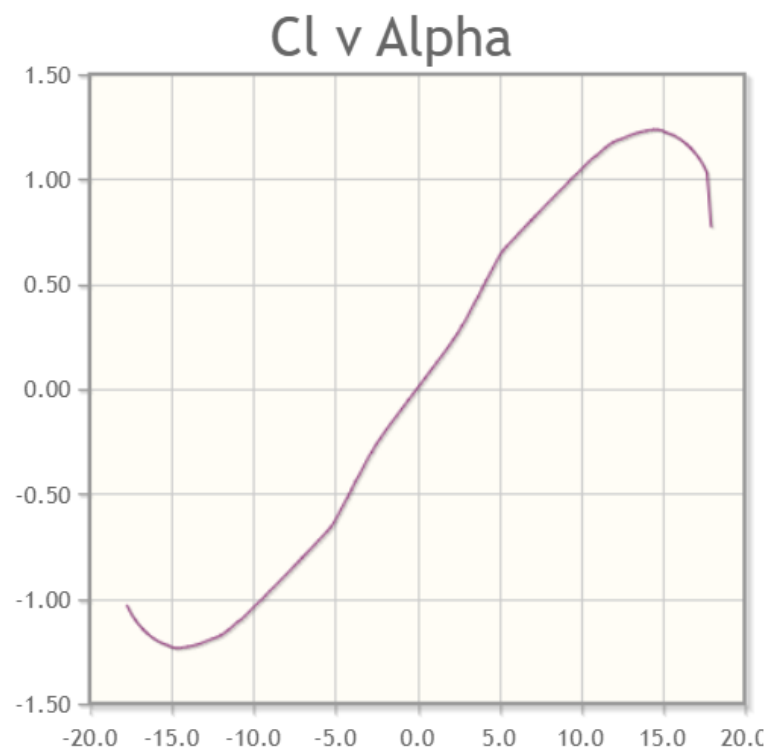
Figure 2.5: Lift coefficient VS angle of attack [55].
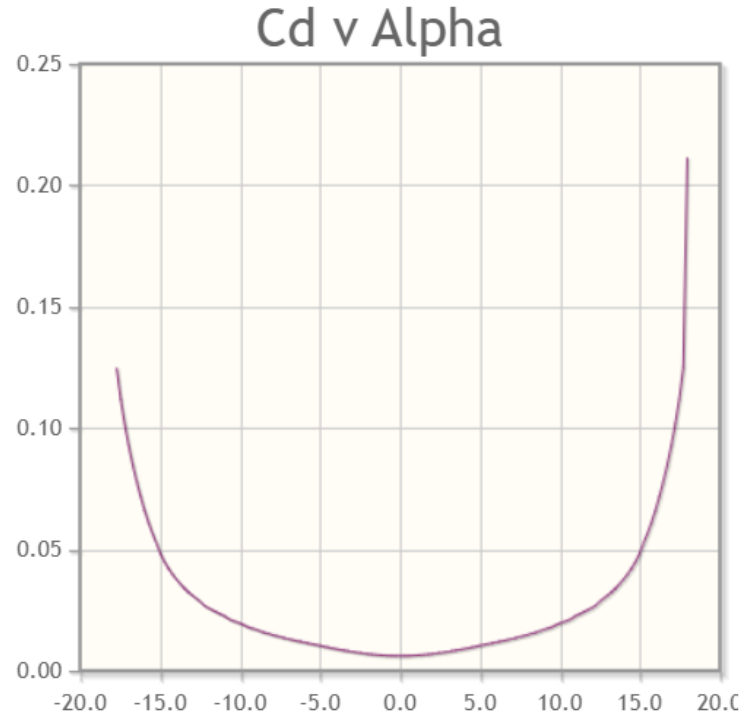
Figure 2.6: Drag coefficient VS angle of attack [55].

2.3 Vehicle system dynamics

There are three important dynamic characteristics of a ground vehicle – its performance, handling, and ride. Performance characteristics describe the ability of the vehicle to accelerate/decelerate, negotiate road grade, and overtake obstacles; handling characteristics describe the ability to stabilize the vehicle itself against external disturbances and reflect the response of the vehicle to the driver's commands; ride characteristics describe how the vibration of the vehicle excited by surface irregularities make efforts on passengers/cargos. The interactions among the driver, vehicle, and environment accomplish the behavior of a ground vehicle [61].
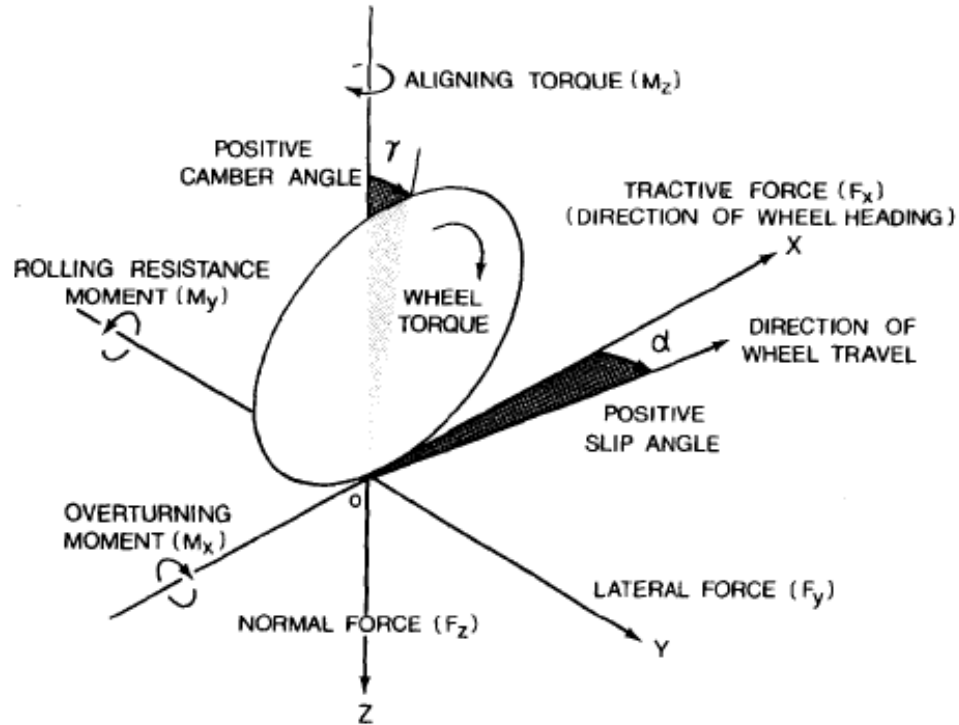
Figure 2.7: Tire axis system [61].

To understand the above characteristics further, it is necessary to have a rough idea of the basic laws of the interaction between the tire and ground. There are three major external forces acting on the vehicle – aerodynamic forces, gravitational forces, and rolling resistance forces. The first two types of forces act on the vehicle body and then affect the tire forces, while the rolling resistance force acts on the tire directly. Figure 2.7 shows the tire axis system; it illustrates the direction of tire forces and moments and how those forces/moments exert on one tire.

The total tractive effort in the longitudinal direction can be expressed by Equation (2.3), where F is the total tractive effort on tires, R_a the aerodynamic resistance force, R_r the total tire rolling resistance force, R_g the grade resistance force, a the linear acceleration in the

longitudinal direction, W the vehicle weight, g the gravity constant, and $\frac{aW}{g}$ denotes the inertial force due to acceleration a.

$$F = R_a + R_r + R_g + \frac{aW}{g} \tag{2.3}$$

The maximum tractive effort that the tire-ground contact patch can provide is described in Equation (2.4), where μ is the coefficient of road adhesion.

$$F_{\max} = \mu W \tag{2.4}$$

The handling characteristics reflect the response of direction of motion changes to driver's steering commands and road disturbances. The handling of a vehicle should embody the control of the direction of motion of the vehicle and should have the ability to stabilize the vehicle against external disturbances. For a typical six degrees of freedom (DOF) rigid vehicle body, it has six motions including longitudinal, lateral, bounce, yaw, roll, and pitch. Longitudinal, lateral, and yaw motion are indispensable in the design and analysis of the handling characteristics. While roll, pitch, and bounce motion are generally considered when exploring vehicle's ride characteristics [61].

Equation (2.5) express the required steering angle δ for a two-axle ground vehicle to negotiate a given curve, where L is the wheelbase, R the curve radius, K_{us} the understeer coefficient, and a_y the lateral acceleration. When $K_{us} > 0$, the vehicle is in understeer; when $K_{us} = 0$, the vehicle is in neutral steer; when $K_{us} < 0$, the vehicle is in oversteer. A neutral steer is an ideal case for the vehicle handling characteristics [62].

$$\delta = \frac{L}{R} + K_{us}\frac{a_y}{g} \tag{2.5}$$

The third important characteristic of vehicle dynamics is ride quality. This characteristic is more about the passenger's sensation or feeling when sitting in a moving vehicle. The main factor that causes uncomfortable to passengers is the vibrations. The common resources that introduce the vibrations include road surface irregularities, aerodynamic forces, vibrations from the engine and transmission unit, and imbalances of the tire assembly. In the case of turning, an excessive lateral acceleration would make the passenger feel uncomfortable as well [61].

A vehicle active control system utilizes the subsequent results from the study of the vehicle's dynamic characteristics. To design an active control system for a vehicle, the first step is to use a proper dynamic model to receive the system input and then feedback on the output of the system so that every required vehicle state and output variables can be presented, calculated, and manipulated. Based on different requirements, two, three, seven, or even fourteen degree of freedom vehicle models are usually used for exploring handling and stability performance. A vehicle dynamic model is generally presented in ordinary differential equations (ODE's) [63].

2.4   Model predictive control

Model predictive control (MPC) is a multi-input and multi-output control method that is efficient to deal with the model uncertainties and system constrains on states and inputs [64]. The original idea came up as early as 1960s but it became popular since later 1970s [65]. An MPC-based tracking-control is usually formulated as a real-time quadratic optimization problem, in which the current action is attained by solving on-line. At each

sampling instant, it uses the current state of the plant as the initial state to solve a finite horizon open-loop optimal control problem. The optimization yields an optimal control sequence and the first control in the sequence is applied to the plant. The essence of MPC is 'prediction', i.e., predicting the future evolution of the system and the future action effects over a finite time window. Based on the prediction, MPC determines the control actions while minimizing predicted errors subject to operating constraints at each sample time [66].

Some implementations of MPC in automotive field are the steering and braking control for the obstacle avoidance and vehicle lateral stability control [67,68]. Another version of MPC, i.e., nonlinear model predictive control (NLMPC), is used to deal with the nonlinearity in model plant [69-71]. NLMPC was developed from MPC, it has all the functions and characteristics of general MPC but with addition of managing nonlinearities in the dynamic system [72]. Recently, further attempts have been made to study the integration of local motion-planning and tracking-control to enhance autonomous driving control for road vehicles. To track the centerline of the road while avoiding obstacles, a two-stage control scheme was proposed [73]: an outer-loop NLMPC technique was used to generate the collision-free trajectory; in the inner-loop was a linear feedback trajectory tracking controller. In [74], an MPC-based controller was proposed, which is featured with simultaneous trajectory planning and tracking-control. The aforementioned studies focused on the integrated autonomous driving control for given vehicle mechanical systems. Like road vehicles with active safety control systems, AVs are mechatronic systems. For vehicular mechatronics, there exist strong interactions between mechanical and control subsystems [75-79].

Many attempts have been made to explore effective techniques for tuning MPC controllers applied in the process industries [80, 81]. The usual tuning parameters of MPC controllers include prediction horizon, control horizon, output weighting, and control input variation weighting [82]; choosing these tuning parameters appropriately is not trivial; reliable guidelines for choosing prediction horizon and control horizon were established, however selecting output weighting and control input weighting is still open for discussions. While the established guidelines may facilitate MPC tuning using the trial-and-error methods, these ad hoc approaches rely upon the uniqueness either of the plant model or MPC formulation, or both. Although, with the established guidelines, the trial-and-error tuning methods may achieve good controllers, the tuning processes are still time-consuming and do not necessarily yield optimal performance. To circumvent these shortcomings, auto- and optimal-tuning methods have been proposed and studied in recent years [83]. In these auto- and optimal-tuning algorithms, a bi-level optimization process was implemented, in which the tuning parameters for MPC controllers were computed automatically at the upper-level using meta-heuristic search algorithms, e.g., particle swarm optimization (PSO) and genetic algorithm (GA), then the resulting parameters were sent to the lower-level MPC problem; the MPC used the tuned weights to calculate optimal control inputs for the plant [84].

2.5 Particle swarm optimization

Particle swarm optimization (PSO) was proposed in 1995 [85]. Since then, this optimization search method has advanced, and its performance has been improved [86]. PSO is a meta-heuristic search technique inspired by the choreography of a bird flock [83].

This technique uses a swarm of volumeless particles, which 'fly' through a multi-dimensional search space to find the global minimum of an objective function. The flying trajectory of each particle is governed by a simple rule, which considers the current particle velocity and explores the histories of the particle and its neighbors [86]. Due to its simplicity, flexibility, and reliability, PSO has been applied successfully to a variety of optimization problems. Moreover, PSO is more suitable for multi-objective optimization problems owning to its higher search efficiency compared to evolutionary computations (ECs), among which Gas, evolutionary programming, and evolutionary strategies are well-known examples [87-89].

There exist similarities and differences between PSO and ECs. Both PSO and ECs are population-based. They operate in a similar way, through which these algorithms update their populations using some types of operators based on the fitness information attained; thus, the individuals of the populations are expected to move towards better solution areas in the respective search spaces [88]. To update individuals in the population, ECs usually use two types of operators, including selection and mutation [89]. With a selection operator, poorly performing individuals are removed, and they are replaced with copies of other population members, namely parents. In ECs, mutation operations take different forms, e.g., crossover [90]. By means of a mutation operator, an EC randomly varies a subset of the individuals in the population. Unlike ECs, the selection operation is not implemented in PSO [88]. Each particle in PSO remains in the population over all population manipulating operations. The updating of individuals in PSO is similar to the use of a crossover operator in ECs. However, the mutation mechanisms used in these techniques

are different. In PSO, every particle, i.e., each individual, is updated in accordance with its own flying experience and the swarm's experience.

2.6   Research gaps identified from the literature review

The study and the results from the above literature review have paved a road for the further development of autonomous vehicle control. Vehicle dynamics is the stable 'subgrade' of the road, which provides the fundamental knowledge to support the MPC application to become the 'pavement' so that any vehicle can run smoothly; PSO is the 'road sign' that leads the system to find the optimal path from all candidate paths, thereby achieving better performance and efficiency; active aerodynamics control is the 'road markings', which helps the high-speed vehicle running safely in its desired position.

The past studies provide direction and inspiration to the current research. Little research effort has been made of developing systematic approaches to tuning MPC controllers for AVs, as well as the active control of aerodynamic devices in high-speed scenarios. By utilizing the NLMPC technique and the PSO algorithm, a bi-level synthesis design method is proposed in this thesis. At the upper layer is the optimizer process that finds the optimal controller weights and/or suitable vehicle parameters; at the lower layer is the virtual vehicle with four independent NACA-0012 spoilers. Those spoilers can be controlled individually and actively, and the generated down/lift forces will be delivered to each tire during the path following operation in the high-speed scenario, therefore, it helps the vehicle reduce the roll motion and improve its safety and comfort performance.

The proposed design method is distinguished from the aforementioned auto- and optimal-tuning approaches (introduced in Section 2.4) due to the following feature: in the former, the interactions between the mechanical vehicle and the MPC controller are considered by coordinating the variations of mechanical vehicle parameters and MPC control parameters in the permitted design space. The effectiveness of the proposed design method is demonstrated by applying it to the design of a road vehicle with autonomous steering control. It should also be noted that no research has been reported on applying active aerodynamic control to improve vehicle safety and passenger's ride quality while designing the synthesis design method for AVs.

Chapter 3

Design synthesis method

3.1 Proposed design synthesis method

Figure 3.1 shows the proposed framework for the design synthesis of road vehicles with autonomous driving control. At the upper layer is an optimizer using PSO or GA algorithm, while at the lower layer is the coupled components of the motion-planner, NLMPC controller, and virtual vehicle. This section introduces the structure and functionality of the proposed design synthesis method, which includes PSO algorithm, vehicle models, and design of the NLMPC controller. This section also outlines the local motion-planning method.
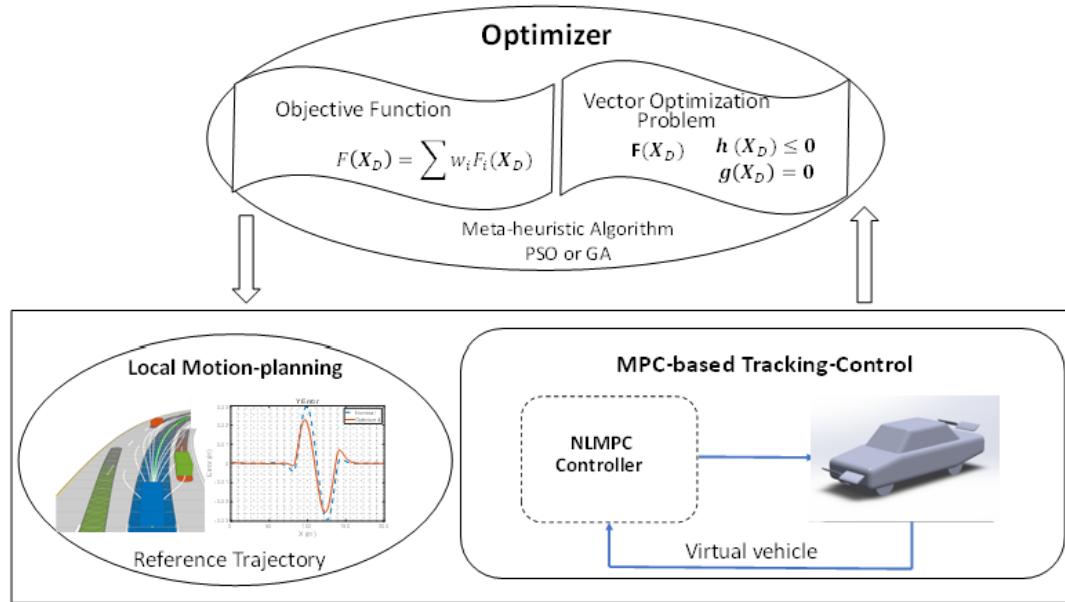
Figure 3.1: Schematic representation of the proposed method for the design synthesis of road vehicles with autonomous driving control.

3.2 Structure of proposed design synthesis method

As shown in Figure 3.1, the proposed method is featured with a framework with two layers: at the lower layer are the dynamically coupled local motion-planning and tracking-control modules; at the upper layer is an optimizer.

Given the constraints and design variable set X_D from the upper layer, the local motion-planning module, and the MPC-based tracking-control module, including the NLMPC controller and the plant (e.g., a vehicle model), are updated. With the data from forward-looking sensors and the higher-level behavioral-planning, the local motion-planning is carried out. The detected path boundaries, which consider various road features and hazard factors, establish constraints on projected vehicle location and orientation. By providing the reference trajectory generated by the motion-planner, the NLMPC controller determines the desired control inputs to drive the virtual vehicle to track the reference trajectory for optimal performance. Via the coupled dynamic analysis between the two modules through closed-loop simulations, the resulting data are sent back to the upper layer. Then, the fitness values and constraints are evaluated at the upper layer. The acquired fitness values, $F(X_D)$, and constraints, $h(X_D) \leq 0$ and $g(X_D) = 0$, are formulated as a vector optimization problem. With a scalarization technique, the vector optimization problem is converted to a scalar one with a utility function taking the form of $\sum w_i F_i(X_D)$, where $w_i, i \in \{1, 2, \dots, n\}$ are weights [77, 91]. The design variable set X_D may include subsets of X_{Dt}, X_{Dm}, and X_{Dv}, which characterize and represent the reference trajectories (X_{Dt}), e.g., the tuning parameters for the parametric trajectories, the MPC controller (X_{Dm}), i.e., the tuning parameters of the controller, and the mechanical vehicle (X_{Dv}), e.g., geometric and inertial parameters of the vehicle, respectively. The formulation of the utility

function is to be discussed in Section 3.4.

As introduced in literature review, the MPC-based tracking-control itself is an optimization problem. Thus, the design synthesis shown in Figure 3.1 is a bi-layer optimization problem. Using a bi-layer optimization technique for the design of mechatronic vehicles usually leads to a complex non-convex optimization problem, where a variation of the initial conditions may result in different design solutions [92]. Nevertheless, such a situation can be attenuated by using meta-heuristic search algorithms, e.g., GA and PSO, which have been preferred over gradient-based techniques. In this research, a PSO algorithm is used for solving the upper layer optimization problem shown in Figure 3.1.

3.3 Optimizer at upper layer – PSO

A PSO algorithm is used for solving the upper layer optimization problem shown in Figure 3.1. Given a D-dimensional search space, the i-th particle in the swarm is denoted by $\boldsymbol{Z}_{D,i} = (z_{i1}, \ z_{i2}, \ \cdots, z_{iD})$; the velocity of the particle is represented by $\boldsymbol{V}_i = (v_{i1}, v_{i2}, \cdots, v_{iD})$; $\boldsymbol{P}_i = (p_{i1}, p_{i2}, \cdots, p_{iD})$ is the position in the search space visited so far by this individual, which provides the best fitness value, i.e., the minimum fitness value, and this position is called the personal best for the individual; $\boldsymbol{P}_g = (p_{gi}, p_{g2}, \cdots, p_{gD})$ is the position in the search space visited so far by the g-th particle, which gives the minimum fitness value among all the particles in the population, and this position of the g-th particle is called the global best for all the individuals of the population. In the PSO algorithm, the particles are updated using the following equations:

$$v_{id}(k+1) = w \cdot v_{id}(k) + c_1 \cdot r_{i,1} \cdot [p_{id} - z_{id}(k)] + c_2 \cdot r_{i,2} \cdot [p_{gd} - z_{id}(k)],$$

$$d \in \{1,2,\dots,D\} \tag{3.1}$$

$$z_{id}(k+1) = z_{id}(k) + v_{id}(k+1) \tag{3.2}$$

where k+1 is the total number of updating the particle swarm so far, i.e., the generation number, w the inertia weight, c_1 and c_2 denote two positive constants, and $r_{i,j} \in [0,1], j \in \{1,2\}$, are random and independent sequences employed to enhance the stochastic nature of the PSO algorithm. As shown in Equation (3.1), the velocity v_{id} is updated towards p_{id} and p_{gd}, weighted by constants c_1 and c_2, with randomness induced by $r_{i,1}$ and $r_{i,2}$, respectively [86]; the inertia weight, w, poses its impact on a local or global search of the PSO algorithm: a large inertia weight is in favor of a global search, while a small inertia weight facilitates a local search [88]. The pseudo code is shown in Figure 3.2, it provides the basic logic to operate the PSO algorithm.
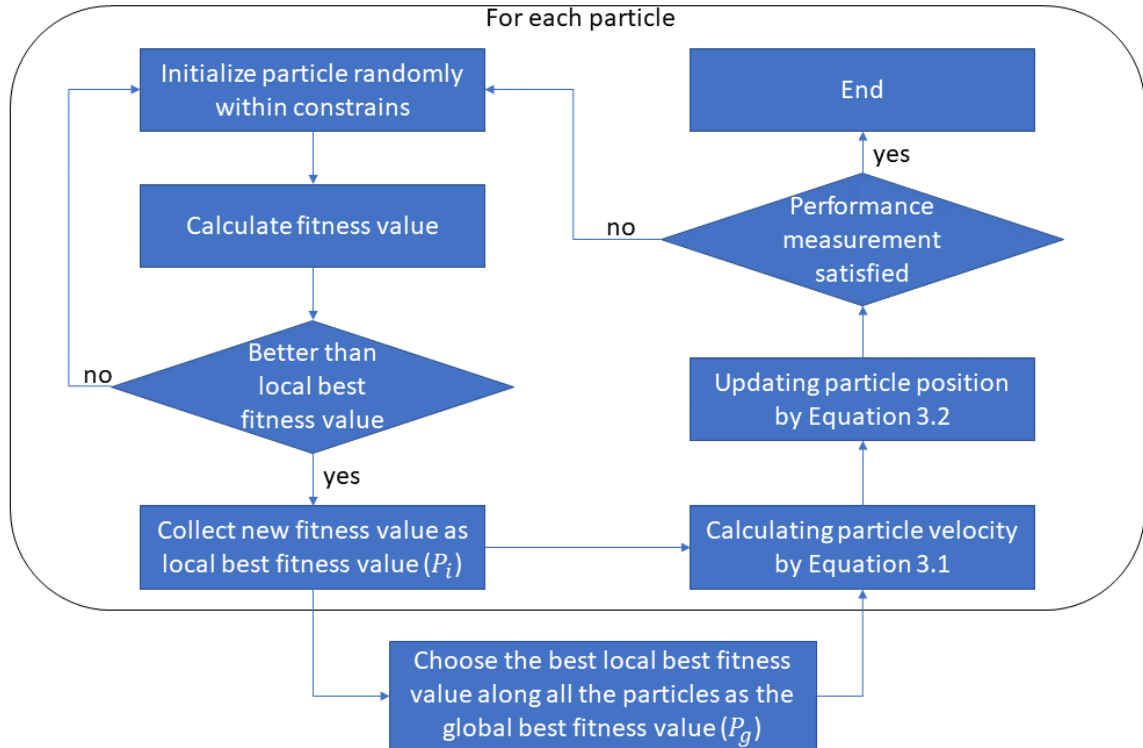
Figure 3.2: PSO flow chart.

3.4   Vehicle models

In the NLMPC based tracking-controller design, two applications and three cases are considered. In the first application, the tracking-controller will be applied to an autonomous vehicle without active aerodynamic control functionality; the vehicle performance will be evaluated in two cases, that is, an evasive maneuver at two forward speeds, 60 and 100 km/h. In the second application, the tracking-controller will be applied to a high-speed vehicle with active aerodynamic control functionality; the vehicle performance will be evaluated in one case, that is, an obstacle avoidance at a high speed, 180 km/h. Considering the two applications, two predictive vehicle models are generated: 1) a 2 degrees of freedom (DOF) nonlinear yaw-plane single track model for the first application; 2) a 2-DOF nonlinear yaw-plane double track model for the second application. Accordingly, two 3-dimensional (3-D) vehicle models generated using CarSim software [93]. In the NLMPC controller design, the first CarSim model (without active aerodynamic control functionality) is used as the virtual vehicle plant for the first application, while the second CarSim model (with active aerodynamic control functionality) is utilized as the virtual vehicle plant for the second application. In the following subsections, these vehicle models are introduced.

3.4.1 2-DOF nonlinear yaw-plane single-track vehicle model

Figure 3.3 shows the single-track (bicycle) model to simulate the lateral dynamics of the vehicle. As seen in the figure, the vehicle system is telescoped laterally and each axle set is represented by one wheel. Two coordinate systems are introduced, which are the inertial

coordinate system, $X - O - Y$, and the vehicle body fixed coordinate system, $x - o - y$. For the latter, the origin, o, is located at the center of gravity (CG) of the vehicle, and the coordinate system moves with the vehicle. The notation of the vehicle model is given in Figure 3.3.

Figure 3.3: 2-DOF nonlinear yaw-plane single-track vehicle model.

The vehicle modelling is based on the following assumptions: 1) the vehicle forward speed v_x remains constant; 2) given the constant forward speed, the longitudinal forces on the tires and the aerodynamic drag on the vehicle are neglected; 3) the vehicle mass is lumped at the CG with a mass moment of inertia about the vertical axis, z; 4) the vertical, roll and pitch motions are neglected; 5) road bank angle is ignored. In the modelling, the motions considered are vehicle lateral velocity and yaw-rate, i.e., v_y and $\dot{\varphi}$. Based on Newton's law of dynamics, the equation of motions of the vehicle are expressed as

$$m(\dot{v}_y + v_x\dot{\varphi}) = F_{cf}\cos\delta + F_{cr} \qquad (3.3)$$

$$I\ddot{\varphi} = l_f F_{cf}\cos\delta - l_r F_{cr} \qquad (3.4)$$

where m and I are the vehicle mass and moment of inertia about z axis, respectively, F_{cf} and F_{cr} the cornering force of the front and rear tire, accordingly, l_f and l_r the respective distance from the CG to the front and rear axle, and δ is the front wheel steer angle. Note that as shown in Figure 3.3, v_f and v_r denote the velocity at the center of the contact area of the front and rear wheel with the road, respectively. Using the 'Magic Formula' tire model by Pacejka [89], the tire cornering forces are determined by

$$F_{ci} = f_{ci}(\alpha_i, \mu, F_{zi}), \quad i \in \{f, r\} \tag{3.5}$$

where $i \in \{f, r\}$ denotes the front or rear tire, α_i the front or rear tire slip angle, μ the friction coefficient between tire and the road, and F_{zi} the vertical load on front or rear wheel. As shown in Figure 3.3, the tire slip angles are given by

$$\begin{cases} \alpha_f = \delta - \dfrac{l_f \dot{\varphi} + v_y}{v_x} \\ \alpha_r = \dfrac{l_r \dot{\varphi} - v_y}{v_x} \end{cases} \tag{3.6}$$

The vertical load on the front and rear wheel are determined by

$$\begin{cases} F_{zf} = \dfrac{mgl_r}{l_f + l_r} \\ F_{zr} = \dfrac{mgl_f}{l_f + l_r} \end{cases} \tag{3.7}$$

Under an operating condition, with a given steer angle input δ and at a constant forward speed, Equation (3.3) to Equation (3.7) determine the lateral dynamic responses of the vehicle.

Without loss of generality, the vehicle tracks a target path as shown in Figure 3.4. At an arbitrary instant, it is assumed that point S is the closest point on the target path to the vehicle CG, which is located on the normal axis of the target path coordinate system at

point S. The orientation of the tangent line of the target path at point S is determined by angle φ_{ref}, which is measured in the inertial coordinate system. The orientation of the vehicle is specified by its heading angle φ. As seen in Figure 3.4, at the given instant, the position and orientation of the vehicle with respect to the target path can be determined by

$$e_1 = \varphi - \varphi_{ref} \tag{3.8}$$

$$\dot{e}_2 = v_y \cos(e_1) + v_x \sin(e_1) \tag{3.9}$$

where e_1 denotes the vehicle yaw angle error with respect to the target path, and e_2 the vehicle lateral path deviation.

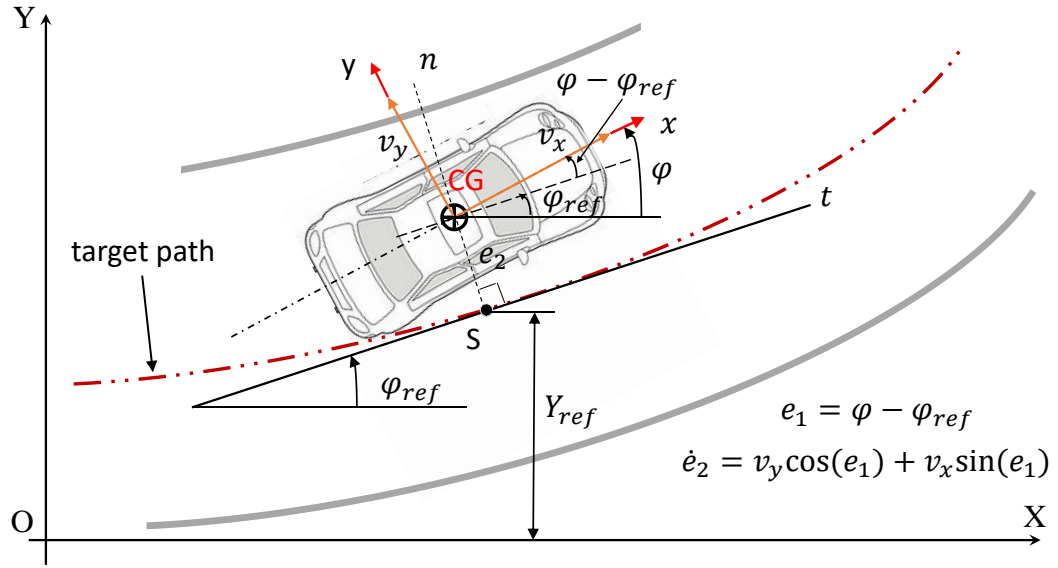Figure 3.4: Definition of the lateral path deviation and yaw angle error of the vehicle with respect to a target path.

In the inertial coordinate system, the velocities at the vehicle CG are corelated with the heading angle and the velocities measured in the vehicle body fixed coordinate system by

$$\begin{cases} \dot{X} = v_x \cos\varphi - v_y \sin\varphi \\ \dot{Y} = v_x \sin\varphi + v_y \cos\varphi \end{cases} \tag{3.10}$$

The nonlinear vehicle dynamics expressed in Equation (3.3) to Equation (3.10) can be cast in the compact form as follows

$$\dot{x}(t) = f\big(x(t), u(t)\big) \tag{3.11}$$

where the state and input vectors are defined as $x(t) = \begin{bmatrix} v_y & \dot{\varphi} & \varphi & e_1 & e_2 & X & Y \end{bmatrix}^T$ and $u(t) = \delta(t)$.

The results based on simulated obstacle avoidance maneuvers, e.g., single lane-change scenarios, indicate that single-track yaw-plane vehicle models are effective for controller designs for various active safety systems of road vehicles [64, 95]. In this research, for urban application at speed of 60 km/h and highway application at speed of 100km/h, the derived 2-DOF nonlinear yaw-plane vehicle model is used for designing the NLMPC controller for automated steering and the design synthesis shown in Figure 3.1.

3.4.2 2-DOF nonlinear yaw-plane double-track vehicle model

In the NLMPC tracking-controller design, we also consider its application to high-speed vehicles operating at high speed, e.g., 180 km/h. In this case, active aerodynamic control functionality is introduced. With the active aerodynamic control functionality, above each of the wheels allocated at four corners of the vehicle is installed a spoiler to manipulate lift/down force of each wheel for improving the safety of the vehicle. To this end, a 2-DOF nonlinear yaw-plane double-track vehicle model is generated as the prediction model for the NLMPC controller design. Figure 3.5 shows the double-track vehicle model, with which the effect of aerodynamic associated lift/down force on each of the four tires can be considered. With the same assumptions previously made for the single-track vehicle model,

the double-track vehicle model shares the same governing equations of motion with the single-track vehicle model. Thus, governing equations of motion for the single-track vehicle model are still applicable for the high-speed vehicle application at the high speed of 180 km/h. As shown in Figure 3.5, F_{cf_1} and F_{cf_2} denote to the left and right front tire cornering force, respectively, F_{cr_1} and F_{cr_2} represent the left and right rear tire cornering force, accordingly, and w_t is the track width of the vehicle.
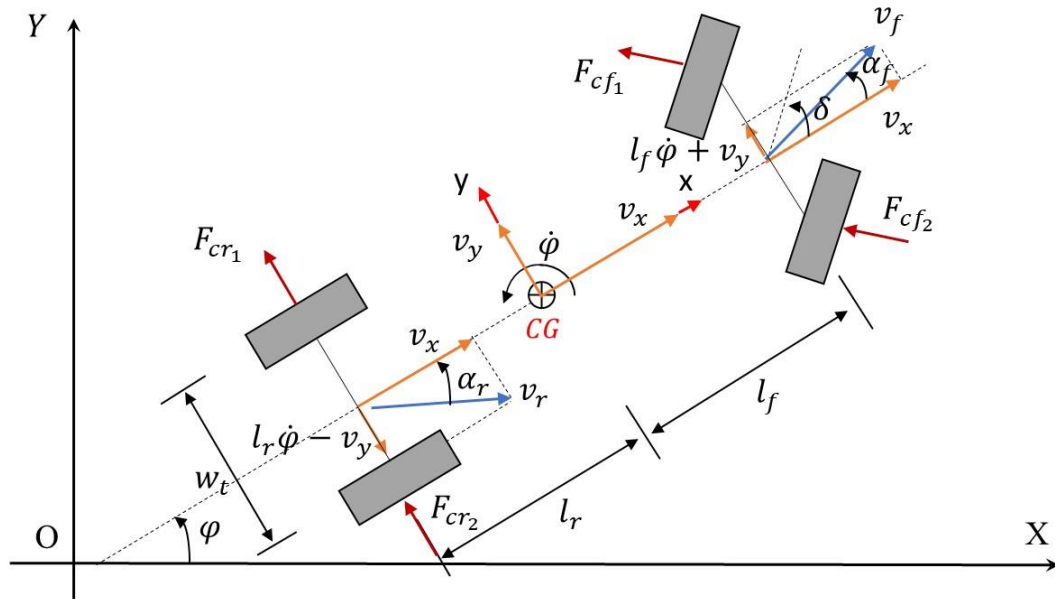
Figure 3.5: 2-DOF nonlinear yaw-plane double-track vehicle model.

3.4.3 CarSim model without active aerodynamic control

The 3-D CarSim model consists of a rigid vehicle body, two suspensions, and four wheels. The motions considered include the longitudinal, lateral, vertical, roll, pitch, and yaw motion of the body, as well as the vertical and spinning motions of each wheel. The nonlinear features of vehicle components, e.g., suspensions and pneumatic tires, are

mimicked in the model.

In the CarSim software, a symbolic multibody program, called VehicleSim (VS) Lisp, is used to derive equations of motion for vehicle systems [93]. VS Lisp takes an input as the description of the 3-D vehicle model configuration mostly in geometric terms, such as the body DOF, point locations and the directions of force vectors. With the input information, VS Lisp generates equations of motion in terms of ordinary differential equations and produces a source code (C or Fortran) to solve them.

The CarSim software involves three key components: VS browser, CarSim databases, and VS solver. The VS browser is a graphical user interface. The CarSim databases are used to choose vehicle configuration templates, e.g., dependent or independent suspension, and to define the system parameters, the tire-road interactions, the test maneuvers, etc. The VS solver is used to solve the derived governing equations of motion and to execute the defined simulations. The VS browser can also be applied to other applications, e.g., incorporating the NLMPC controller to be designed in Matlab/Simulink in the 3-D vehicle model via an interface for co-simulation.

In this study, the parameter values of the 3-D CarSim model are provided in the Appendix.

3.4.4 CarSim model with active aerodynamic control

Built upon the above CarSim model, the 3-D vehicle model is developed with active aerodynamic functionality. As shown in Figure 3.6, at each corner of the vehicle is installed an independent NACA-0012 spoiler. Each NACA-0012 spoiler has a symmetrical shape, which is assumed to provide the same drag and lift/down force if the absolute value of the angle of attack is the same. Figure 2.5 shows the asymmetrical trends between the lift

coefficient and the angle of attack; Figure 2.6 visualizes the symmetrical trends between the drag coefficient and the angle of attack. Based on those features, NACA-0012 is chosen to significantly reduce the computation time by half when acquiring the aerodynamic results in the CFD simulations. Technically, the spoiler in the design method can be replaced by any type of airfoil as long as the aerodynamic results are provided.

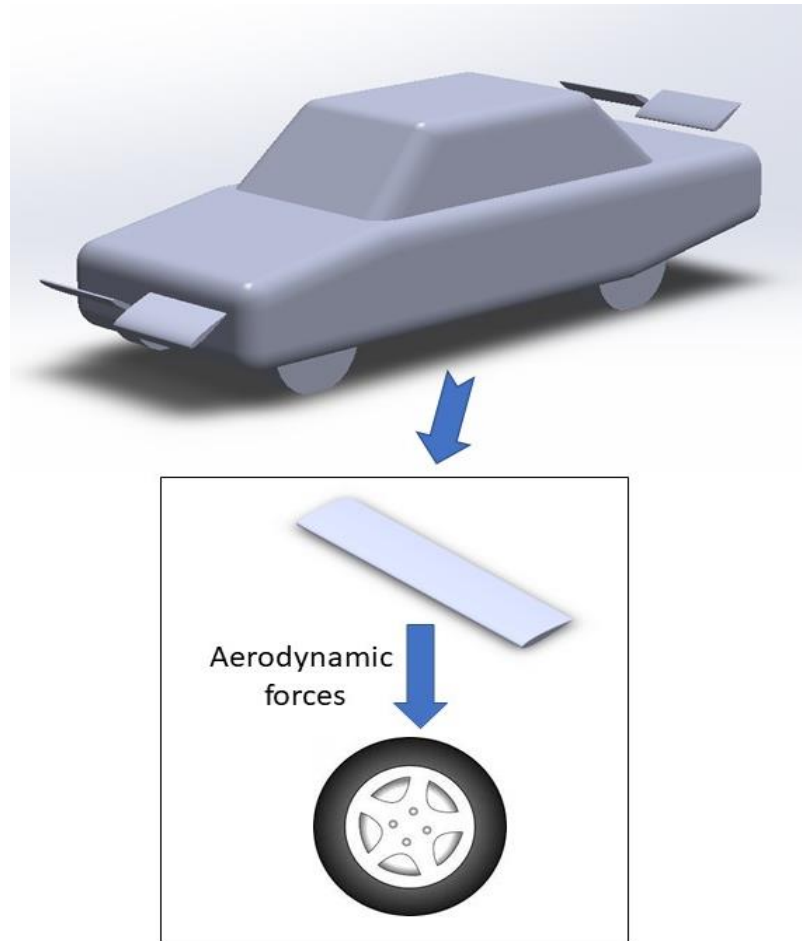Figure 3.6: Vehicle installed with four NACA-0012 spoilers.

It should be noted that one of the objectives of this research is to design an active aerodynamic control system utilizing spoilers to produce the required lift/down forces to increase the safety of the vehicle, thereby ignoring the spoilers' effects on the other aspects of aerodynamic behaviors, e.g., aerodynamic drag. Considering the fact that the spoilers

have much less impacts on the dynamic behaviors at low speed [55], these spoilers only operate while the vehicle travels at high speed, e.g., 180 km/h. In this research, the spoiler model is generated, and the CFD setup is established [96].

3.4.4.1 Spoiler modelling

The dimensions of each single NACA-0012 are listed in Table 3.1. The 3-D spoiler was modelled using SolidWorks. Figure 3.7 shows the various view of the CAD model.

Table 3.1: Dimensions of NACA-0012 spoiler.

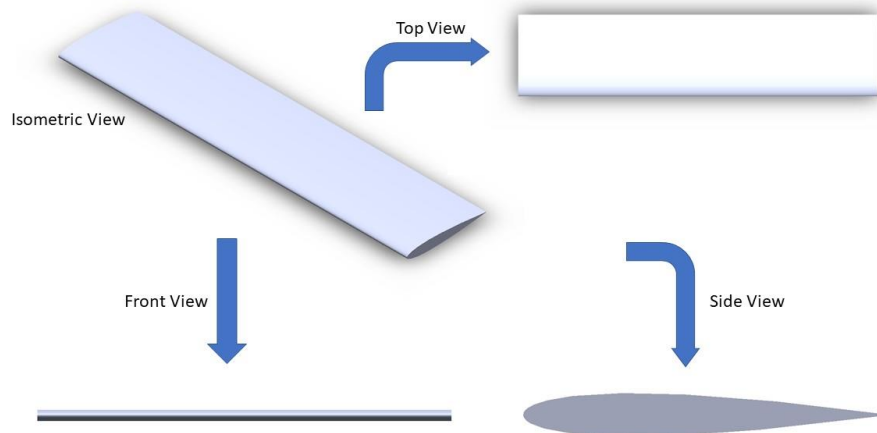| NACA-0012 Dimensions		
Length	Chord length	Thickness
660 mm	300 mm	36 mm

Figure 3.7: Various views of NACA-0012 spoiler.

The assembled CAD model is shown in Figure 3.6. The aerodynamic lift/down forces generated by each spoiler will be only acting on the corresponding tire. Each spoiler can only rotate individually around a lateral axis in the clockwise or counter-clockwise directions.

The spoiler CAD model is exported to Ansys/Fluent software to perform the CFD simulations. The computational domain (as shown in Figure 3.8) is created as a 3000 mm × 800 mm × 1000 mm rectangular box and all the side and top boundaries are set as no shear stress stationary wall. As shown in Figure 3.8, the left green face is the flow inlet and the right green face is the flow outlet. Uniform distributed flow will go through the inlet perpendicularly. For the purpose of accuracy, a cylinder is placed around the spoiler so that element size in meshing process can be refined within that region. The region occupied by the cylinder is called the refined volume mesh region.
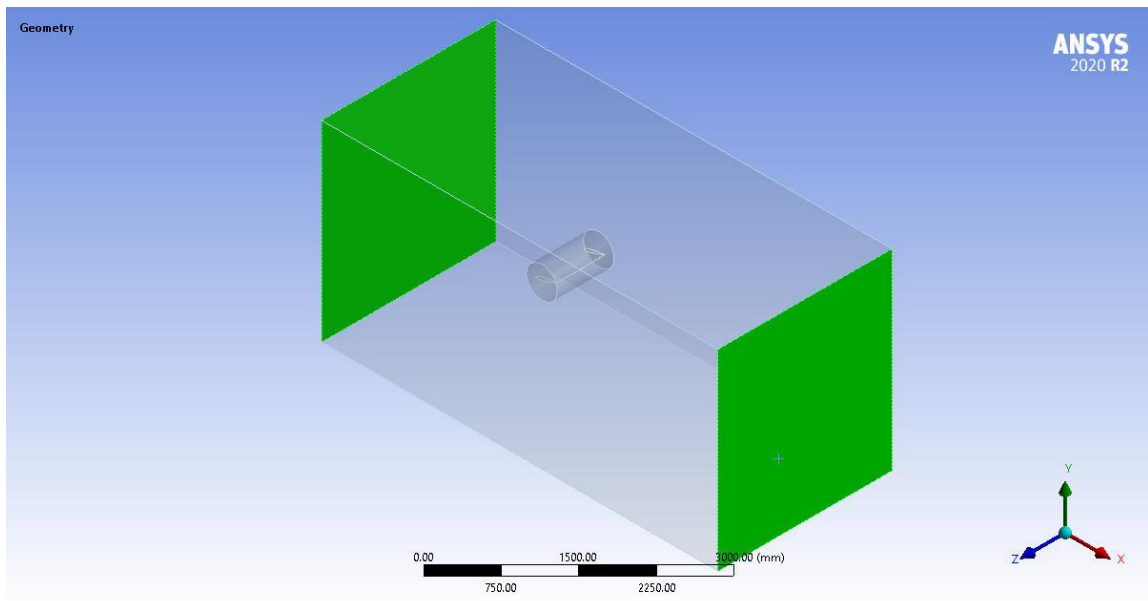
Figure 3.8: Computation domain of NACA-0012.

3.4.4.2 Meshing

For a vehicle spoiler, the pressure is dominant over the skin friction thus the accuracy of the predicted static pressure distribution on the body decides the accuracy of the aerodynamic force calculations. Also, the locations of the flow separation and reattachment is the key affection of the pressure distribution. Therefore, the surface mesh should contain all the relevant details of the geometry [96].
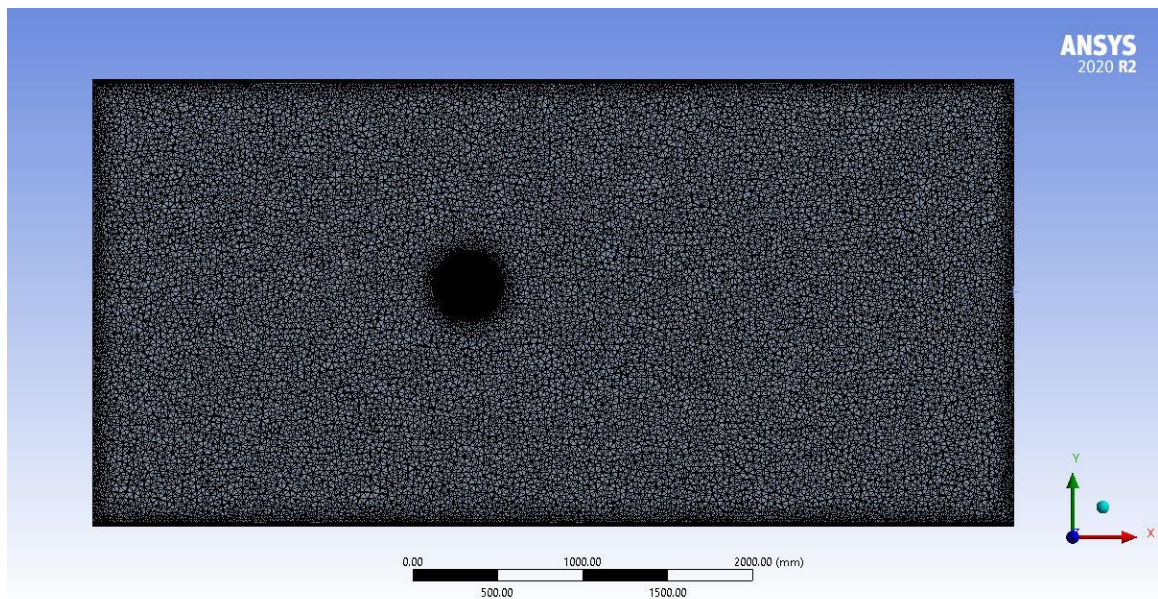
Figure 3.9: Mesh view inside the computation domain.

There are 14130091 elements created in the meshing process. Figure 3.9 shows the inside mesh from the view of cutting the model in half from its flow inlet. The volume outside the cylinder, it has an element size of 20 mm, while the element size is 8 mm inside the cylinder (as shown in Figure 3.10).
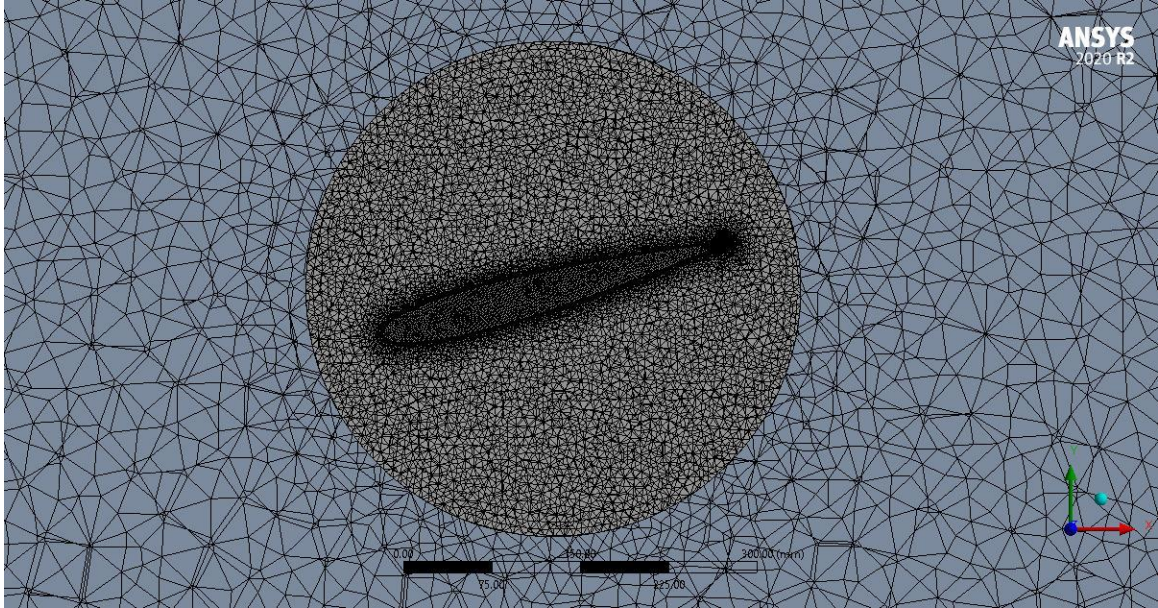
Figure 3.10: Mesh inside refined volume mesh region.

As shown in Figure 3.11, the face of the spoiler was meshed with element size of 2 mm and it equipped with the inflation layers to smooth the transition from smaller elements to larger elements. The overall mesh growth rate is 1.2 and it has the capability to capture the curvature and proximity of the geometry.

Figure 3.11: Mesh of the surface of NACA-0012.

3.4.4.3 CFD results

The calculation model used in this CFD simulation is called the k-omega shear stress transport (SST). This is a hybrid model from the two equation Eddy Viscosity Models, which combined both k-omega and k-epsilon, i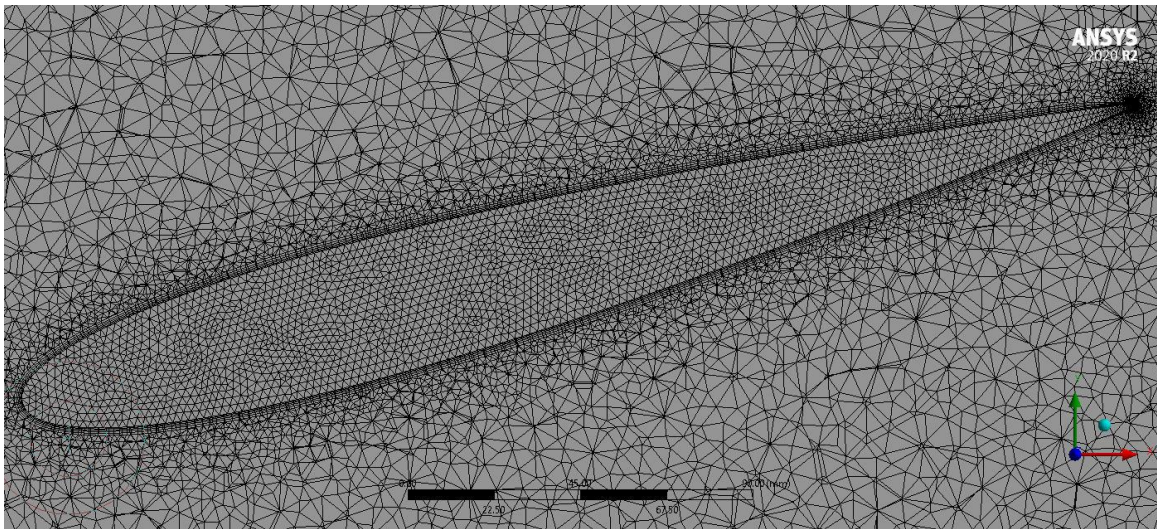t can activate k-omega near the wall and k-epsilon in the free stream. The model sits in a constant pressure of one atmosphere environment, details of the rest of the setups are showing in the following Table 3.2.

Table 3.2: CFD setup.

Solver	Pressure based – Steady time	
Model	K – omega SST	
Initial Velocity	50 m/s (180 km/h)	
Method	Scheme	Coupled
	Gradient	Least squares cell based
	Pressure	Second order
	Moment	Second order upwind
	Turbulent Kinetic Energy	First 100 runs – First order upwind Rest 200 runs – Second order upwind
	Turbulent Dissipation Rate	First 100 runs – First order upwind Rest 200 runs – Second order upwind

There are 12 simulations for different angle of attack in this study, and each simulation has 300 runs. Their results are based on the velocity of 180 km/h and they are listed in Table 3.3. As one characteristic of aerodynamics, different travelling speed will have different

results. Thus, 180 km/h was chosen only for design testing convenience. As mentioned previously, the objective is not to pursue the spoiler's aerodynamic behavior or its effects on the flow around the vehicle body; therefore, only lift and drag forces were collected in the table below.

Table 3.3: Aerodynamic results of one single NACA-0012.

Angle of Attack (°)	Lift Force (N)	Drag Force (N)
0	0.0017	7.9257
5	144.6378	13.6007
10	294.0678	31.4225
13	381.9419	48.4634
15	455.0574	61.1899
17	411.9820	101.1271
20	325.9045	124.6727
25	351.4644	177.5363
30	369.1325	228.6332
35	377.4673	278.8235
40	381.4918	332.1318
45	381.0785	385.8338

It is observed that the lift force increases as the angle of attack (AOA) varies from 0° to 15°, then the lift force starts to drop until the AOA increased to 20°. Although the lift force increases again after 20°, at which the drag force is approximately twice larger than the drag force as AOA equals 15°. To attenuate the effects of the drag force, it was decided

that the spoiler is constrained and operates within the ranges of 0° to 15° in the clockwise direction and 0° to 15° in the counter-clockwise direction. Within the constrained operation ranges, the lift force may vary from zero to the maximum value, while the drag force remains a small value. By choosing the lift force results from 0° to 17°, the lift/down force fitting function can be determined as follow:

$$\boldsymbol{Liftforce = p1 \cdot X^8 + p2 \cdot X^7 + p3 \cdot X^6 + p4 \cdot X^5 + p5 \cdot X^4 + p6 \cdot X^3 + p7 \cdot X^2 + p8 \cdot X + p9;}$$

(3.19)

Where $p1 = -1e - 21; p2 = -2.36e - 06; p3 = 3.683e - 19;$
$p4 = 0.0009377; p5 = -1.618e - 17; p6 = -0.09872;$
$p7 = -3.744e - 15; p8 = 31.5; p9 = 9.398e - 14;$

Based on the lift/down force fitting function, a curve can be plotted as shown in Figure 3.12. The curve follows the trends in Figure 2.5 which validate the CFD results that can be used in a Matlab function to calculate the lift/down forces for the active control of the spoiler.
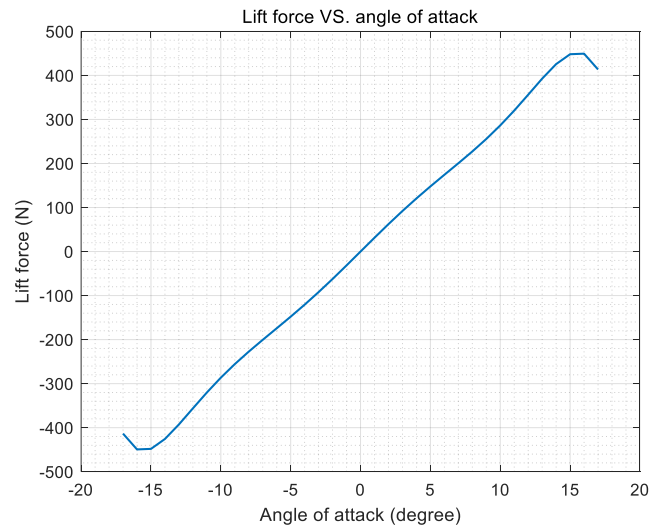

Figure 3.12: Lift force VS. angle of attack (clockwise is the positive direction).

3.5 Nonlinear model predictive control

The NLMPC controller consists of two core elements: the discretized vehicle model represented by Equations (3.13) to (3.15), and an optimizer with a cost function and a batch of constraints. Note that Equation (3,13) is the discretized version of Equation (3.11). The discretized model is used to derive a prediction of future output vehicle dynamic behavior. With the prediction, optimization is conducted to find a sequence of control input moves, which minimizes the selected measures of the output deviation from their respective reference trajectories, while satisfying all the given constraints. To improve the quality of prediction, adequate measurements are collected; however, only the first of the calculated control input sequences is implemented. The optimization is repeated at the next sampling time. This 'receding horizon implementation' makes the MPC algorithm a feedback controller.

To design the NLMPC controller, we need to discretize the nonlinear vehicle model described in Equation (3,11). At sampling step k, discretizing the nonlinear vehicle model with the forward Euler method leads to

$$x(k + 1) = f\big(x(k), u(k)\big) \tag{3.13}$$

$$u(k) = u(k - 1) + \Delta u(k) \tag{3.14}$$

where $x(k) = \left[v_y(k)\ \dot{\varphi}(k)\ \varphi(k)\ e_1(k)\ e_2(k)\ X(k)\ Y(k)\right]^T$, $u(k) = \delta(k)$, $\Delta u(k) = \Delta \delta(k)$, and $y(k)$ denotes the output variable vector determined by

$$y(k) = Cx(k) = \begin{bmatrix} 0 & 0 & 1 & 0 & 0 & 0 & 0 \\ 0 & 0 & 0 & 0 & 0 & 0 & 1 \end{bmatrix} x(k) \tag{3.15}$$

It is assumed that the reference trajectory is defined as

$$r(k) = [\varphi_{ref}(k)\ Y_{ref}(k)]^T \tag{3.16}$$

Considering the control input, output variable vector, and the desired outputs specified by Equation (3.14), (3.15), and (3.16), respectively, we formulate the NLMPC controller design as an optimization problem with the following cost function subject to the specified constraints:

$$\min_{\Delta u(k|k),\cdots,\Delta u(k+H_c-1|k)} J\big(x(k), \Delta u(k)\big) =$$

$$\sum_{i=1}^{H_p} \|y(k+i|k) - r(k+i|k)\|_Q^2 + \sum_{i=0}^{H_c-1} \|\Delta u(k+i|k)\|_R^2 \tag{3.17a}$$

subject to:

$$x(k+1+i|k) = f\big(x(k+i|k), u(k+i|k)\big), i \in \{0,\cdots,H_p-1\} \tag{3.17b}$$

$$u(k+i|k) = u(k-1+i|k) + \Delta u(k+i|k), i \in \{0,\cdots,H_p-1\} \tag{3.17c}$$

$$y(k+i|k) = Cx(k+i|k), i \in \{1,\cdots,H_p\} \tag{3.17d}$$

$$\delta_{min} \le u(k+i|k) \le \delta_{max}, i \in \{0,\cdots,H_c-1\} \tag{3.17e}$$

$$\Delta\delta_{min} \le \Delta u(k+i|k) \le \Delta\delta_{max}, i \in \{0,\cdots,H_c-1\} \tag{3.17f}$$

$$\Delta u(k+i|k) = 0, i \in \{H_c,\cdots,H_p-1\} \tag{3.17g}$$

where the symbol '$|k$' indicates the sampling step k, at which the control input $u(k)$ is given for the closed-loop control of vehicle plant, H_p and H_c are the prediction and the control horizon, respectively; $Q \in \mathbb{R}^{2\times2}$ and $R \in \mathbb{R}^{1\times1}$ the matrices corresponding to weights on the output and control input vectors, accordingly, $\Delta u(k) = [\Delta u(k|k),\cdots,\Delta u(k+H_c-1)|k]^T$ denotes the predicted control input series at time series of $k,\cdots,k+H_c-1$, and $y(k+i|k)$ the output vector predicted at time $k+i$ attained by starting from the state vector $x(k)$. Note that $H_p > H_c$, and the predicted control inputs are

assumed constant in the time interval from H_c to H_p.

In Equation (3.17a), the first summand imposes the penalty on trajectory tracking deviation, while the second summand is to prevent large control effort for the automated steering. Solving the optimization problem described in Equation (3.17), we obtain the optimal control input increments evaluated at the sampling step k for the currently observed vehicle state vector $\boldsymbol{x}(k)$, and denote the optimally predicted control input increments by

$$\Delta\boldsymbol{u}^*(k) \triangleq [\Delta\boldsymbol{u}^*(k|k), \cdots, \Delta\boldsymbol{u}^*(k + H_c - 1)|k]^T \tag{3.18}$$

where the first control input increment is used to update the required control action as described in Equation (3.14). The resulting state feedback control law is thus cast as

$$\boldsymbol{u}(k + 1) = \boldsymbol{u}(k) + \Delta\boldsymbol{u}^*(k|k) \tag{3.19}$$

At the next sampling step $k + 1$, the control action $\boldsymbol{u}(k + 1)$ will be applied to the vehicle plant and be fed to the observer to acquire the new vehicle state vector estimation $\boldsymbol{x}(k + 1)$, with which the optimization problem formulated by Equation (3.17) is to be solved again over a shifted horizon.

To summarize the design of the NLMPC controller, the interrelations are visualized among the controller and the vehicle plant using the block diagram shown in Figure 3.13. In the operation of motion-planning module, with the global route determined by the route planner, the behavioral planner decides on a local driving task with a motion specification. Following the directives of the behavioral planner, the local motion-planner generates the reference trajectory (i.e., r(·)) for the NLMPC controller to manipulate the track action, as shown in Figure 3.13.
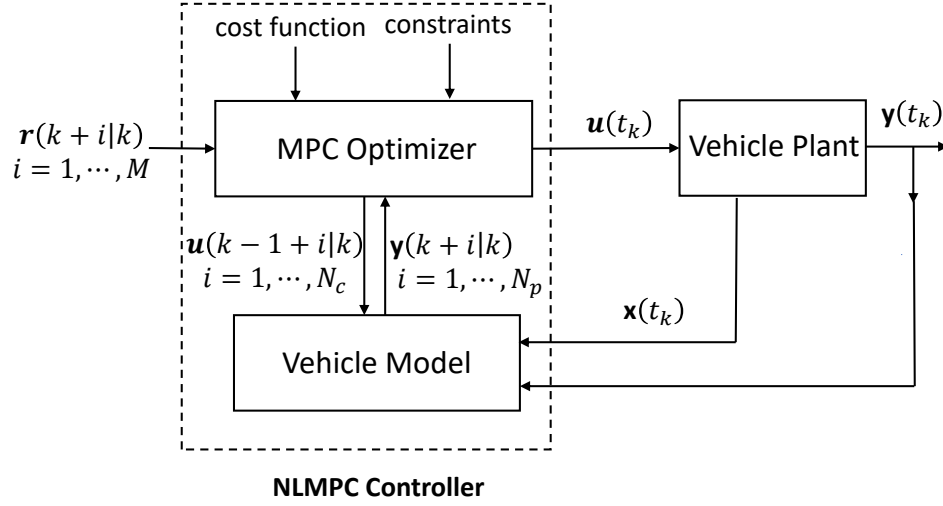
Figure 3.13: Block diagram describing the interrelations among NLMPC controller and

vehicle plant.

To date, studies have been conducted to explore techniques for local motion-planning. These techniques may be classified into two groups [97]: 1) separated methods, by which spatial maneuver (e.g., a single lane-change (SLC) for obstacle avoidance at a constant forward speed) and temporal maneuver (e.g., speeding up along a predefined SLC path to overtake a front vehicle) are separately planned; 2) integrated approaches, with which the spatial and temporal maneuvers are planned simultaneously. The integrated techniques exhibit poor performance in terms of computational efficiency. In contrast, the separated methods significantly improve the computational efficiency because of the layered nature [98].

In this research, the separated methods are adopted. Due to the fact that only autonomous steering control at a constant forward speed is considered in this study, the local motion-planning is reduced to a path planning problem. It is indicated that the testing maneuver with a single cycle sine wave steering input is well-accepted for assessing road vehicles'

handling performance in terms of path-following and yaw stability under SLC maneuver at a constant forward speed [99]. To facilitate systematic and repeatable tests of the proposed design synthesis method, it is assumed that the local motion-planning results in a SLC path at a given speed. Under the evasive maneuver, the vehicle with automated steering will be evaluated in terms of path-following, yaw stability, and driving quality.

3.6   Implementation of The Design Synthesis Problem

The design of the vehicle with automated steering is conducted with the proposed framework. This section outlines the design in terms of: 1) design objectives, variables, and constraints, 2) design synthesis implementation of urban and highway scenarios, and 3) design synthesis implementation for high-speed vehicle with active aerodynamic control.

3.6.1 Design objectives, variables and constrains

The design of the vehicle with automated steering aims at improving path-following, ensuring yaw stability, and enhancing ride quality under severe operating conditions. To this end, obstacle avoidance maneuvers in highway, urban area operations, and high-speed operations at 180 km/h are simulated. It is assumed that, under these SLC maneuvers, the paths to be tracked by the AV are determined by the motion-planner. Under each SLC maneuver, the AV follows the path at a constant forward speed, v_x. Under the maneuver, the NLMPC controller adjusts the steer angle, δ, to improve path-following, ensure yaw stability, and enhance ride quality by minimizing the path-following off-tracking, J_1, yaw

angle deviation, J_2, and the ride quality measure, J_3.

As shown in Figure 3.4, the target path can be defined by the lateral position, $Y_{ref}(t)$, and the tangential angle, $\varphi_{ref}(t)$, of the path at point S; the path-following off-tracking of the AV is directly associated with the vehicle lateral path deviation (e_2) defined by Equation (3.9); the yaw angle deviation of the AV is related to the vehicle yaw angle error (e_1) specified by Equation (3.8); the ride quality of the AV is determined by the lateral acceleration of the vehicle, $a_y = \dot{v}_y + v_x \varphi$. Over the SLC maneuver, the forward speed (v_x) remains constant. Assuming the time duration for completing the SLC maneuver is T_{slc}, we define the path-following off-tracking performance measure as

$$J_1 = \left\{ \frac{1}{T_{slc}} \int_0^{T_{slc}} [e_2(t)]^2 \, dt \right\}^{\frac{1}{2}} \tag{3.20}$$

where J_1 represents the root of mean square (RMS) value of the vehicle lateral path deviation, e_2, over the SLC maneuver.

Similarly, the yaw angle deviation of the AV is specified as

$$J_2 = \left\{ \frac{1}{T_{slc}} \int_0^{T_{slc}} [e_1(t)]^2 \, dt \right\}^{\frac{1}{2}} \tag{3.21}$$

where J_2 denotes the RMS value of the vehicle yaw angle error, e_1, over the SLC maneuver.

Finally, the ride quality measure is determined by

$$J_3 = \left\{ \frac{1}{T_{slc}} \int_0^{T_{slc}} [a_y(t)]^2 \, dt \right\}^{\frac{1}{2}} \tag{3.22}$$

where J_3 represents the RMS value of the vehicle lateral acceleration, a_y, over the maneuver. A quantitative assessment of the ride quality can be performed with the respective measures by ISO-2631-1 [100], which specifies metrices to quantify the

evaluation of human exposure to whole-body vibration in relation to vehicle occupant health and comfort, probability of vibration perception and incidence of motion sickness. This research considers one index, i.e., an acceleration along the y axis ($a_{eq,y}$). This index corresponds to the performance measure (J_3). The evaluation of the ride comfort based on $a_{eq,y}$ is attained by examining the approximate human reactions at various magnitudes of the index provided by ISO-2631-1, which are presented in Table 3.4.

Table 3.4: Human reactions to various RMS values of acceleration recommended by ISO-2631-1 [100].

RMS values of acceleration, m/s^2	Human reaction
$a_{eq,y} \leq 0.315$	Not uncomfortable
$0.315 \leq a_{eq,y} \leq 0.63$	A little uncomfortable
$0.5 \leq a_{eq,y} \leq 1.0$	Fairly uncomfortable
$0.8 \leq a_{eq,y} \leq 1.6$	Uncomfortable
$1.25 \leq a_{eq,y} \leq 2.5$	Very uncomfortable
$a_{eq,y} \geq 2.5$	Extremely uncomfortable

For this optimization problem, the design variable set $\boldsymbol{X}_D$ consists of two subsets, i.e., $\boldsymbol{X}_{Dm}$ and $\boldsymbol{X}_{Dv}$, which represent the tuning parameters of the NLMPC controller, as well as the geometric and inertial parameters of the mechanical system of the AV, respectively.

In MPC controller designs, the tuning parameters generally include [82], [101]: prediction horizon, H_p, control horizon, H_c, sample time, T_s, output weighting matrix $\boldsymbol{Q}$, and control input variation weighting matrix $\boldsymbol{R}$. Tuning of MPC controllers is of importance due to the fact that a good choice of tuning parameters is likely to significantly increase control quality [81]. In real-time implementation of MPC controls, practical limitations often restrict the availability of sample time, T_s, as a tuning parameter [101]. In MPC controller

designs for AVs, it is recommended that sample time, T_s, take 0.05 s [6]. In this research, we adopt the recommended sample time. Reliable guidelines for selecting the tuning parameters of the prediction horizon, H_p, and control horizon, H_c, are well established [82]. Following these guidelines, this research makes a reliable selection, i.e., $H_p = 20$, and $H_c = 10$.

It is indicated that the selection of output weighting (Q) and control input variation weighting (R) is still open for discussions [82]. Moreover, the tuning of these weighting matrices using the trial-and-error method is difficult, and the tuning process is time-consuming [6]. With the above considerations, we treat the elements of the weighting matrices Q and R as the components of the design variable subset X_{Dm}. In the design synthesis, the NLMPC controller design is formulated as the lower-layer optimization problem as expressed in Equation (3.17). The vectors of output, reference output, and control input variation are specified as

$$\hat{\boldsymbol{y}}(k) = [\hat{\varphi}(k) \quad \hat{Y}(k)]^T \tag{3.23a}$$

$$\boldsymbol{r}(k) = [\varphi_{ref}(k) \quad Y_{ref}(k)]^T \tag{3.23b}$$

$$\Delta u(k) = \Delta\delta(k) \tag{3.23c}$$

With the vectors of output, reference output, and control input variation defined in Equation (3.23), the weighting matrix $Q \in \mathbb{R}^{2\times2}$ and $R \in \mathbb{R}^{1\times1}$ are reduced to

$$\boldsymbol{Q} = \begin{bmatrix} q_1 & 0 \\ 0 & q_2 \end{bmatrix} \tag{3.24a}$$

$$\boldsymbol{R} = [R] \tag{3.24b}$$

Thus, the design variable subset (X_{Dm}) is defined as

$$X_{Dm} = [q_1 \quad q_2 \quad R] \tag{3.25}$$

Among various geometric and inertial parameters of road vehicles, total mass (m), wheelbase (l), and distance from CG to front axle (l_f) are directly associated with path-following capability, yaw stability, and ride quality under severe evasive maneuvers [75]. In this research, these three parameters constitute the mechanical vehicle design variable subset (X_{Dv}), which is specified as

$$X_{Dv} = [m \quad l \quad l_f] \tag{3.26}$$

In the design synthesis, the evaluations of the performance measures defined by Equations (3.20) to (3.22) are attained based on the dynamic responses of the vehicle plant shown in Figure 3.13, which is represented by the nonlinear vehicle model defined by Equation (3.11), over the simulated SLC maneuver. The design variable subsets, X_{Dm} and X_{Dv}, are allowed to vary from their lower bounds $(X_{Dml}$ and $X_{Dvl})$ to the respective upper bounds $(X_{Dmu}$ and $X_{Dvu})$. Following the design framework shown in Figure 3.1, the upper layer optimization problem is formulated to realize the aforementioned design objectives subject to the specified constraints. The formulation is constructed as

$$\min_{X_{Dm}, X_{Dv}} F(X_D) = \sum_{i=0}^{3} \rho_i J_i(X_D) \tag{3.27a}$$

subject to:

$$\dot{x}(t) = f(x(t), u(t)) \tag{3.27b}$$

$$X_{Dm_l,i} \leq X_{Dm,i} \leq X_{Dm_u,i}, \quad i \in \{1,2,3\} \tag{3.27c}$$

$$X_{Dv_l,i} \leq X_{Dv,i} \leq X_{Dv_u,i}, \quad i \in \{1,2,3\} \tag{3.27d}$$

where ρ_1, ρ_2, and ρ_3 are the normalized weighting factors for the vehicle performance

measures, J_1, J_2, and J_3, respectively; Equation (3.27b) defines the nonlinear vehicle model, by which the objective function and constraints are evaluated; $X_{Dm,1}$, $X_{Dm,2}$, and $X_{Dm,3}$ denote q_1, q_2, and R, while $X_{Dm_l,i}$ and $X_{Dm_u,i}$, $i \in \{1,2,3\}$, are the lower and upper bounds of the respective design variables $X_{Dm,i}$; $X_{Dv,1}$, $X_{Dv,2}$, and $X_{Dv,3}$ represent m, l, and l_f, while $X_{Dv_l,i}$ and $X_{Dv_u,i}$, $i \in \{1,2,3\}$, are the lower and upper bounds of these vehicle design variables, accordingly.

To facilitate the design optimization, each term of the right-hand side of Equation (3.27a) is normalized with the respective norm [76], [77]. For the case concerned, the norm of each term is the inverse of the respective weighting factor, that is,

$$\rho_i = 1/J_i^{norm}, i \in \{1,2,3\} \tag{3.28}$$

where J_i^{norm} are the performance measure defined and calculated using Equations (3.20) to (3.22), respectively, with the design variables taking their nominal values, which will be provided in Chapter 4.

3.6.2 Implementation of the bi-layer optimization problem

As shown in Figure 3.14, to run the PSO algorithm, the undetermined parameters in Equation (3.1) are assigned finely tuned values: $w = 1.0$, $c_1 = 1.5$, $c_2 = 1.5$, and the total number of particles is n. In the case concerned, the number of design variables is 6.

Initially, the PSO algorithm randomly selects n particles/designs in the 6-dimensional design variable space. Then, each particle/design ($X_{Di}, i \in \{1,2,\ldots,n\}$) is sent to the coupled local motion-planning and NLMPC tracking-control modules. With a given design variable set, X_{Di}, as shown in Figure 3.13, the specified geometric and inertial parameters

of the vehicle model and the tuning weights of the NLMPC controller are updated. Under

a SLC maneuver, the reference path for the AV is determined by the local motion-planning

module. Over the SLC maneuver, the NLMPC controller determines the steering angle δ

of the vehicle plant (defined by Equation (3.11)) to track the reference path at a constant

forward speed. After completing the SLC maneuver, a fitness value, $F(X_{Di}) = \sum_{j=1}^{3} \rho_j J_j(X_{Di})$, $i \in \{1,2, \dots, n\}$, can be derived using the dynamic responses of the vehicle
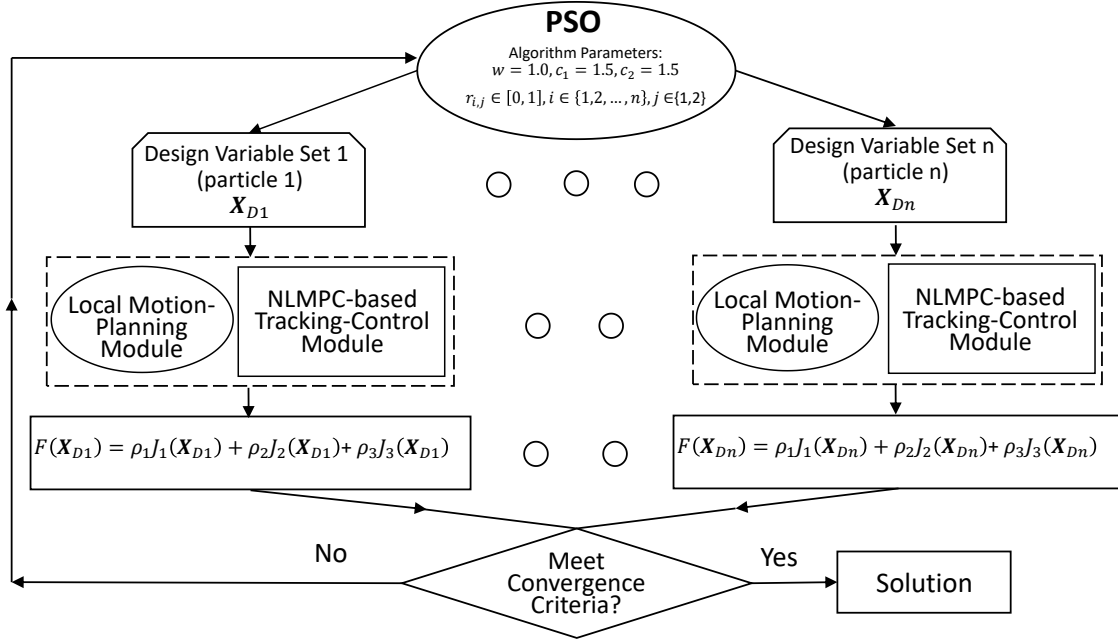
plant over the SLC maneuver.

Figure 3.14: Schematic representation of the implementation of the bi-layer optimization

problem.

With the execution of the equivalent SLC maneuver corresponding to each of the n design

variable sets, a fitness value vector, $[F(X_{D1}), F(X_{D2}), \dots, F(X_{Dn})]$, is obtained. At this

point, if the convergence criteria, e.g., a predefined total generation number, an acceptable

error between the best fitness values of the last two generations, etc., are satisfied, the

optimization process terminates. Otherwise, the achieved fitness value vector is feedbacked

to the PSO at the upper layer. Based on the returned fitness value vector corresponding to the given design variable sets, the PSO creates the next generation of design variable sets (or particles) using the 'particles' updating operator defined in Equation (3.1) and Equation (3.2). This process repeats until the optimal design variable set is found.

3.6.3 Implementation for high-speed vehicles with active aerodynamic control

For the high-speed vehicle application, the implementation of the proposed design synthesis method is similar with the one shown in Figure 3.14. There are two distinct features for the high-speed vehicle case: 1) in the NLMPC controller design, the prediction model is the 2-DOF nonlinear yaw-plane double-track vehicle model shown in Figure 3.5; 2) the respective 3-D CarSim model with the active aerodynamic control functionality is used as the virtual vehicle plant.

Figure 3.15 shows the schematic of the proposed method for the design synthesis of the high-speed vehicles with active aerodynamic control. Different with the urban and highway scenarios, the active aerodynamic control system is introduced in the 3-D CarSim vehicle model. As shown in Figure 3.15, the NLMPC controller sends the control input to the virtual vehicle plant, and the controller receives its feedback for the virtual vehicle plant to form a closed-loop control system. In Figure 3.15, however, there is an inherent close-loop control within the virtual vehicle plant to perform the active aerodynamic control. Noted that the active aerodynamic control is an independent control system with NLMPC as their control input and output parameters are different and they not affect each other's control process.
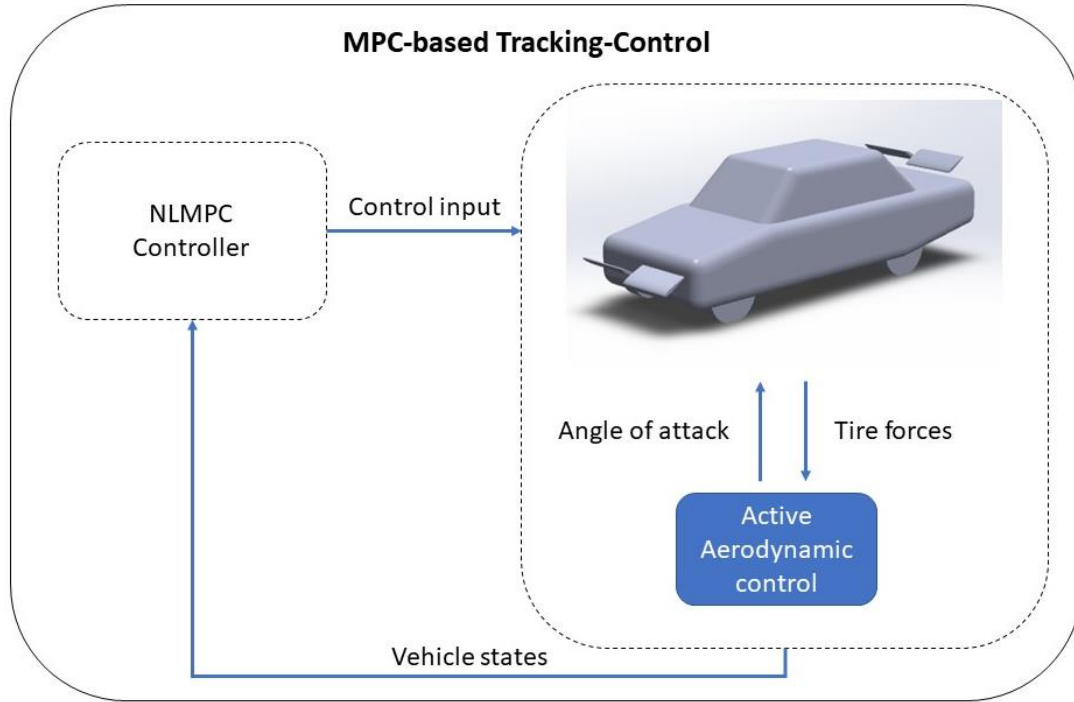
Figure 3.15: Schematic representation of the proposed method for the design synthesis of road vehicles with active aerodynamic control.

The working principle for this active aerodynamic control (AAC) is shown in Figure 3.16, AOA is the angle of attack of the spoiler, F_z is the vertical force on the tire, and F_{z_aero} is the lift force generated by the spoiler. The active aerodynamic control is to compensate the vertical load transformation between the left and right wheels on each axle while the vehicle negotiates curved path. Considering the vertical load difference between the left and right wheels on each axle, the active aerodynamic controller calculates the angle of attack for each spoiler to manipulate the vertical force on each individual wheel.
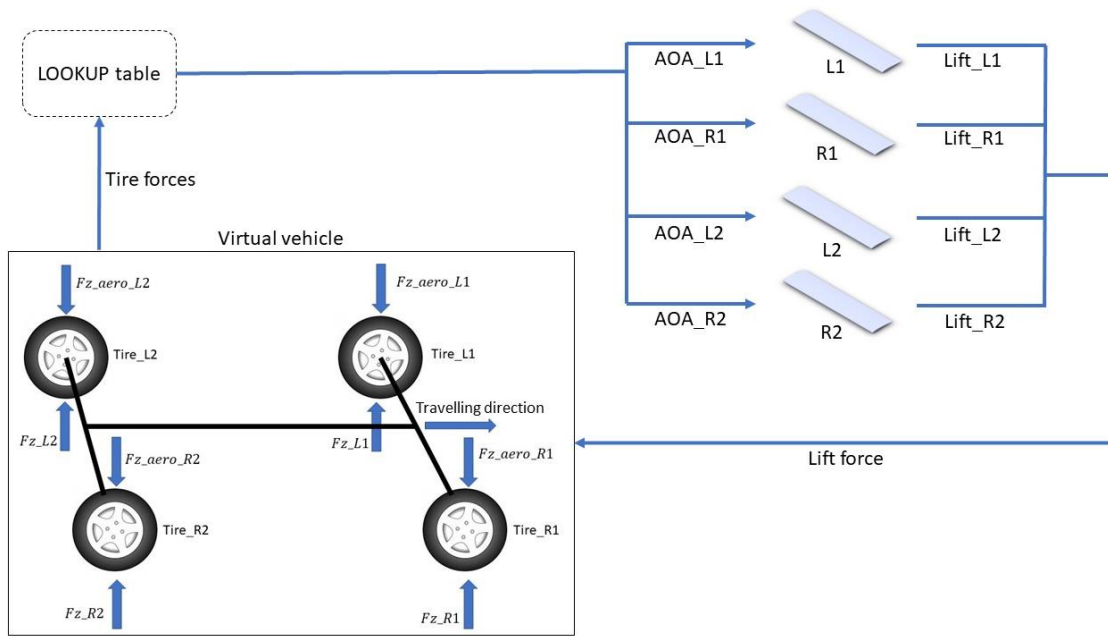
Figure 3.16: Close-loop control of aerodynamic lift/down force.

In Matlab/Simulink, a look-up table is established using the data in terms of the correlation between the angle and attack and the lift force provided in Table 3.3. In the simulation of a curved path negotiation, the 3-D CarSim model sends Matlab/Simulink the vertical load of each wheel. Given the vertical load difference between the left and right wheels of each axle, the active aerodynamic controller determines the angle of attack for each spoiler to diminish the vertical load difference. With the calculated angle of attack for each spoiler, the lift/down force of the respective wheel can be determined using the look-up table. The resulting lift/down force for each wheel is then sent back to the virtual vehicle plant in CarSim. This close-loop control is implemented to compensate the vertical load transformation between the left and right wheels on each axle.

Chapter 4

Results and Discussion

4.1 Case studies specification and testing maneuvers

The bi-layer design optimization shown in Figure 3.14 is implemented considering three operating scenarios or case studies: 1) urban, 2) highway, and 3) high-speed consider active aerodynamic control (AAC) application. In each of case studies, the respective SLC maneuver is simulated, and the reference path is prescribed. These reference paths are mathematically defined by

$$Y(X) = \frac{L}{T}\left[\frac{X}{V_x} - \frac{T}{2\pi}\sin\left(\frac{2\pi X}{TV_x}\right)\right] \tag{4.1}$$

where X and Y are the horizontal and vertical displacement (in *meters*) of a point on the reference path displayed in the inertial coordinate system, V_x (in *m/s*) is vehicle forward speed, L (in *meters*) is the maximum SLC lateral displacement, and T (in *seconds*) is the time period. For the three case studies, the values of the reference path parameters are provided in Table 4.1.

Table 4.1: Parameter values for each of the reference path of the three operation scenarios.

Reference path parameters	Urban SLC	Highway SLC	AAC SLC
Vehicle forward speed, $V_x, m/s$	16.67 (*60 km/h*)	27.78 (*100 km/h*)	50 (180 km/h)
Time period, T, s	3.00	2.00	2.00
Maximum lateral displacement, L, m	3.00		

To implement the optimizations, the nominal values are selected, as well as the lower and upper bound values of the design variables, which are listed in Table 4.2. It should be noted that to highlight the effects of AAC and retain the other vehicle aerodynamic

characteristics, the vehicle parameters take their nominal values, and they are not considered as the design variables in the case study of AAC. Therefore, the number of design variable in the case of AAC is three (i.e., only controller parameters), whereas the other two cases have 6 design variables (that is, controller parameters and vehicle parameters). Note that the design optimization is implemented independently in the three cases, i.e., urban, highway, and AAC. For implementing these design optimizations, both the population number (i.e., the total number of particles), n, and the total number of generations of the PSO algorithm are assigned the value of 100.

Table 4.2: Design variables with nominal values, lower and upper bound values, as well as optimized variable values.

X_D	Nominal values	Lower bound values	Upper bound values	Optimal values (urban)	Optimal values (highway)	Optimal values (AAC)
q_1	15.00	0.00	20.00	4.30	16.40	17.8
q_2	5.00	0.00	20.00	11.52	4.51	2.9
R	10.00	0.00	40.00	2.25	4.77	5.3
$m\ (kg)$	1,530.0	1,200.0	2,000.0	1,934.0	1986.0	
$l\ (m)$	2.87	2.00	3.60	3.16	3.55	
$l_f(m)$	1.11	1.00	2.00	1.08	1.43	

After the execution of the design optimizations under the three operating scenarios, the optimal design variable sets and the respective performance measures defined in Equations (3.20) to (3.22) are attained. The resulting values of the optimal design variables are also provided in Table 4.2.

To analyze and evaluate the attained optimization results, co-simulations are conducted by integrating the virtual vehicle, i.e., the CarSim model, with the coupled motion-planning and NLMPC tracking-control modules designed in Matlab. In the co-simulations, the

urban, highway, and AAC SLC maneuvers are simulated; in these operating scenarios, the NLMPC controller and the vehicle models take the respective nominal and optimal design variable values listed in Table 4.2. In the following subsections, the co-simulation results in terms of the performance measures of the nominal and optimal designs in all the three cases are examined first, then the effects of optimal design variables on the performance improvements are evaluated.

4.2   Performance measures of urban and highway scenarios

In the urban scenario, the nominal and optimal designs are compared and evaluated, as shown in Figures 4.1, 4.3, 4.5, 4.7, and 4.9. Figure 4.1 shows the reference path and the trajectories of the vehicle CG for the nominal and optimal designs. It seems difficult to distinguish the differences among the three paths without the aid of the focused and enlarged windows accompanying the figure. By means of the accompanying window in the figure, it is observed that the path of the optimal design is closer to the reference one with a lower overshoot compared to the counterpart of the nominal design. The simulation results illustrated in Figures 4.3 and 4.5 justify our observation. As shown in Figure 4.3, in the nominal design, the maximum peak lateral position deviation of the vehicle CG from the reference path $\left(Y_{err\_Max}\right)$ is 0.0287 *m*; while in the optimal design, this measure is 0.0115 *m*, decreasing by 59.9% from the counterpart of the nominal design. Figure 4.5 shows that in the optimal design, the maximum peak vehicle yaw angle deviation from the reference value $\left(Yaw\_ang_{err\_Max}\right)$ is 0.6357º, reducing by 14.8% from the corresponding measure of 0.7462º for the nominal design.
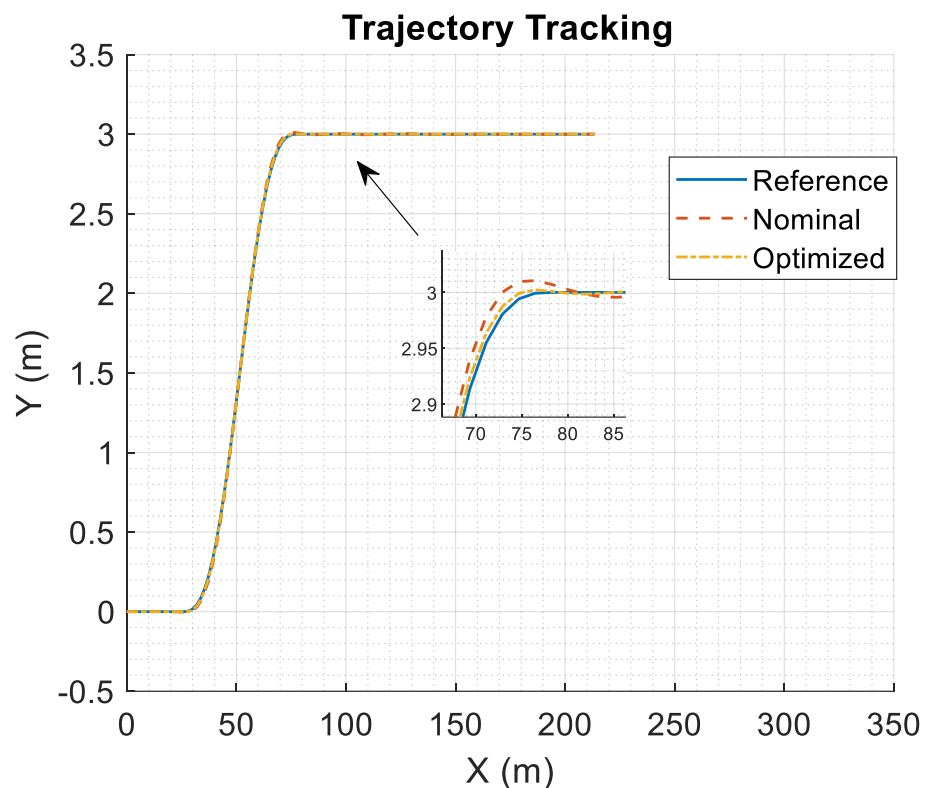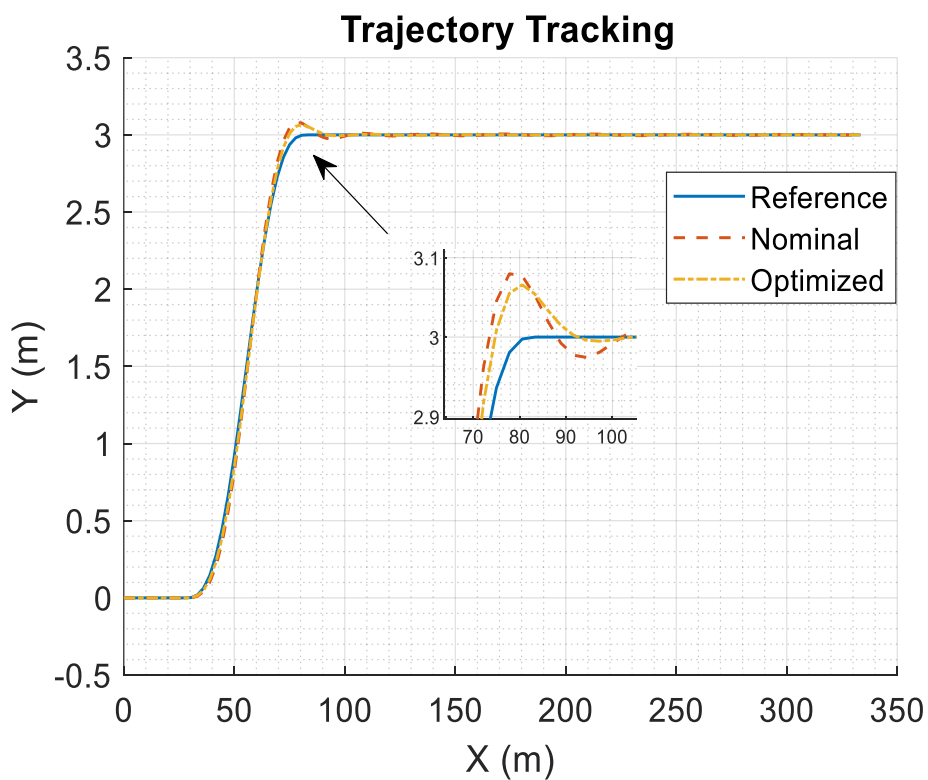
Figure 4.1: Path tracking in urban scenario.

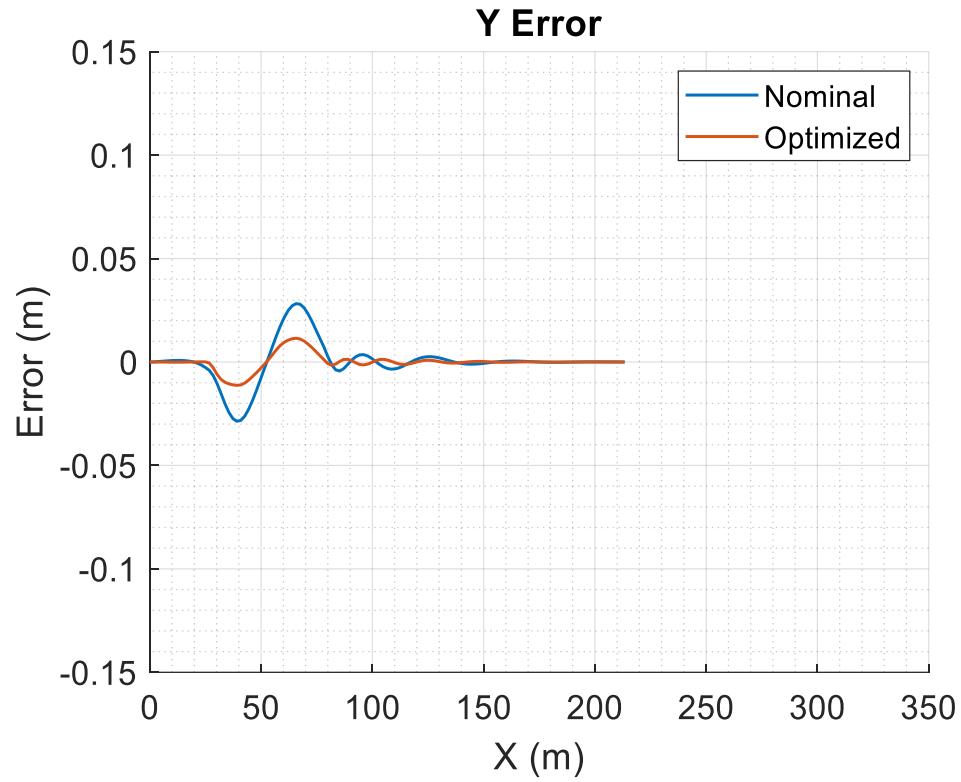Figure 4.2: Path tracking in highway scenario.

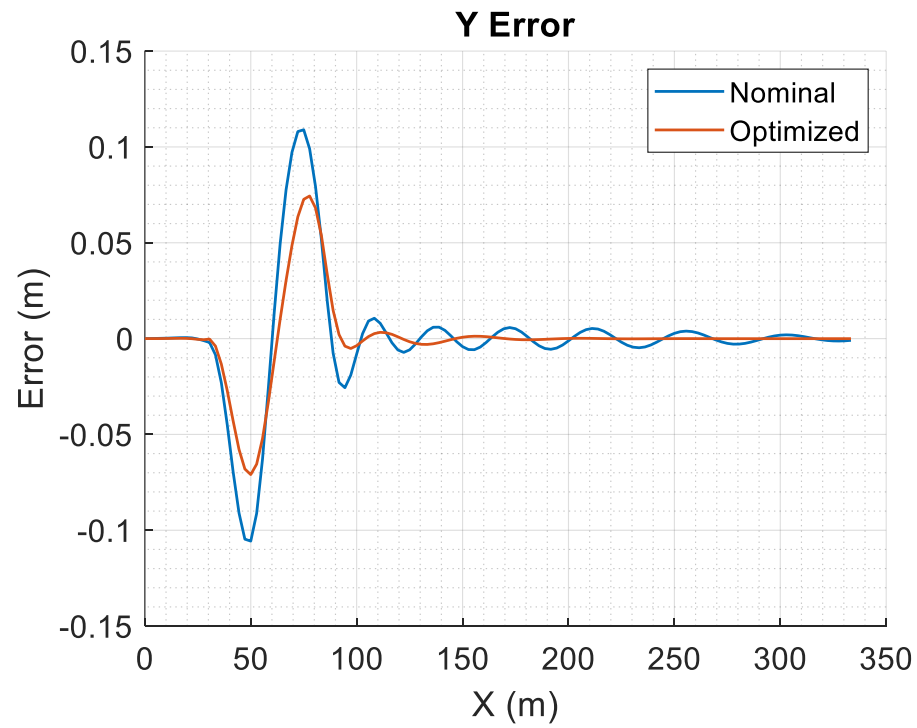Figure 4.3: Lateral position deviation in urban scenario.

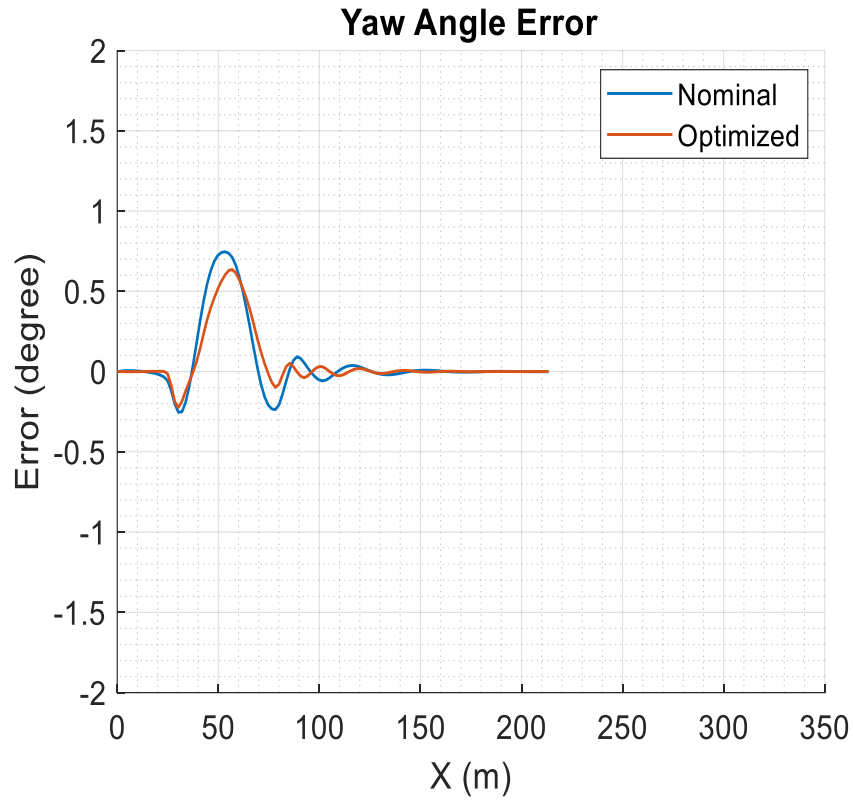Figure 4.4: Lateral position deviation in highway scenario.

Figure 4.5: Yaw angle deviation in urban scenario.

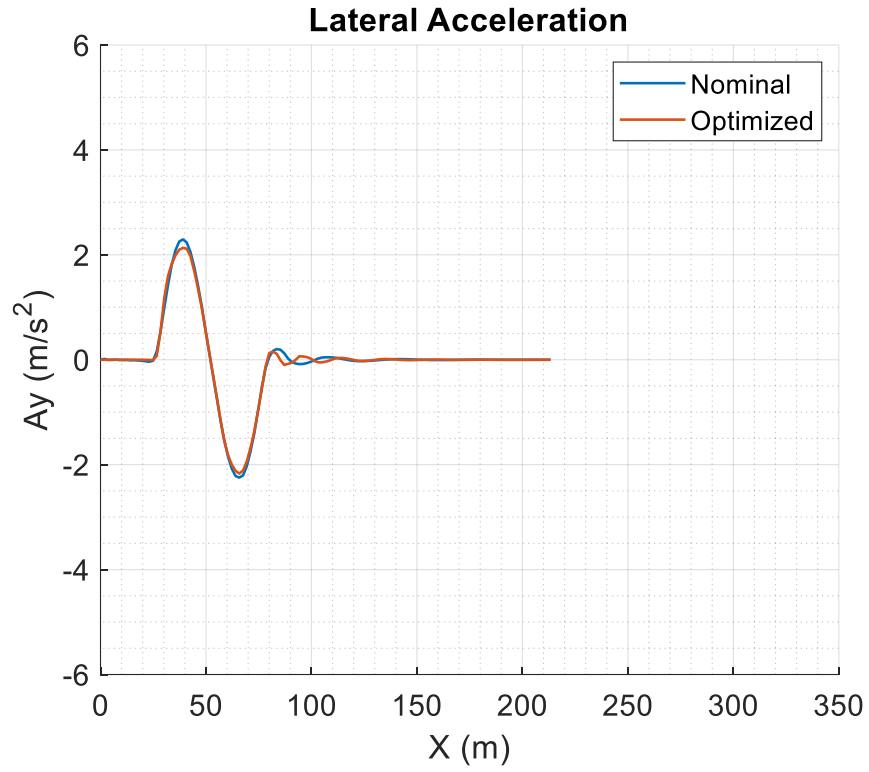Figure 4.6: Yaw angle deviation in highway scenario.

Figure 4.7: Lateral acceleration variation in urban scenario.
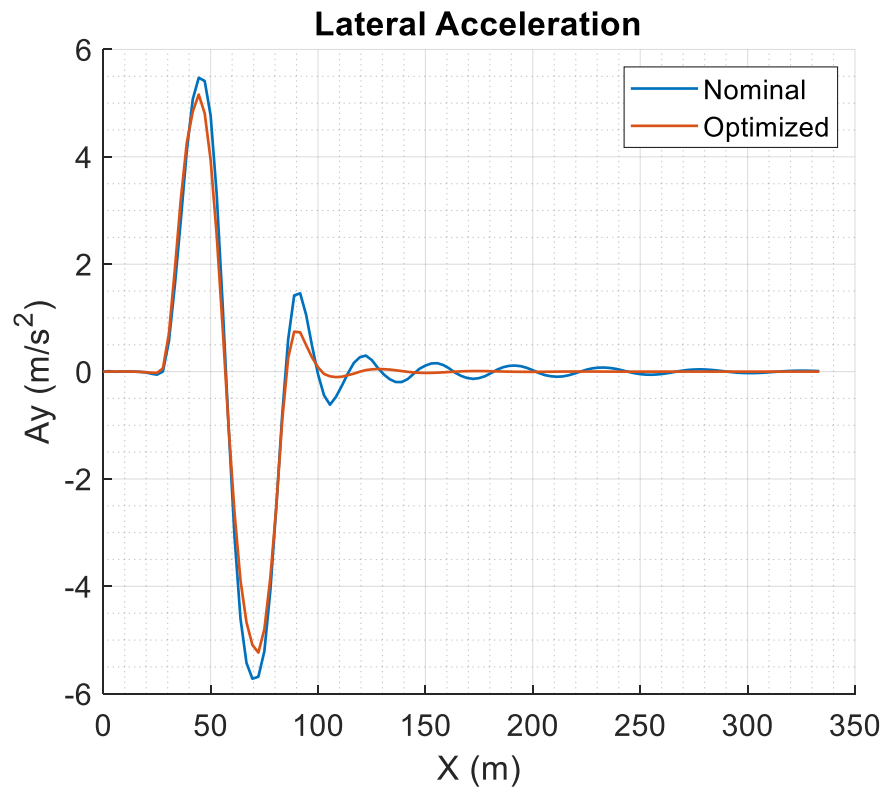

Figure 4.8: Lateral acceleration variation in highway scenario.

Figure 4.7 displays the vehicle dynamic response in terms of the variation of the lateral acceleration at the vehicle CG in both the nominal and optimal designs. Obviously, the fluctuation of the lateral acceleration in the nominal design is more violent with larger peak values than its counterpart in the optimal design. To evaluate the ride comfort of the designs, RMS values of lateral acceleration (a_y) over the SLC maneuver are calculated using Equation (3.22). In the optimal design, this measure takes the value of $0.7599\ m/s^2$, reducing by 3.1% from its nominal value of $0.7845\ m/s^2$. Assessing the ride quality based on the ISO-2631-1 specifications listed in Table 3.4, it can be found that for both the optimal and nominal designs, the vehicle occupants will feel fairly uncomfortable during the urban SLC maneuver.
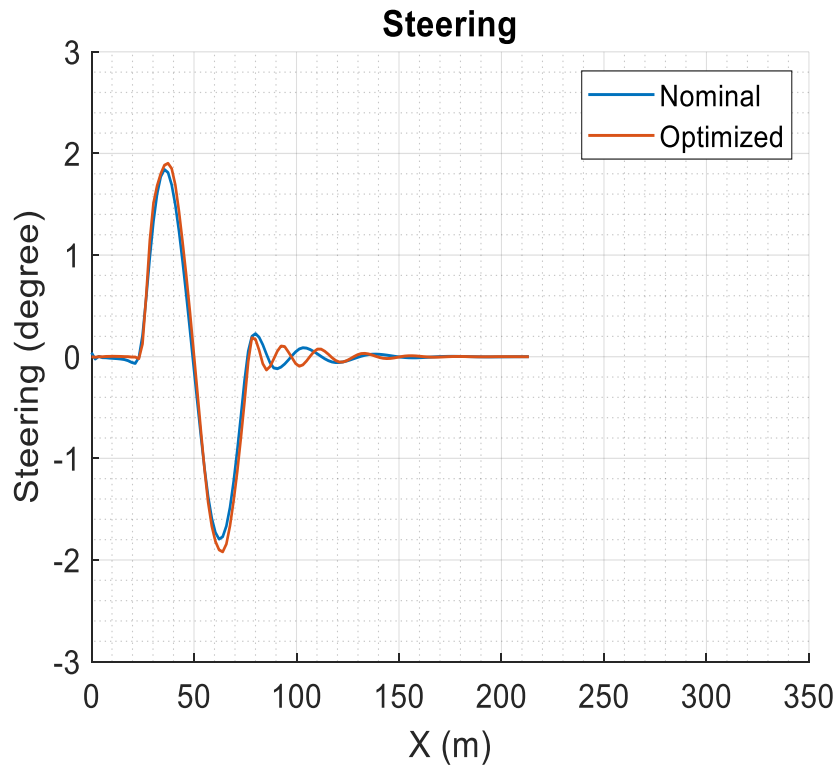

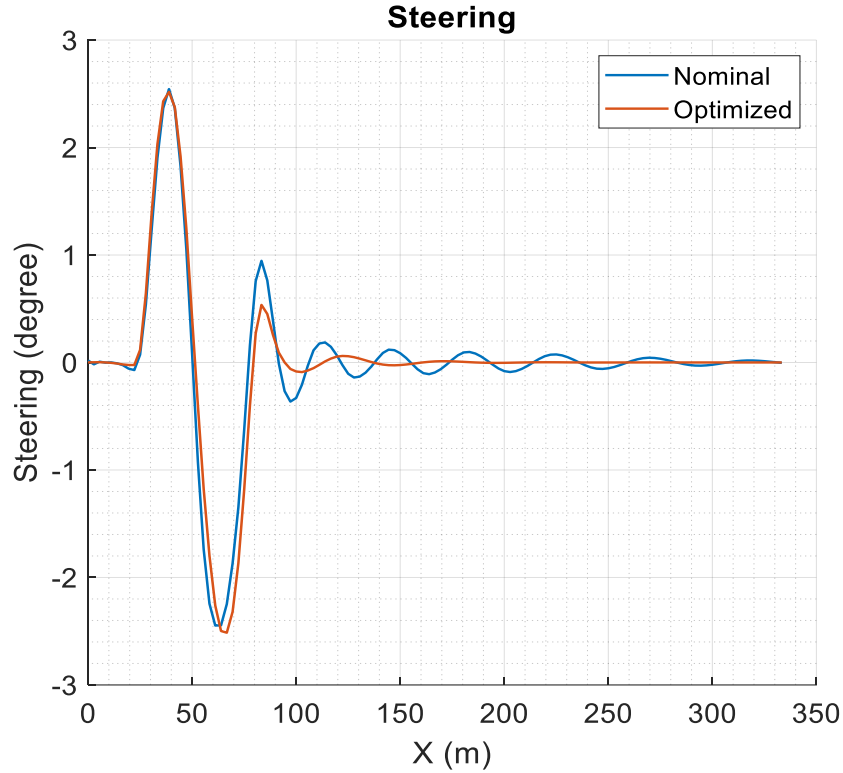Figure 4.9: Front wheel steer angle variation in urban scenario.

Figure 4.10: Front wheel steer angle variation in highway scenario.

Figure 4.9 illustrates the front wheel steer angle input controlled by the respective NLMPC controller over the SLC maneuver for each of the two designs. As expected, each of the steer inputs takes a single cycle sine wave form for the SLC maneuvers. It is found that with the approximate same time period, the two sine wave inputs have different amplitudes. For the optimal design, the maximum amplitude ($Steer\_ang_{Max}$) is 1.9201°, which is increased by 4.2% from its nominal value of 1.8425°. It has been found that for a given SLC maneuver, the total area (absolute value) enclosed by the vehicle front-wheel steer angle curve and the horizontal axis may be viewed as an indicator for steering control effort [102]. A close observation of Figure 4.9 discloses that the overall steering control effort of the optimal design is larger than its counterpart of the nominal design.

All the aforementioned performance measures of the nominal and optimal designs, as well as their relative variations, are listed in Table 4.3. The above analysis indicates that the

optimal design outperforms the nominal one in the performance measures of path-following off-tracking, yaw angle deviation, and ride quality. The performance improvement of the optimal design may be attributed to its larger steering control effort of the front wheel.

In the case of the highway scenario, the respective performance measures of the nominal and optimal designs are also provided in Table 4.3. Interestingly, the performance improvement of the optimal design over the nominal design in the highway scenario is similar to that in the urban scenario. To dig out the root causes leading to these performance improvements, the Section 4.4 analyzes the effects of design variables and justify the optimal designs.

Table 4.3: Performance measures of the nominal and optimal designs for both the urban and highway cases.

Performance measures	Urban			Highway		
	Nominal design	Optimal design	Variation[*] (%)	Nominal design	Optimal design	Variation[*] (%)
Y_{err_Max}, m	0.0287	0.0115	-59.9	0.1090	0.0744	-31.7
$Yaw\_ang_{err\_Max}, (^o)$	0.7462	0.6357	-14.8	1.7948	1.6982	-5.4
$a_y, m/s^2$ (RMS)	0.7845	0.7599	-3.1	1.6573	1.5026	-9.3
$Steer\_angle_{Max}, (^o)$	1.8425	1.9201	4.2	2.4473	2.5177	2.9

[*] Relative variation of the optimal design with respect to the nominal design.

4.3 Performance measures of high-speed case with AAC

To emphasize the effect of AAC, this section compares three designs, i.e., nonimal design without AAC, optimal design without AAC, and optimal design with AAC. The nominal, optimal, and optimal with AAC designs are evaluated and shown in Figures 4.11 to 4.19.

From Figures 4.11 to 4.15, the performance improvement of the optimal with AAC design over the nominal design has the similar consequence as those for the urban and highway scenario. These results also indicate that the optimal with AAC design outperforms the optimal design without AAC in the performance measures of path-following off-tracking, yaw angle deviation, and ride quality. All the performance measures of the nominal, optimal, and optimal with AAC designs, as well as their relative variations, are listed in Table 4.4.
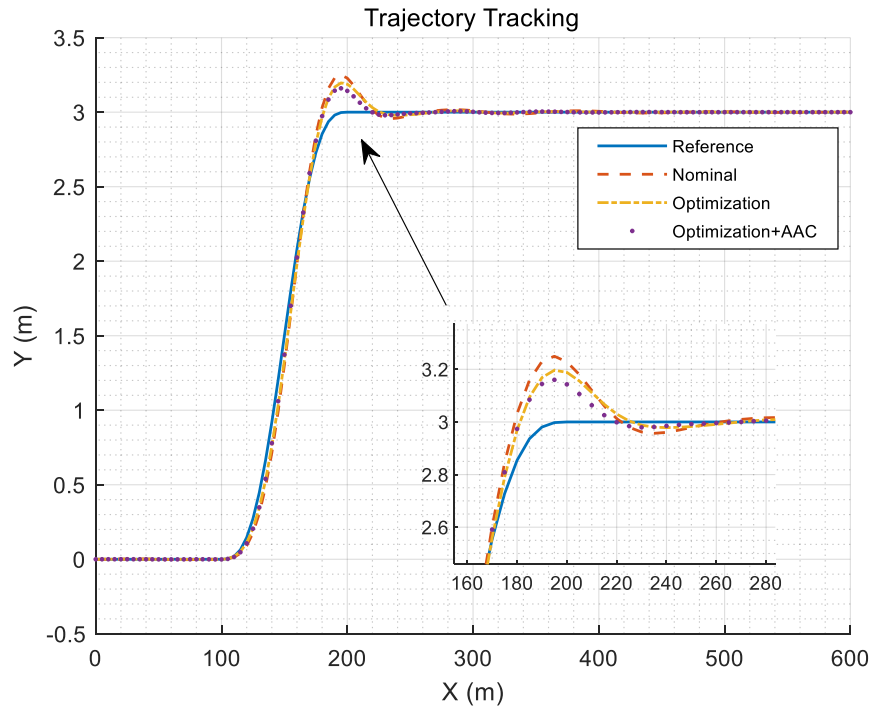

Figure 4.11: Co-simulation results for the AAC operating scenarios - path tracking.

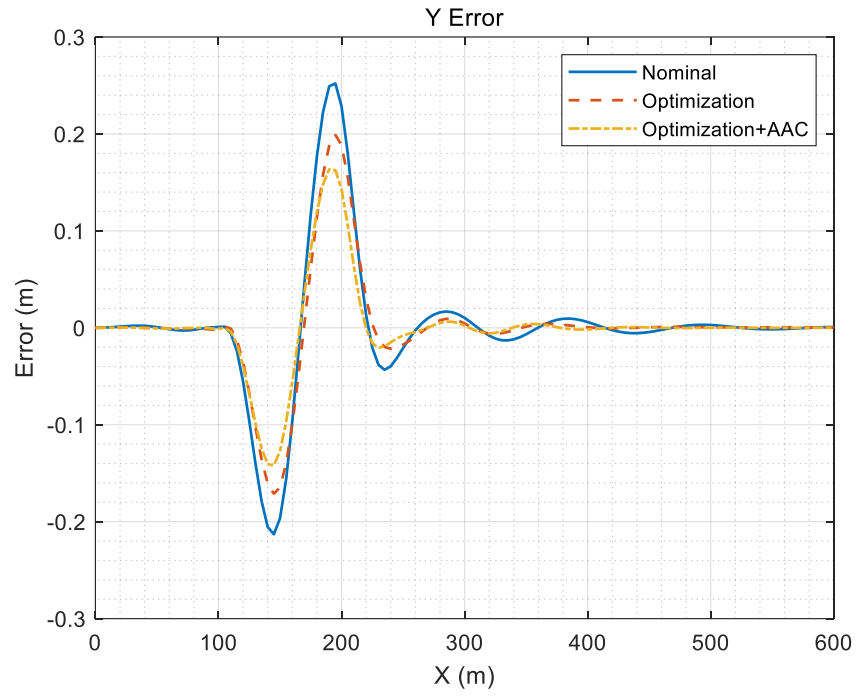Figure 4.12: Co-simulation results for the AAC operating scenarios - lateral position deviation.
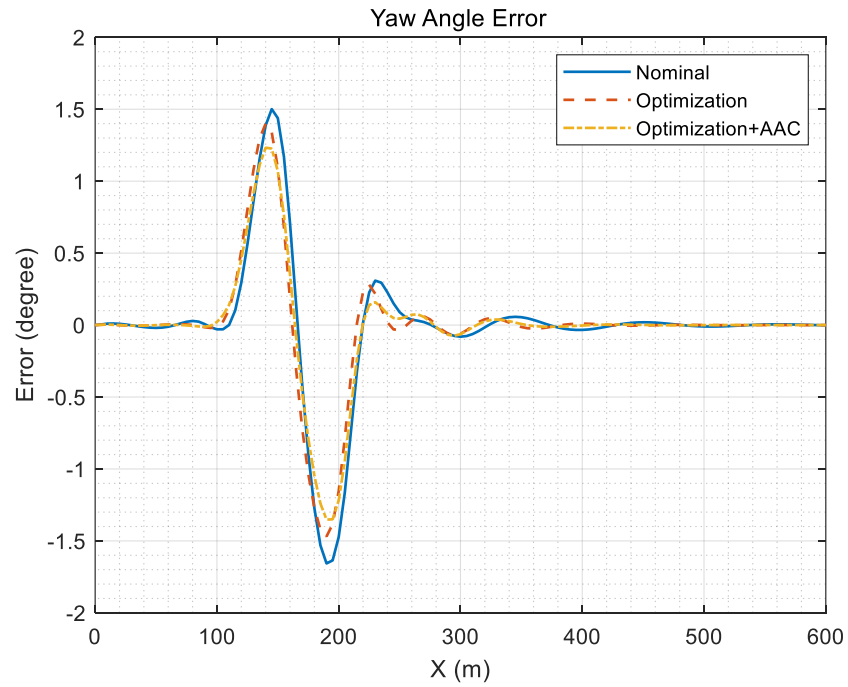

Figure 4.13: Co-simulation results for the AAC operating scenarios - Yaw angle deviation.
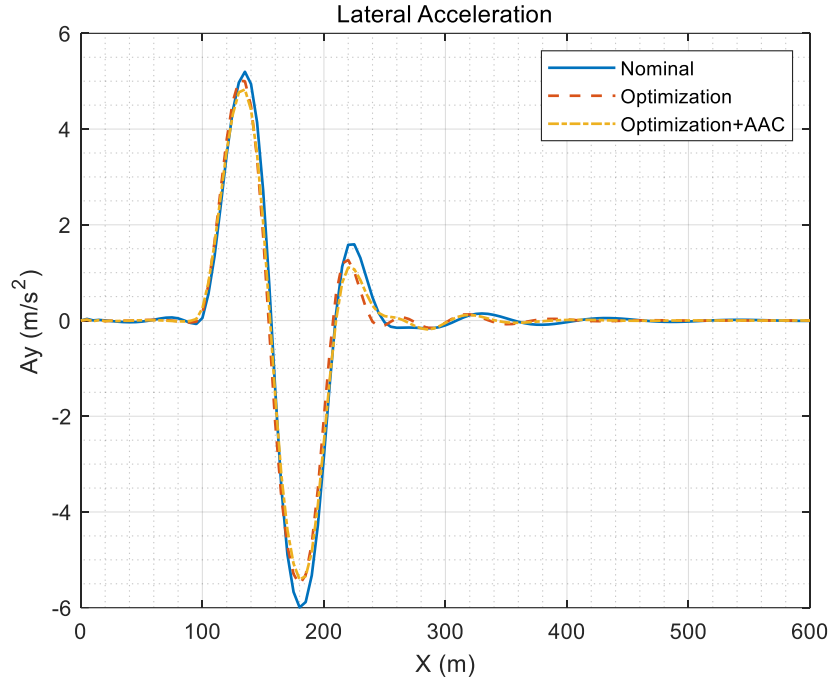
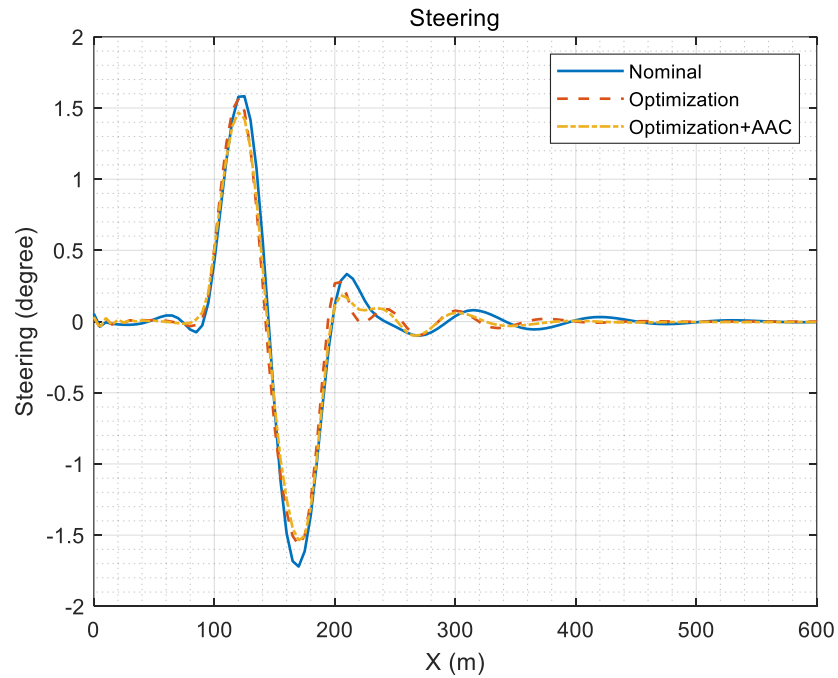Figure 4.14: Co-simulation results for the AAC operating scenarios - lateral acceleration variation.

Figure 4.15: Co-simulation results for the AAC operating scenarios - front wheel steer angle variation.

Table 4.4: Performance measures of the nominal and optimal designs for AAC cases.

Performance measures	Nominal design	Optimal design	$Variation^1$ (%)	Optimal design with AAC	$Variation^2$ (%)
Y_{err_Max}, m	0.2520	0.1991	-21.0	0.1626	-35.5
$Yaw\_ang_{err\_Max}, (°)$	1.6566	1.3992	-15.5	1.2329	-18.4
$a_y, m/s^2$ (RMS)	1.6939	1.5792	-6.8	1.5459	-8.7
$Steer\_angle_{Max}, (°)$	1.7209	1.5631	-9.2	1.4692	-10.7
$F_{z\_diff\_front\_max}, (N)$	2700.0	2478.1	-8.2	1530.7	-43.3
$F_{z\_diff\_rear\_max}, (N)$	2832.5	2602.4	-8.1	1660.2	-41.4
$Roll_{max}, (°)$	0.8967	0.8702	-3.0	0.7233	-19.3

1. Relative variation of the optimal design with respect to the nominal design.
2. Relative variation of the optimal design with AAC with respect to the nominal design.

Figures 4.16 to 4.19 show each tire's vertical force variation over the SLC maneuver. To identify the effects of the spoilers, once again the three designs are compared in these figures. Figures 4.16 and 4.17 present the vertical force variation of the tires (tire L1 and R1) on front axle, while Figures 4.18 and 4.19 illustrate the vertical force variation of the tires (tire L2 and R2) on rear axle. Note that the active aerodynamic controller is to determine the angle of attack of each spoiler to manipulate the respective lift/down force to compensate the transformation of vertical load between the right and left tires on each axle. The ideal situation is to retain a constant vertical force on each tire over the SLC maneuver for achieving optimal overall performance. In the active aerodynamic control, the angle of attack is calculated based on the vertical force difference between the two tires on each axle. A lift force will be applied on the tire that has a higher vertical force; on the contrast, a down force will be exerted on the tire that has a lower vertical force.

In Table 4.4, three important performance measures of the AAC system were listed: the maximum vertical tire force difference of the front axle ($F_{z\_diff\_front\_max}$), the maximum

vertical tire force difference of the rear axle ($F_{z\_diff\_rear\_max}$), and the maximum roll angle of the vehicle in its inertial frame ($Roll_{max}$). These three measures can precisely describe the difference of vehicle roll dynamics due to the effects of the designs of nominal, optimal, and optimal with AAC. For the optimal design without AAC, $F_{z\_diff\_front\_max}$ is 2478.1 N, $F_{z\_diff\_rear\_max}$ is 2602.4 N, and $Roll_{max}$ is0.8702°, while for the optimal with AAC, $F_{z\_diff\_front\_max}$ is 1530.7 N, $F_{z\_diff\_rear\_max}$ is 1660.2 N, and $Roll_{max}$ is 0.7233°. Obviously, the performance of the optimal design with AAC outperforms those of nominal and the optimal designs without AAC. Thus, the optimal design with AAC can improve the vehicle SLC performance at the forward speed of 180 km/h.

Figure 4.16: Co-simulation results for the AAC operating scenarios - vertical force variation of tire L1.

Figure 4.17: Co-simulation results for the AAC operating scenarios - vertical force variation of tire R1.
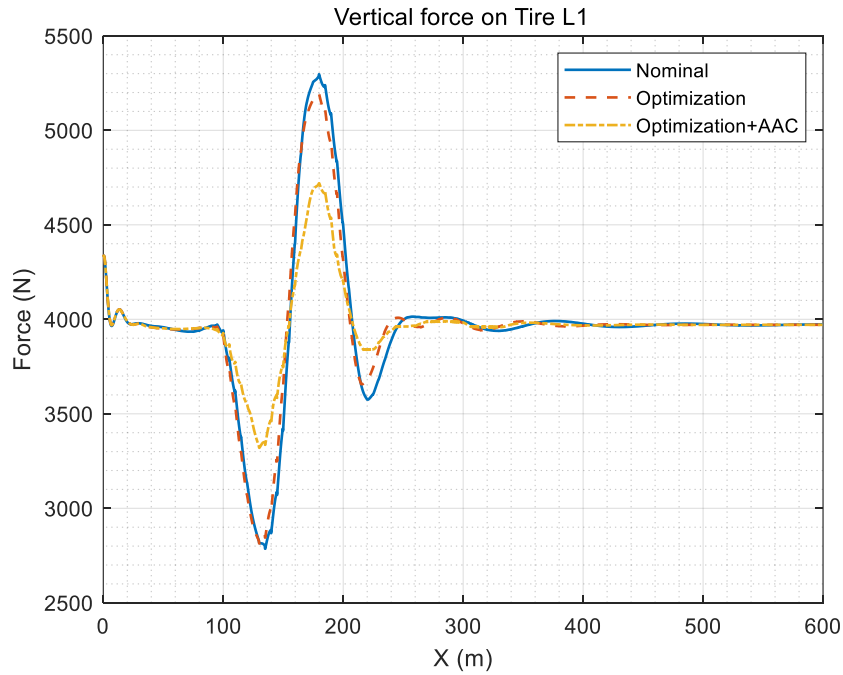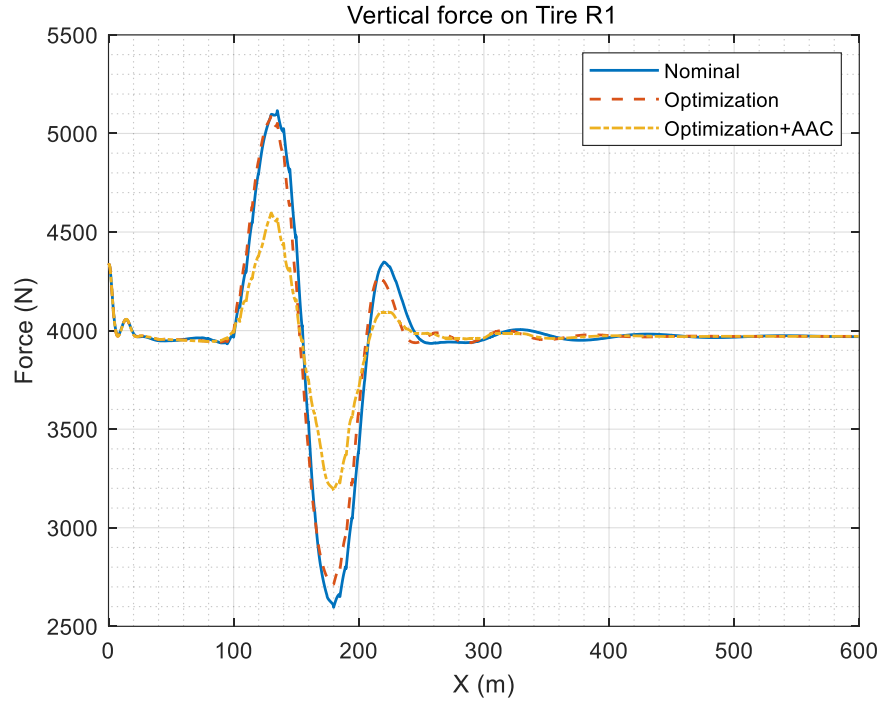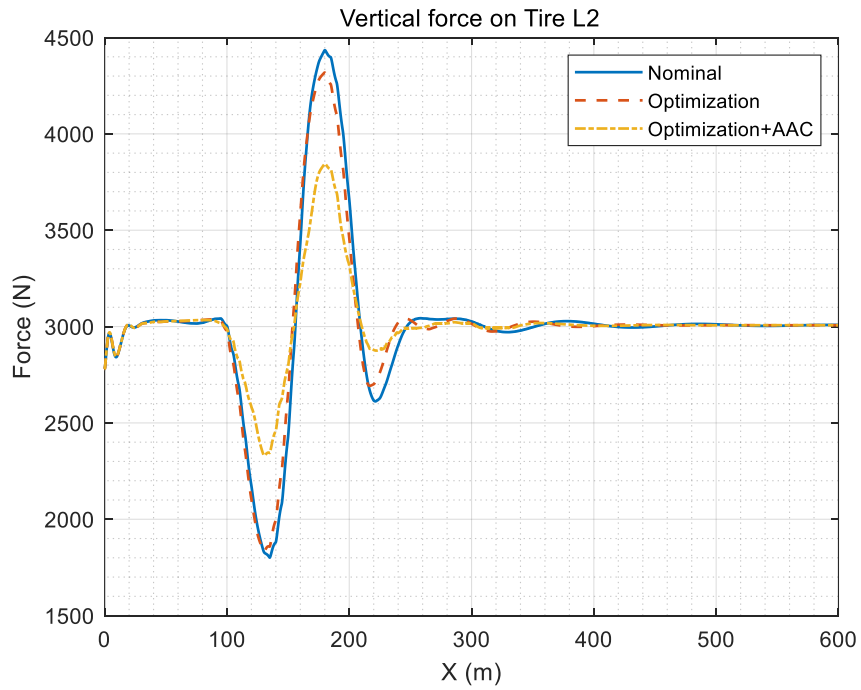

Figure 4.18: Co-simulation results for the AAC operating scenarios - vertical force variation of tire L2.
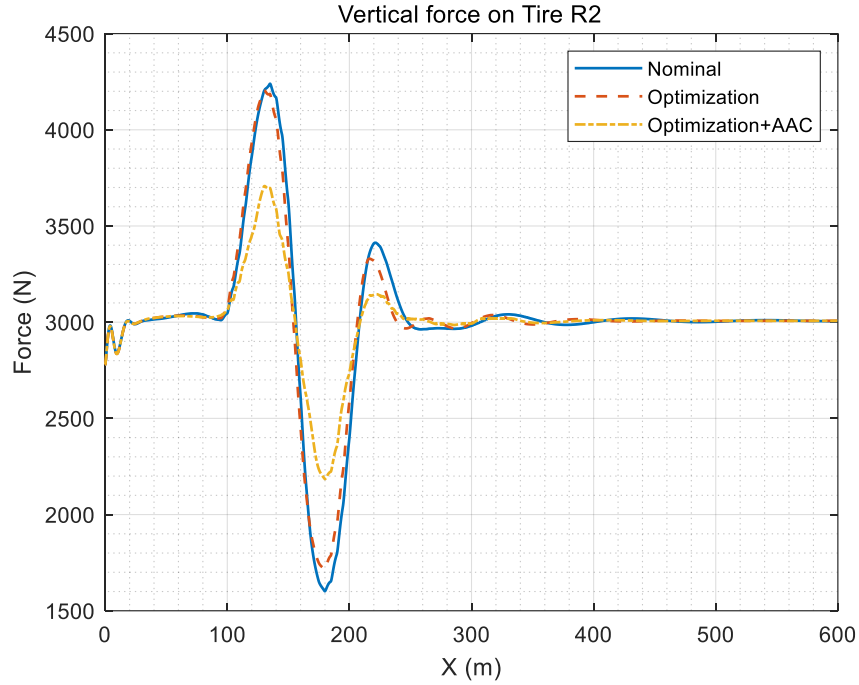
Figure 4.19: Co-simulation results for the AAC operating scenarios - vertical force variation of tire R2.

4.4 Effects of design variables

To make this thesis concise, only select two design variables, i.e., l (vehicle wheelbase) and q_1 (weight on yaw angle deviation), and evaluate the impacts of each of the two variables on the performance measures of Y_{err} (vehicle CG lateral position deviation from the reference path) and Yaw_ang_{err} (vehicle yaw angle deviation from the reference angle). In the following sensitivity analysis for evaluating the effects of the selected design variables, for each case study, only the chosen one varies, while others remain fixed with their nominal values provided in Table 4.2. The simulation results for the sensitivity analysis are derived from the simulated urban SLC (USLC) maneuver and the highway SLC (HSLC) maneuver.

Figures 4.20 and 4.21 illustrate the impact of l on Y_{err} in the USLC and HSLC, respectively. It is found that in both scenarios, the maximum peak Y_{err} value decreases with the increase of l value. It appears that a larger l benefits for achieving a better measure of Y_{err}. Figures 4.22 and 4.23 show the influence of l on Yaw_ang_{err}. In the HSLC case, a larger l also benefits for achieving a better measure of Yaw_ang_{err}. A close observation of Figure 4.23 reveals that the larger the l value becomes, the smaller the maximum peak Yaw_ang_{err} value will attain. This observation may explain why in the HSLC case, the optimal l takes the value of 3.55 m, which is very close to the upper bound value of 3.6 m. However, in the USLC case as shown in Figure 4.22, the above conclusion derived from the observation based on the result illustrated in Figure 4.23 is not true. As seen in Figure 4.22, when the vehicle wheelbase l takes the value of 3.6, 3.2, and 2.866 m, the corresponding maximum peak Yaw_ang_{err} values are $0.7702°$, $0.7346°$, and $0.7462°$. The above values of l and the respective maximum peak Yaw_ang_{err} values are not consistent with the aforementioned observation, that is, 'the larger the l value becomes, the smaller the maximum peak Yaw_ang_{err} value will attain'. Interestingly, among the above three listed l values, the one with the value of 3.2 m leads to the Yaw_ang_{err} measure of $0.7346°$, which is the least among the three measures. The l value of 3.2 m is very close to the optimized value of 3.16 m listed in Table 4.2.
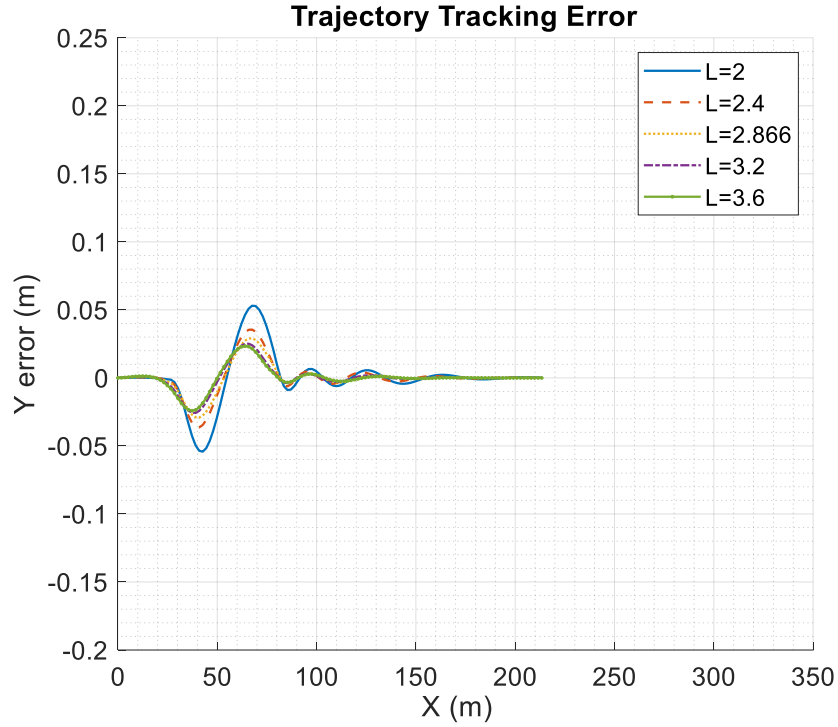
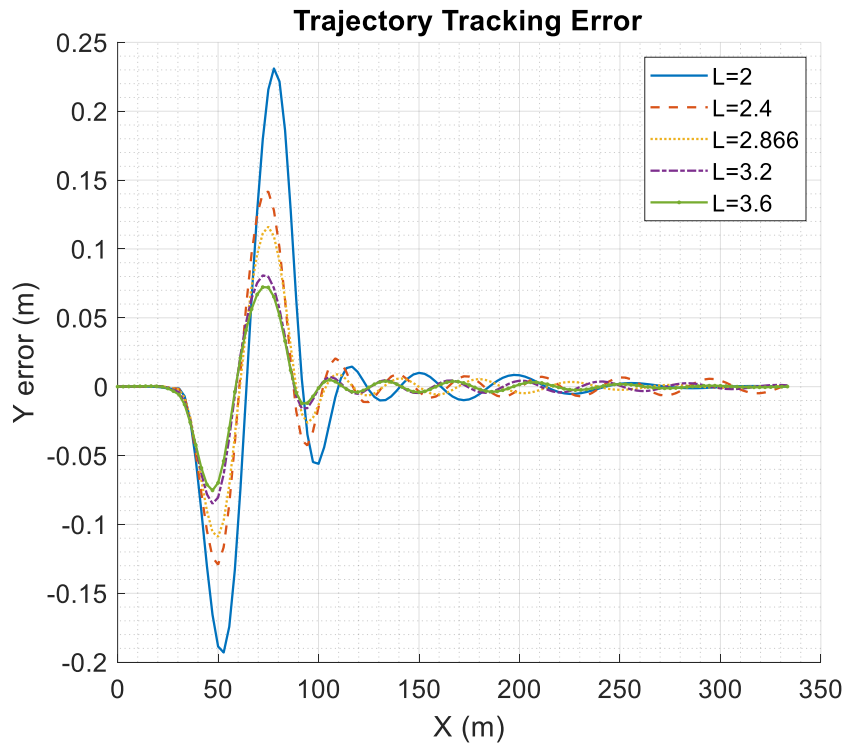Figure 4.20: Sensitivity analysis of the effects of l on Y_{err} in USLC.

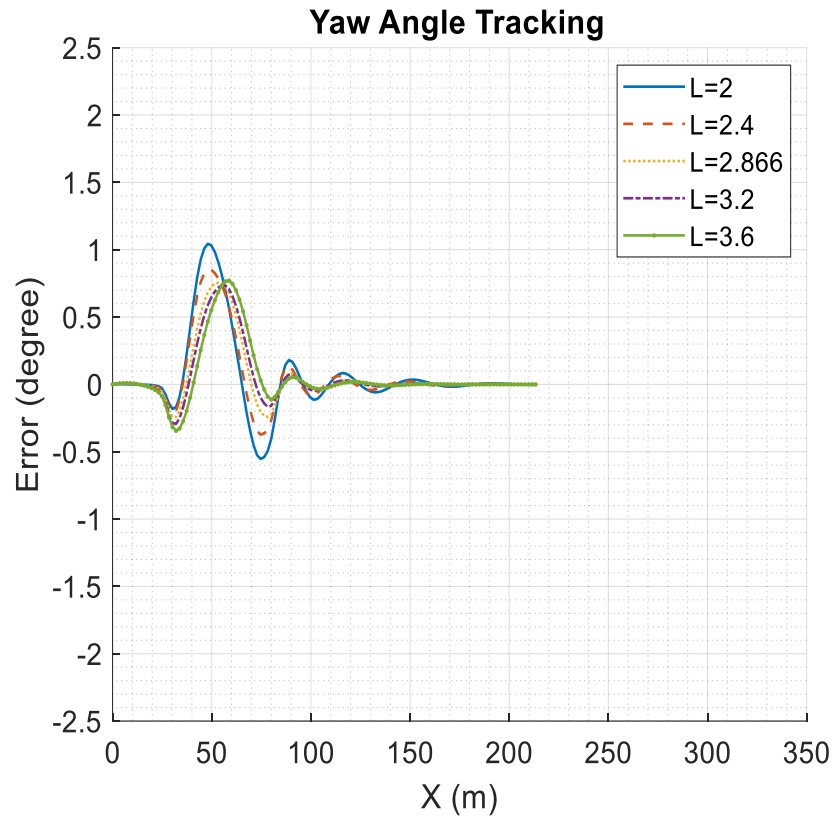Figure 4.21: Sensitivity analysis of the effects of l on Y_{err} in HSLC.

Figure 4.22: Sensitivity analysis of the effects of l on Yaw_ang_{err} in USLC.
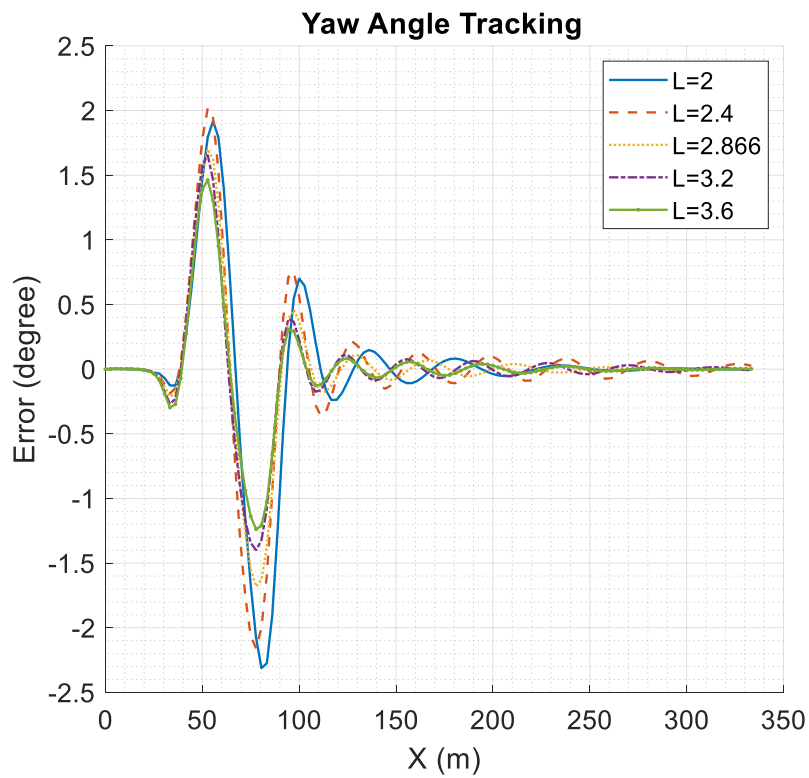

Figure 4.23: Sensitivity analysis of the effects of l on Yaw_ang_{err} in HSLC.

The above analysis regarding the effect of l on the measures of Y_{err} and Yaw_ang_{err} discloses that as vehicle forward speed increases, a longer wheelbase benefits for decreasing cross path error and enhancing yaw stability. This observation is consistent with the conclusion reported in [92]: a shorter wheelbase is advantageous to achieving a better low-speed (less than 15 km/h) path-following performance; while in high-speed evasive maneuvers, an ideal wheelbase value selection is a trade-off solution between transient path-following off-tracking and yaw/lateral stability. The aforementioned sensitivity and dynamic analysis well explain the optimal wheelbase value for the USLC and HSLC scenarios.

Figures 4.24 and 4.25 display the effect of q_1 on Y_{err} in the USLC and HSLC, accordingly. In the USLC case, the influence of q_1 on the peak values of Y_{err} is weak. This is reflected by the curves shown in Figure 4.24. It is shown that with the variation of q_1, the change of the two peak values of Y_{err} is not evident. In the HSLC case (as shown in Figure 4.25), it is observed that the larger the weight of q_1, the larger the maximum peak Y_{err}. Based on Equation (3.16), (3.17a), (3.23b) and (3.24a), we know that q_1 is the weight imposed on the output of Yaw_ang_{err}. For the weighted-sum-method-based multi-objective optimization of the NLMPC problem formulated in Equation (3.17), with the fixed weights of q_2 and R, increasing the weight of q_1 leads to a heavier penalty on Yaw_ang_{err}; in contrast, this results in a relatively lighter penalty on Y_{err}. The results shown in Figure 4.25 visualize the above inference.

Shown in Figures 4.26 and 4.27 are the effect of q_1 on Yaw_ang_{err} in the USLC and HSLC scenarios, respectively. By means of imposing a penalty on the magnitude of Yaw_ang_{err}, increasing the weight value of q_1 leads to the decrease of the maximum peak

value of this measure in both scenarios. Thus, the measures of Y_{err} and Yaw_ang_{err} pose the contradicted requirements on q_1 in both the cases and, in particular, the HSLC case. An ideal weight of q_1 is, generally, a compromised solution between the conflicting design criteria; the corresponding optimal q_1 will be a value between the lower and upper bound values of 0 and 20. As shown in Table 4.2, in the USLC case, the optimal value is 4.30, which is smaller than the nominal value, i.e., 15.00; while in the HSLC case, the counterpart is 16.40, which is bigger than the nominal value.
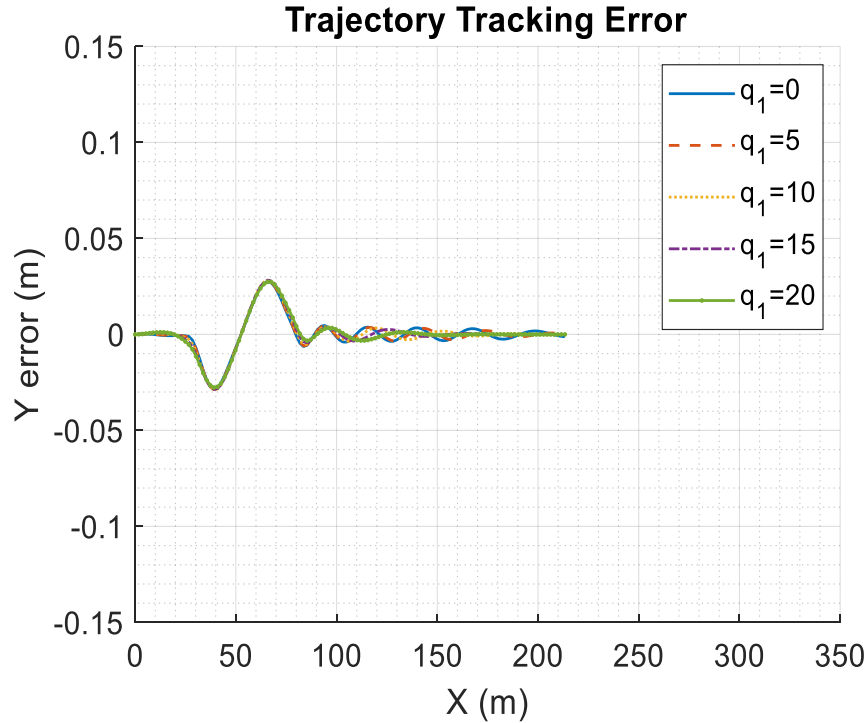
Figure 4.24: Sensitivity analysis of the effects of q_1 on Y_{err} in USLC.
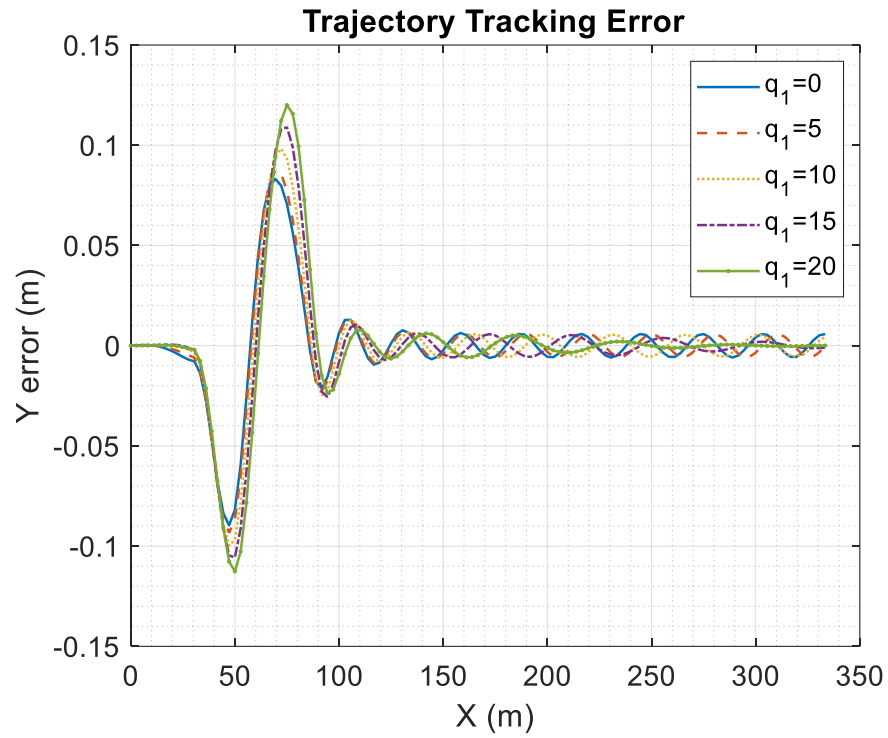
Figure 4.25: Sensitivity analysis of the effects of q_1 on Y_{err} in HSLC.
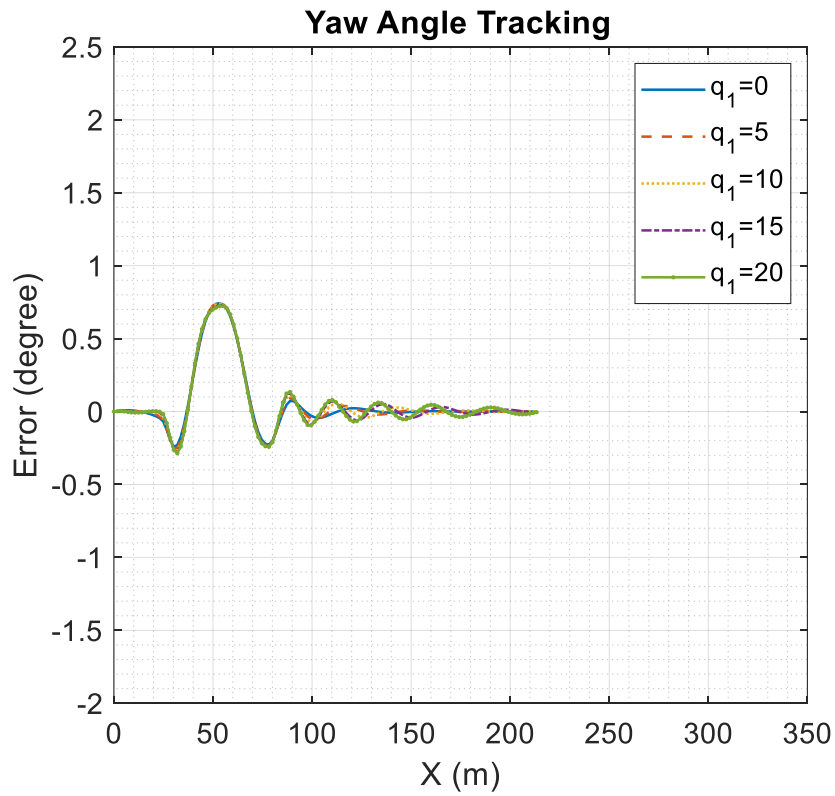
Figure 4.26: Sensitivity analysis of the effects of q_1 on Yaw_ang_{err} in USLC.
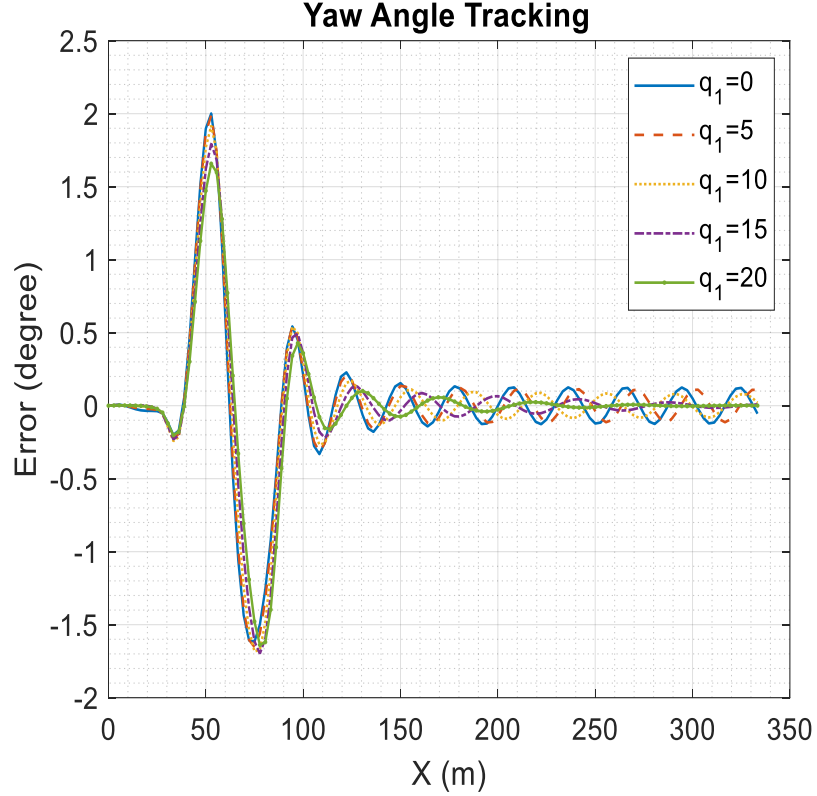
Figure 4.27: Sensitivity analysis of the effects of q_1 on Yaw_ang_{err} in HSLC.

The difference between the optimal values of q_1 in the USLC and HSLC scenarios is consistent with the vehicle design principle proposed in [78, 92]: in low-speed curved road negotiations, emphasis should be placed on improving path-following performance (i.e., lateral position deviation), whereas in the high-speed evasive maneuvers, more attention should be paid to ensuring yaw stability (i.e., yaw angle deviation).

In addition to the above sensitivity and vehicle dynamic analysis, the effects of the other individual design variables had also evaluated, including q_2, R, m, and l_f, on the performance measures of Y_{err}, Yaw_ang_{err}, and the RMS value of a_y, respectively. The comprehensive sensitivity and vehicle dynamic analysis justifies the optimal designs of the road vehicle with autonomous steering functions in both the USLC and HSLC scenarios. The successful implementation of the design optimization demonstrates the effectiveness

of the proposed design synthesis method shown in Figure 3.1.

Chapter 5

Conclusions

5.1 Conclusions

Considering the fact that an autonomous vehicle (AV) is a complex mechatronic system consisting of multi-subsystems, including mechanical vehicles, motion-planning, tracking-control, etc., this thesis proposes a bi-layer design synthesis method for AVs. At the lower layer, these dynamically coupled subsystems are modelled and synthesized as an integrated AV; the virtual AV is then simulated with the modules of motion-planning and tracking-control to operate in 'real-time' under a given operating maneuver. At the upper layer, a multi-objective optimization problem is formulated with the design criteria of path-following off-tracking, lateral/yaw stability, ride comfort, etc. The proposed method aims at finding ideal solutions to the complex AV optimization problem to satisfy the specified design requirements and constraints. With the aid of active aerodynamic control (AAC) system, it is expected that this method can achieve better performance during high-speed operating scenarios.

To assess the applicability and effectiveness of the proposed method, it is applied to the design synthesis of a road vehicle with an automated steering function. For implementing this design synthesis, a PSO search algorithm is introduced to solve the upper layer optimization problem; at the lower layer, the AV is modelled with the subsystems of a motion-planning, a mechanical vehicle, and an NLMPC tracking-control; an ideal AV design with the optimal design variables of a mechanical vehicle and NLMPC controller is sought under the simulated USLC and HSLC maneuvers. Due to the enlarged design space,

including the design variable sets for a mechanical vehicle and a tracking controller, the optimal AV is superior to its nominal design in terms of path-following off-tracking, lateral/yaw stability, and ride quality. The respective sensitivity and dynamic analyses justify the selected optimal design. It is disclosed that the optimal designs are operating condition dependent.

A special case is conducted under high-speed operating conditions considering the application of active aerodynamic control functionality. Vehicle aerodynamics lift/down forces and corresponding dynamic effects at high speed, e.g., 180 km/h, are simulated in a high-speed SLC maneuver. This case study is intended to test the design of active aerodynamic control with the installation of four independent spoilers. The virtual vehicle plant with the AAC system, and the resulting vehicle plant is used for the design of the NLMPC tracking-controller. The virtual vehicle plant utilizes the aerodynamic characteristics of the spoilers to enhance vehicle stability and handling capability. The simulation results indicate that the AAC system can improve high-speed handling and driving performance in terms of path-following off-tracking, yaw stability, ride quality, vertical tire force transformation, and roll stability.

The proposed design synthesis method may be applied in the early design stages of AVs for identifying desired design variables and predicting performance envelops.

5.2   Future research work

To improve the proposed design synthesis method, the function of tracking-control can be enhanced by introducing vehicle forward speed control, incorporating the perception module in the AV, and further enlarging the design space by adding the design variables for the modules of perception and motion-planning. Extended Kalman filter can be also considered in the design synthesis method to make the autonomous driving control become more robust and gain a better capability of filtering undesired noises.

Furthermore, research attempts can be made in active aerodynamic control. By building a physical vehicle prototype with spoilers, the spoiler profile can be validated in a wind tunnel. The validated active aerodynamic control system may be tested and evaluated with the in-vehicle experiment.

Lastly, AAC system can be controlled by the NLMPC system rather than divide into two independent system. It has the advantages of better system unity so that improve system's robustness and reliability. The control input of AAC can also be optimized by using the PSO algorithm therefore reduce the process in the lookup table. The proposed design method and AAC system can be tested in a physical vehicle to explore the capability and stability of the overall system.

REFERENCES

[1] B. Paden, M. Cáp, S. Z. Yong, et al., "A survey of motion planning and control techniques for self-driving urban vehicles," *IEEE Transactions on intelligent vehicles*, vol. 1, no. 1, pp.33-55, 2016.

[2] F. Rosique, P. J. Navarro, C. Fernández and A. Padilla, "A systematic review of perception system and simulators for autonomous vehicles research," *Sensors*, vol. 19, no. 3, pp. 1-29, 2019.

[3] E. Javanmardi, M. Javanmardi, Y. Gu and S. Kamijo, "Autonomous vehicle self-localization based on multilayer 2D vector map and multi-channel LiDAR," 2017 IEEE Intelligent Vehicles Symposium (IV), 2017, pp. 437-442.

[4] I. Sung, B. Choi, and P. Nielsen, "On the training of a neural network for online path planning with offline path planning algorithms," Int. J. Inf. Manage., vol. 57, no. May 2020, p. 102142, 2020.

[5] X. Hu, L. Chen, B. Tang, D. Cao, and H. He, "Dynamic path planning for autonomous driving on various roads with avoidance of static and moving obstacles," Mech. Syst. Signal Process., vol. 100, pp. 482–500, 2018.

[6] P. Falcone, H. E. Tseng, F. Borrelli, et al., "MPC-based yaw and lateral stabilisation via active front steering and braking," Vehicle System Dynamics, vol 46, supplement, pp. 611-628, 2008.

[7] E. Tofighi, and A. Mahdizadeh, "Automatic weight determination in nonlinear model predictive control of wind turbines using swarm optimization technique," Journal of

Physics: Conference Series, vol. 753, pp. 1-10, 2016.

[8]   "The   United   Nations   and   Road   Safety."   [Online].   Available: https://www.un.org/en/roadsafety/report.shtml. [Accessed: 07-June-2022].

[9] Y. He, "Design of an actively controlled aerodynamic wing to increase high-speed vehicle safety," SAE Technical Paper 2013-01-0802, 2013.

[10] T. Sikder, S. Kapoor, and Y. He, "Optimizing Dynamic Performance of High-Speed Road Vehicles Using Aerodynamic Aids," presented at the ASME 2016 International Mechanical Engineering Congress and Exposition, 2016, p. V007T09A060-V007T09A060.

[11] A. Rahimi and Y. He, "A review of essential technologies for autonomous and semi-autonomous articulated heavy vehicles", *Proceedings of the Canadian Society for Mechanical Engineering (CSME) International Congress 2020*, Charlottetown, PE, Canada, June 21-24, 2020.

[12] M. P. Ananda, H. Bernstein, K. E. Cunningham, W. A. Feess, and E. G. Stroud, "Global Positioning System (GPS) autonomous navigation," *IEEE Symp. Position Locat. Navig. A Decad. Excell. Navig. Sci.*, pp. 497–508, 1990.

[13] W. Rahiman and Z. Zainal, "An overview of development GPS navigation for autonomous car," in *Proceedings of the 2013 IEEE 8th Conference on Industrial Electronics and Applications, ICIEA 2013*, 2013.

[14] S. A. S. Mohamed, M. H. Haghbayan, T. Westerlund, J. Heikkonen, H. Tenhunen, and J. Plosila, "A survey on odometry for autonomous navigation systems," *IEEE*

Access, 2019.

[15] D. Göhring, M. Wang, M. Schnürmacher, and T. Ganjineh, "Radar/Lidar sensor fusion for car-following on highways," In *Proceedings of the 2011 5th International Conference on Automation, Robotics and Applications (ICARA)*, Wellington, New Zealand, December 6–8, 2011.

[16] L. Wei, C. Cappelle, and Y. Ruichek, "Camera/laser/GPS fusion method for vehicle positioning under extended NIS-based sensor validation," *IEEE Trans. Instrum. Meas.*, vol. 62, no. 11, pp. 3110–3122, 2013.

[17] A. V. Goldberg and C. Harrelson, "Computing the shortest path: A search meets graph theory," in *Proc. 16th Annu. ACM-SIAM Symp. Discrete Algorithms*, 2005, pp. 156–165.

[18] R. Geisberger, P. Sanders, D. Schultes, and C. Vetter, "Exact routing in large road networks using contraction hierarchies," *Transp. Sci.*, vol. 46, pp. 388–404, 2012.

[19] H. Bast *et al.*, "Route planning in transportation networks," arXiv:1504.05140, 2015.

[20] P. Jagannathan, S. Rajkumar, J. Frnda, et al., "Moving vehicle detection and classification using Gaussian mixture model and ensemble deep learning technique," *Wireless Communications and Mobile Computing*, vol. 2021, 15 pages, May 2021.

[21] D. M. Steinberg, S. B. Williams, O. Pizarro and M. V. Jakuba, "Towards autonomous habitat classification using Gaussian mixture models," *The 2010 IEEE/RSJ International Conference on Intelligent Robots and Systems*, Taipei, Taiwan, October 18-22, 2010.

[22] W. Fang, S. Zhang, H. Uuang, et al., "Learn to make decision with small data for autonomous driving: Deep Gaussian process and feedback control," *Journal of Advanced Transportation*, vol. 2020, 11 pages, August 2020.

[23] L. Xin, P. Wang, C. Chan, et al., "Intention-aware long horizon trajectory prediction of surrounding vehicles using dual LSTM networks," *2018 21st International Conference on Intelligent Transportation Systems*, Maui, HI, USA, November 4-7, 2018.

[24] S. Liu, K Zheng, L. Zhao and P. Fan, "A driving intention prediction method based on hidden Markov model for autonomous driving," *Computer Communications*, vol. 157, pp. 143-149, 2020.

[25] Z. Shiller and S. Sundar, "Emergency lane-change maneuvers of autonomous vehicles," *J. Dyn. Sys., Meas., Control,* vol. 120, no. 1, pp. 37-44, 1998.

[26] Y. Hattori, E. Ono, and S. Hosoe, "Optimal vehicle trajectory control for obstacle avoidance problem," IEEE/ASME Transactions on Mechatronics, vol. 11, no. 5, pp. 507-512, 2006.

[27] S. Lazard, J. Reif and H.Wang, "The complexity of the two dimensional curvature constrained shortest-path problem," in *Proc. 3rd Int. Workshop Algorithmic Found. Robot.*, 1998, pp. 49–57.

[28] L. E. Kavraki, M. N. Kolountzakis, and J.-C. Latombe, "Analysis of probabilistic roadmaps for path planning," *Trans. Robot. Autom.*, vol. 14, pp. 166–171, 1998.

[29] J. Reif and M. Sharir, "Motion planning in the presence of moving obstacles," *J. ACM*, vol. 41, pp. 764–790, 1994.

[30] Z. Shiller and S. Sundar, "Emergency maneuvers for AHS vehicles," SAE Technical Paper 951893, 1995.

[31] T. Fraichard, "Trajectory planning in a dynamic workspace: A 'state-time space' approach," *Adv. Robot.*, vol. 13, pp. 75–94, 1998.

[32] T. Gu, J. Snider, J. M. Dolan, and J. Lee, "Focused trajectory planning for autonomous on-road driving," *2013 IEEE Intelligent Vehicle Symposium (IV)*, pp. 547-552, 2013.

[33] I. Kaminer, A., Pascoal, E. Hallberg, and C. Silvestre, "Trajectory tracking for autonomous vehicles: An integrated approach to guidance and control," Journal of Guidance, Control, and Dynamics, vol. 21, no.1, pp.29-38, 1998.

[34] J. Yu, T. Sharma, and Y. He, "Design optimization of autonomous steering control schemes for articulated vehicles," Proceedings of the Canadian Society for Mechanical Engineering International Congress 2021, Charlottetown, PE, Canada, June 27-30, 2021.

[35] J. Wit, C. D. Crane, and D. Armstrong, "Autonomous ground vehicle path tracking," J. Robot. Syst., vol. 21, pp. 439–449, 2004.

[36] Z.-P. Jiang and H. Nijmeijer, "Tracking control of mobile robots: A case study in backstepping," Automatica, vol. 33, pp. 1393–1399, 1997.

[37] A. Rahimi, W. Huang, and Y. He, "A longitudinal speed controller for autonomous multi-trailer articulated heavy vehicles," Proceedings of the Canadian Society for Mechanical Engineering International Congress 2021, Charlottetown, PE, Canada, June 27-30, 2021.

[38] Y. Kanayama,Y.Kimura, F. Miyazaki, and T.Noguchi, "A stable tracking control method for an autonomous mobile robot," in Proc. Int. Conf. Robot. Autom., 1990, pp. 384–389.

[39] B. d'Andr´ea Novel, G. Campion, and G. Bastin, "Control of nonholonomic wheeled mobile robots by state feedback linearization," Int. J. Robot. Res., vol. 14, pp. 543–559, 1995.

[40] L. Liu, B. Wang, and Y. He, "Research on path-tracking control of articulated vehicle with a trailer based on advanced model prediction control strategy," Proceedings of the Canadian Society for Mechanical Engineering International Congress 2021, Charlottetown, PE, Canada, June 27-30, 2021.

[41] W. Gao, Z. Deng, Y. Feng, and Y. He, "On aerodynamic drag reduction of road vehicles in platoon," Int. J. Vehicle Systems Modelling and Testing, vol. 16, no.1, pp.1-24, 2022.

[42] W. Gao, Z. Deng, and Y. He, "A comparative study of tail air-deflector designs on aerodynamic drag reduction of medium-duty trucks," Int. J. Vehicle Performance, vol. 8, nos, 2/3, pp. 316-333, 2022.

[43] C. Fu, M. Uddin, and C. Zhang, "Computational Analyses of the Effects of Wind Tunnel Ground Simulation and Blockage Ratio on the Aerodynamic Prediction of Flow over a Passenger Vehicle," Vehicles, vol. 2, no. 2, pp. 318–341, Jun. 2020.

[44] S. Kandasamy, B. Duncan, H. Gau, F. Maroy, A. Belanger, N. Gruen, and S. Schäufele, "Aerodynamic performance assessment of BMW validation models using computational fluid dynamics." SAE 2012 World Congress & Exhibition. No. 2012-01-0297. 2012.

[45] Barnard, R. H. Road Vehicle Aerodynamic Design: An Introduction. Mechaero Publishing, 2009.

[46] Katz, Joseph. "Aerodynamics of race cars." Annual Review of fluid mechanics, vol.38, no.1, pp. 27-63, Jan. 2006.

[47] M. Hammad, K. Qureshi, and Y. He, "Safety and lateral dynamics improvement of a race car using active rear wing control," SAE Technical Paper 2019-01-0643, 2019.

[48] J. Cai, S. Kapoor, T. Sikder, and Y. He, "Effects of active aerodynamic wings on handling performance of high-speed vehicles," SAE Technical Paper 2017-01-1592, 2017.

[49] Le Good, G. and Garry, K., "On the Use of Reference Models in Automotive Aerodynamics," SAE Technical Paper 2004-01-1308, 2004.

[50] Ahmed, Syed R., G. Ramm, and Gunter Faltin. "Some salient features of the time-averaged ground vehicle wake." SAE Transactions (1984): 473-503.

[51] Closed-test-section Wind Tunnel Blockage Corrections for Road Vehicles. Warrendale, PA: Society of Automotive Engineers, 1996.

[52] Carr, G. and Stapleford, W., "Blockage Effects in Automotive Wind-Tunnel Testing," SAE Technical Paper 860093, 1986

[53] J. Piechna, L. Rudniak, and A. Piechna. "CFD analysis of the central engine generic sports car aerodynamics." 4th European automotive simulation conference, Munich. 2009.

[54] M. Szudarek and J. Piechna, "CFD Analysis of the Influence of the Front Wing Setup on a Time Attack Sports Car's Aerodynamics," Energies, vol. 14, no. 23, p. 7907, Nov. 2021.

[55] D. Ayyagari and Y. He, "Aerodynamic analysis of an active rear split spoiler for improving lateral stability of high-speed vehicles", International Journal of Vehicle Systems Modelling and Testing, vol. 12, no. 34, p. 217, 2017.

[56] T. Burton, N. Jenkins, D. Sharpe, E. Bossanyi and M. Graham, Wind energy handbook. 2021.

[57] M. Yılmaz, H. Köten, E. Çetinkaya and Z. Coşar, "A comparative CFD analysis of NACA0012 and NACA4412 airfoils", Journal of Energy Systems, pp. 145-159, 2018.

[58] H. Shan, L. Jiang, C. Liu, M. Love and B. Maines, "Numerical study of passive and active flow separation control over a NACA0012 airfoil", Computers & Fluids, vol. 37, no. 8, pp. 975-992, 2008.

[59] L. Huang, P. Huang, R. LeBeau and T. Hauser, "Numerical Study of Blowing and Suction Control Mechanism on NACA0012 Airfoil", Journal of Aircraft, vol. 41, no. 5, pp. 1005-1013, 2004.

[60] "NACA 0012 AIRFOILS (n0012-il)", Airfoiltools.com, 2022. [Online]. Available: http://airfoiltools.com/airfoil/details?airfoil=n0012-il. [Accessed: 02- June- 2022].

[61] J. Wong, Theory of ground vehicles. New York: John Wiley, 2001.

[62] S. Zhu and Y. He, "A driver-adaptive stability control strategy for sport utility vehicles," Vehicle System Dynamics, vol 55, no 8, pp. 1206-1240, 2017.

[63] R. Rajamani, Vehicle dynamics and control[M]. Springer Science & Business Media, 2011.

[64]   M. Morari, C. E. Garcia, and D. M. Prett, "Model predictive control: Theory and practice," IFAC Proc. Vol., vol. 21, no. 4, pp. 1–12, 1988.

[65]   M. Morari and J. H. Lee, "Model predictive control: Past, present and future," Comput. Chem. Eng., vol. 23, no. 4–5, pp. 667–682, 1999.

[66]   J. B. Rawlings, "Tutorial overview of model predictive control," IEEE Control Syst. Mag., vol. 20, no. 3, pp. 38–52, 2000.

[67] S. Cheng, L. Li, H. Q. Guo, Z. G. Chen, and P. Song, "Longitudinal Collision Avoidance and Lateral Stability Adaptive Control System Based on MPC of Autonomous Vehicles," IEEE Trans. Intell. Transp. Syst., vol. 21, no. 6, pp. 2376–2385, 2020.

[68] A. Gray, M. Ali, Y. Gao, J. K. Hedrick, and F. Borrelli, "Integrated threat assessment and control design for roadway departure avoidance," IEEE Conf. Intell. Transp. Syst. Proceedings, ITSC, pp. 1714–1719, 2012.

[69] T. Keviczky, P. Falcone, F. Borrelli, J. Asgari, and D. Hrovat, "Predictive control approach to autonomous vehicle steering," Proc. Am. Control Conf., vol. 2006, pp. 4670–4675, 2006.

[70] P. Falcone, F. Borrelli, J. Asgari, H. E. Tseng, and D. Hrovat, "Predictive active steering control for autonomous vehicle systems," IEEE Trans. Control Syst. Technol., 2007.

[71] S. G. Vougioukas, "Reactive trajectory tracking for mobile robots based on non linear model predictive control," in Proceedings - IEEE International Conference on Robotics and Automation, 2007.

[72] M. A. Henson, "Nonlinear model predictive control: Current status and future directions," Comput. Chem. Eng., 1998.

[73] U. Rosolia, S. D. Bruyne, and A. G. Alleyne, "Autonomous vehicle control: A nonconvex approach for obstacle avoidance," IEEE Trans. Control Syst. Technol., vol. 25, no. 2, pp. 469–484, Mar. 2017.

[74] H. Guo, H. Zhang, H, Chen, and R. Jia, "Simultaneous trajectory planning and tracking using an MPC method for cyber-physical systems: a case study of obstacle avoidance for an intelligent vehicle," IEEE Trans. Ind. Informat., vol. 14, no. 9, pp. 4273–4283, Sept. 2018.

[75] Y. He, "Design synthesis of mechatronic vehicles with coordinated control systems," Vehicle System Dynamics, vol 46, supplement, pp. 923-936, 2008.

[76] Y. He, and J. McPhee, "Multidisciplinary design optimization of mechatronic vehicles with active suspensions," Journal of Sound and Vibration, vol. 283, pp. 217-241, 2003.

[77] Y. He, and J. McPhee, "A design methodology for mechatronic vehicles: application of multidisciplinary optimization, multibody dynamics and genetic algorithms," Vehicle System Dynamics, vol 43, no 10, pp. 697-733, 2005.

[78] Y. He, and M. M. Islam, "An automated design method for active trailer steering systems of articulated heavy vehicles," Journal of Mechanical Design, vol. 134, no. 4, pp. 1-15, 2012.

[79] Y. He, "Design of rail vehicles with passive and active suspensions using multidisciplinary optimization, multibody dynamics, and genetic algorithms," PhD Thesis, Department of Mechanical Engineering, University of Waterloo, 2003.

[80] J. L. Garrriga, and M. Soroush, "Model predictive control tuning method: a review," Ind. Eng. Chem. Res., vol 49, pp. 3505-3515.

[81] R. Nebeluk, and M. Ławryńczuk, "Tuning of multivariable model predictive control for industrial tasks," Algorithms, vol. 14, no. 10, pp. 1-15, 2021.

[82] A. S. Yamashita, P. M. Alexandre, A. C. Zanin, and D. Odloak, "Reference trajectory tuning of model predictive control," Control Engineering Practice, vol. 50, pp.1-11, 2016.

[83] G. A. N. Júnior, M. A. F. Martins, and R. Kalid, "A PSO-based optimal tuning strategy for constrained multivariable predictive controllers with model uncertainty," ISA Transactions, vol. 53, pp. 560-567, 2014.

[84] E. Tofighi, and A. Mahdizadeh, "Automatic weight determination in nonlinear model predictive control of wind turbines using swarm optimization technique," Journal of Physics: Conference Series, vol. 753, pp. 1-10, 2016.

[85] J. Kennedy, and R. C. Eberhart, "Particle swarm optimization," IEEE International Conf. on Neural Networks, pp. 1942-1948, 1995.

[86] K. Kameyama, "Particle swarm optimization - A survey," IEICE Trans. Inf. & Syst., vol. E92-D, no. 7, pp. 1354-1361, 2009.

[87] C. A. Coello, G. T. Pulido, and M. S. Lechuga, "Handling multiple objectives with particle swarm optimization," IEEE Trans. Evol. Comput., vol.8, no3, pp.256-279, 2004.

[88] Y. Shi, and R. C. Eberhart, "Empirical study of particle swarm optimization," Proceedings of the 1999 Congress on Evolutionary Computation, pp. 1945-1950, 1999.

[89] P. J. Angeline, "Evolutionary optimizaton versus swarm optimizaton: philosophy and performance difference," Proceeding of the 1998 Annual Conference on Evolutionary Programming, pp. 601-610, San Diego, 1998.

[90] Y. He, and J. McPhee, "Optimization of curving performance of rail vehicles," Vehicle System Dynamics, vol 43, no. 12, pp. 895-923, 2005.

[91] Y. He, and J. McPhee, "Multidisciplinary optimization of multibody systems with application to the design of rail vehicles," Multibody System Dynamics, vol. 14, pp. 111-135.

[92] M. M. Islam, X. Ding, and Y. He, "A closed-loop dynamic simulation based design method for articulated heavy vehicles with active trailer steering systems," Vehicle System Dynamics, vol 50, no. 5, pp. 675-697, 2012.

[93] (September 26, 2021). Mechanical Simulation Corporation, CARSIM: Math Models. [online]. Available: https://www.carsim.com/downloads/pdf/CarSim_Math_Models.pdf

[94] E. Bakker, L. Nyborg, and H. Pacejka, "Tyre modelling for use in vehicle dynamics studies," SAE Technical Paper 870421, 1987.

[95] S. Zhu, Y. He, and J. Ren, "On robust controllers for active steering systems of articulated heavy vehicles," International Journal of Heavy Vehicle Systems, vol. 26, no. 1, pp. 1-30, 2019.

[96] M. Lanfrit, "Best practice guidelines for handling Automotive External Aerodynamics with FLUENT." (2005).

[97] C. Liu, W. Zhan, and M. Tomizuka, "Speed profile planning in dynamic environments via temporal optimization," in Proc. Intell. Vehicles Symp. (IV), 2017, pp. 154–159.

[98] T. Gu, J. M. Dolan, and J.-W. Lee, "Runtime-bounded tunable motion planning for autonomous driving," in IEEE Intelligent Vehicles Symposium (IV), 2016, pp. 1301–1306.

[99] K. Koibuchi, M. Yamamoto, Y. Fukada, and S. Inagaki. "Vehicle stability control in limit cornering by active brake," SAE Technical Paper 960487, 1996.

[100] International Organization for Standardization. Mechanical vibration and shock – Evaluation of human exposure to whole-body vibration – Part 1: General requirements – Amendment 1, ISO-2631-1:1997/Amd 1:2010.

Available: https://www.iso.org/standard/45604.html

[101] H. M. Osman, "Optimizing model based predictive control for combustion boiler process at high model uncertainty," Chemical and Biochemical Engineering Quarterly, vol. 31, no. 3, pp. 313-324, 2017.

[102] S. Zhu, and Y. He, "A unified lateral preview driver model for road vehicles," IEEE Transactions on Intelligent Transportation Systems, vol. 21, no. 11, pp. 4858-4868, 2020.

Appendix: Parameter values of the 3-D CarSim vehicle model and the lateral tire dynamics
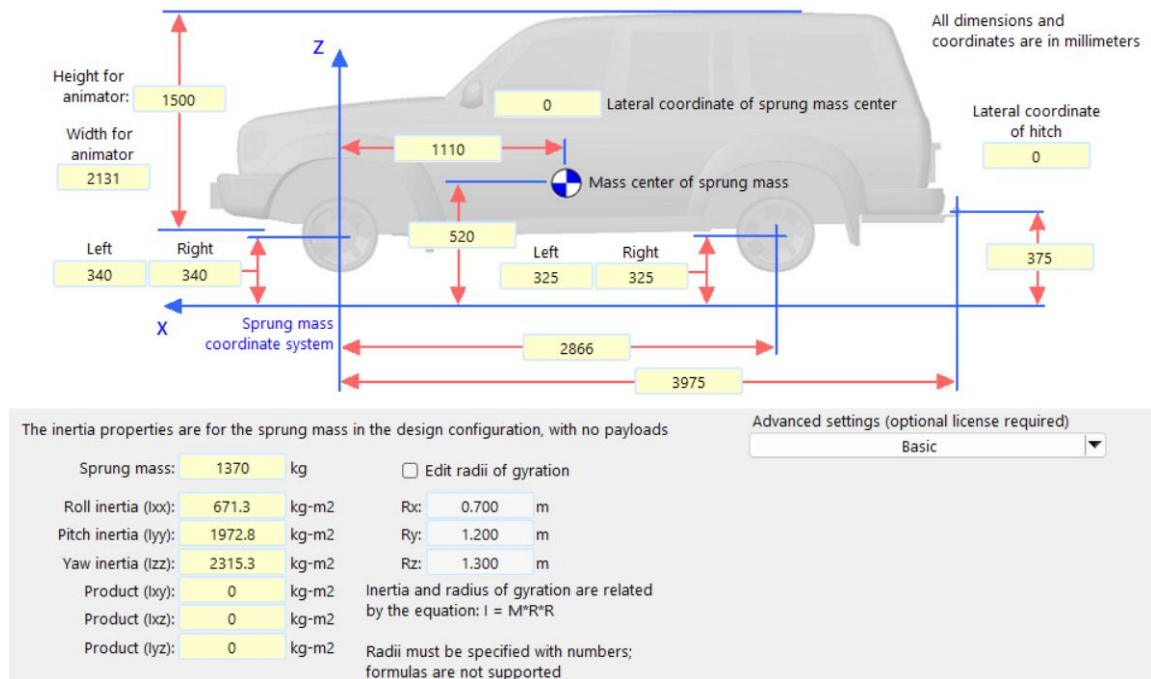

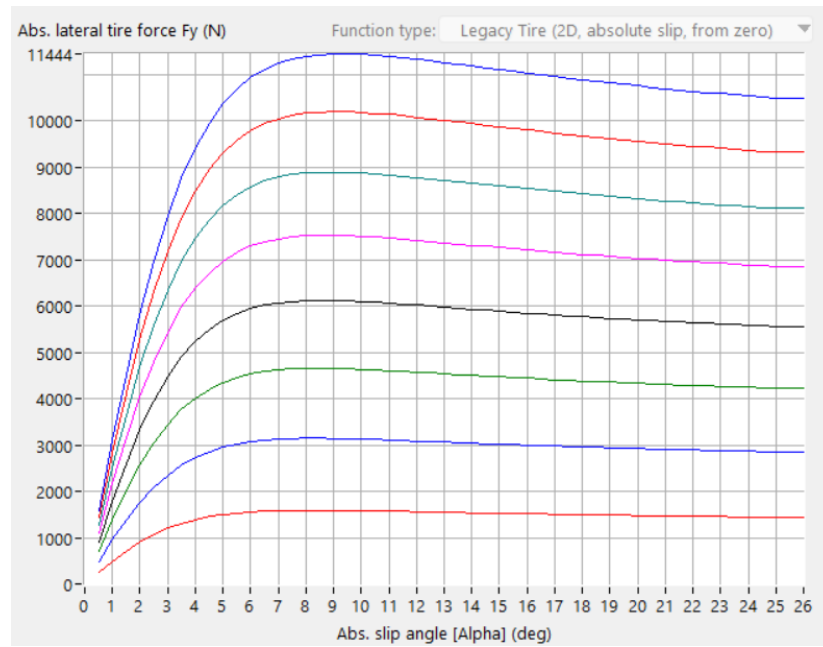Figure A.1: Parameters of virtual vehicle used in Matlab and CarSim co-simulation.

Figure A.2: Lateral tire force profile used in CarSim.